Electron-deuteron deep-inelastic scattering with spectator nucleon tagging and final-state interactions at intermediate x

M. Strikman[1,*] and C. Weiss[2,†]

[1] *Department of Physics, Pennsylvania State University, University Park, PA 16802, USA*
[2] *Theory Center, Jefferson Lab, Newport News, VA 23606, USA*

We consider electron-deuteron deep-inelastic scattering (DIS) with detection of a proton in the nuclear fragmentation region ("spectator tagging") as a method for extracting the free neutron structure functions and studying their nuclear modifications. Such measurements could be performed at a future Electron-Ion Collider (EIC) with suitable forward detectors. The measured proton recoil momentum ($\lesssim 100$ MeV in the deuteron rest frame) specifies the deuteron configuration during the high-energy process and permits a controlled theoretical treatment of nuclear effects. Nuclear and nucleonic structure are separated using methods of light-front quantum mechanics. The impulse approximation (IA) to the tagged DIS cross section contains the free neutron pole, which can be reached by on-shell extrapolation in the recoil momentum. Final–state interactions (FSI) distort the recoil momentum distribution away from the pole. In the intermediate–x region $0.1 < x < 0.5$ FSI arise predominantly from interactions of the spectator proton with slow hadrons produced in the DIS process on the neutron (rest frame momenta $\lesssim 1$ GeV, target fragmentation region). We construct a schematic model describing this effect, using final–state hadron distributions measured in nucleon DIS experiments and low-energy hadron scattering amplitudes. We investigate the magnitude of FSI, their dependence on the recoil momentum (angular dependence, forward/backward regions), their analytic properties, and their effect on the on-shell extrapolation. We comment on the prospects for neutron structure extraction in tagged DIS with EIC. We discuss possible extensions of the FSI model to other kinematic regions (large/small x). In tagged DIS at $x \ll 0.1$ FSI resulting from diffractive scattering on the nucleons become important and require separate treatment.

Keywords: Deep–inelastic scattering, deuteron, neutron, final–state interactions, Electron–Ion Collider

* E-mail: strikman@phys.psu.edu
† E-mail: weiss@jlab.org

CONTENTS

I. INTRODUCTION

Measurements of deep-inelastic lepton scattering (DIS) from nuclei with mass number $A > 1$ address several key topics in short-range nuclear structure and quantum chromodynamics (QCD). One is the partonic structure of the neutron, which is needed for the flavor decomposition of the nucleon's valence and sea quark densities and for the separation of singlet and non-singlet nucleon structure functions in studies of the scale dependence (QCD evolution, higher-twist effects). Another topic are the modifications of the nucleon's partonic structure in the nucleus and their dependence on the scaling variable x (EMC effect at $x > 0.3$, antishadowing at $x \sim 0.1$), which attest to the presence of non-nucleonic degrees of freedom in nuclei and reveal the QCD structure of nucleon-nucleon interactions [1, 2]. Yet another topic are coherence phenomena at $x \ll 0.1$ such as nuclear shadowing, which arise from the participation of multiple nucleons in the DIS process and govern the approach to the unitarity limit at high energies [3]. Experiments in nuclear DIS have been carried out in fixed-target $eA/\mu A$ scattering at several facilities (SLAC, HERMES, CERN EMC and COMPASS, FNAL E665, JLab; see Ref. [4] for a review) and will be extended further with the Jefferson Lab 12 GeV Upgrade. A much wider kinematic range would become accessible in colliding–beam experiments with a future Electron–Ion Collider (EIC) [5–7]. A medium–energy EIC with a squared electron–nucleon center-of-mass energy $s_{eN} \equiv s_{eA}/A \sim$ 200–2000 GeV^2 would be ideally suited for nuclear DIS measurements in the region $x \gtrsim 10^{-3}$ and enable detailed studies of sea quarks and gluons in the nucleon and their nuclear modifications [8, 9]. Complementary information is provided by measurements of hard processes in high-energy hadron and photon scattering on nuclei (RHIC, LHC) [10].

The main challenge in the analysis of nuclear DIS experiments is to account for the multitude of nuclear configurations that can be present in the initial state of the high-energy scattering process and affect its outcome [11]. The scattering can take place on any of the constituent protons and neutrons (p and n), in different states of their quantum–mechanical motion in the nucleus (momentum, spin). In addition, non-nucleonic degrees of freedom such as Δ isobars are excited by the nuclear binding. In the extraction of neutron structure one needs to isolate the DIS cross section arising from scattering on the neutrons and eliminate the effects of nuclear binding (Fermi motion, non-nucleonic degrees of freedom). For neutron spin structure one must also infer the effective polarization of the neutron in the polarized nucleus and account for the polarization of non-nucleonic degrees of freedoms, particularly intrinsic Δ's in polarized ^{3}He [12–14]. In the study of nuclear modifications at $x \gtrsim 0.1$ (EMC effect, antishadowing) one wants to relate the modifications to the nucleon interactions taking place in particular nuclear configurations (short-range correlations, exchange mechanisms). In traditional inclusive nuclear DIS measurements $e + A \to e' + X$ these issues are addressed by modeling the nuclear effects for typical nuclear configurations and averaging over all possible configurations. The resulting theoretical uncertainty usually represents the dominant systematic error in neutron structure extraction. Likewise, this method provides limited possibilities for unraveling the dynamical origin of nuclear modifications. Major progress could come from experiments that provide information on the nuclear configurations present during the high–energy process through measurements of the nuclear final state.

Deep-inelastic scattering on the deuteron ($d, A = 2$) with detection of a nucleon ($N = p$ or n) in the nuclear fragmentation region, $e + d \to e' + N + X$, represents a unique method for performing DIS measurements in controlled nuclear configurations ("spectator tagging"). The nucleon emerges with a typical recoil momentum $|\boldsymbol{p}_N| \sim$ few 10–100 MeV in the deuteron rest frame.[1] At such momenta the deuteron's non-relativistic pn wave function is well known from low–energy measurements and can be used to construct the pn light-front (LF) wave function entering in high–energy processes (see below). Because the deuteron has isospin $I = 0$, Δ isobars in the wave function are strongly suppressed (they can occur only in $\Delta\Delta$ configurations), so that the deuteron can be treated as a pn system for most of the configurations relevant to DIS [11]. Under these conditions the detection of the recoil nucleon and the measurement of its momentum positively identify the active nucleon and control its momentum during the DIS process. By measuring DIS with a tagged proton and extrapolating the measured recoil momentum dependence to the on-shell point near $|\boldsymbol{p}_p| = 0$ (in the deuteron rest frame) one can eliminate nuclear binding effects and extract free neutron structure in a model-independent manner [15]. DIS on the deuteron with proton tagging was measured in the JLab CLAS BONuS experiment at 6 GeV beam energy [16, 17] and will be explored further at 11 GeV [18]. This setup covers recoil momenta $|\boldsymbol{p}_p| \gtrsim 70$ MeV, which are larger than the typical nucleon momenta in the deuteron (the median of the nonrelativistic momentum distribution is ~ 70 MeV). In such fixed–target experiments it is difficult to get slow protons (or neutrons) out of the target and measure their momenta with sufficient resolution, which restricts the measurements to large recoil momenta and prevents on-shell extrapolation.

Much more suitable for tagged DIS measurements are colliding–beam experiments, where the spectator nucleon moves on with approximately half the deuteron beam momentum and can be detected using forward detectors. Both EIC designs presently discussed include capabilities for forward nucleon detection [9, 19, 20]. The JLab EIC detector

[1] We use units in which $\hbar = c = 1$ and quote momenta in MeV/GeV.

is designed to provide full coverage for spectator protons down to zero transverse momentum, and with a momentum resolution corresponding to $|\boldsymbol{p}_p| \sim 20$ MeV in the rest frame, as well as forward neutron detection. This setup would enable measurements of deuteron DIS with spectator tagging over the entire (x, Q^2) range covered by the collider and thus permit extraction of neutron structure and study of nuclear modifications with control of the nuclear configuration. It would also allow for tagged measurements on the polarized deuteron, which is potentially the most precise method for determining neutron spin structure.

The theoretical analysis of tagged DIS on the deuteron relies essentially on the analytic properties of the scattering amplitude (and cross section) in the recoil proton momentum. As a function of the invariant 4–momentum transfer between the deuteron and the recoiling proton, $t \equiv (p_d - p_p)^2$, the cross section has a pole at $t = M_N^2$ (we assume isospin symmetry and denote the common nucleon mass by $M_N \equiv M_{p,n}$). The pole is contained in the impulse approximation (IA) amplitude and corresponds to the scattering from an on-shell neutron in the deuteron in unphysical kinematics. According to the general principles of scattering theory, the residue at the pole is given by the structure function of the *free neutron.* Nuclear binding and final-state interactions (FSI) affect only the tagged deuteron structure functions away from the pole, at $t - M_N^2 \neq 0$, not the residue at the pole. This makes it possible to extract the free neutron structure function, by measuring the proton-tagged DIS cross section as a function of t and extrapolating to the on-shell point $t \to M_N^2$. In terms of the recoil momentum in the rest frame $t - M_N^2 = -2|\boldsymbol{p}_p|^2 + t'_{\rm min}$, where $t'_{\rm min} = -M_d \epsilon_d = -0.0041\,{\rm GeV}^2$ ($\epsilon_d = 2.2$ MeV is the deuteron binding energy), so that the on-shell point corresponds to unphysical values of the recoil momentum extremely close to zero, $|\boldsymbol{p}_p|^2 = -t'_{\rm min}/2$. The method is model-independent and relies only on general properties of the tagged DIS cross section (analyticity, position of singularities). It has considerable theoretical appeal and can be turned into a practical tool, given sufficiently precise data at small recoil momenta.

Away from the nucleon pole, at $t - M_N^2 \neq 0$, the recoil momentum dependence of the tagged DIS cross section is modified by FSI. They result from amplitudes in which the final state produced in the DIS process on the active nucleon rescatters from the spectator nucleon and changes its momentum. They exhibit a complex dependence on the recoil momentum angle and magnitude, dictated by the kinematics of the rescattering process, and on x, because the character of the nucleon DIS final state changes as a function of the latter. The FSI effects in the tagged cross section need to be estimated quantitatively in order to assess the feasibility of neutron structure extraction through on-shell extrapolation. The same is needed in order to explore the possibility of separating initial-state nuclear modifications from final-state interactions in tagged DIS. Such an estimate requires a theoretical model of FSI appropriate to the region of x explored in the tagged DIS experiments.

In this article we develop the theoretical framework for tagged DIS measurements on the deuteron in the kinematic region explored with a medium-energy EIC. We use methods of LF quantum mechanics to separate nuclear and nucleonic structure in the high-energy process and enable dynamical calculations of the deuteron structure elements. We derive the tagged structure functions in the IA and study their symmetries and analytic properties in the recoil momentum. We then develop a dynamical model of nuclear FSI at "intermediate" x, defined as the region between the extreme valence quark regime at $x \gtrsim 0.5$ and the coherent regime at $x \ll 0.1$ (the role of coherent phenomena in FSI at $x \ll 0.1$ will be considered in a separate study [21]). This intermediate region is of prime interest for the study of sea quarks and gluons and their nuclear modifications. We use our model to estimate the magnitude and kinematic dependence of the FSI effects, demonstrate their analytic properties, and study the implications for neutron structure extraction through on-shell extrapolation.

Our treatment is based on a definite physical picture of FSI at intermediate x. The DIS process on the nucleon with momentum transfers $|\boldsymbol{q}| \gg 1\,{\rm GeV}$ (in the deuteron rest frame) produces a broad spectrum of hadrons, ranging in momenta from $|\boldsymbol{p}_h| \sim |\boldsymbol{q}|$ to $|\boldsymbol{p}_h| \lesssim 1\,{\rm GeV}$. The "fast" part of the nucleon DIS final state does not interact strongly with the spectator nucleons in the nucleus. This assertion is supported by empirical and theoretical arguments. Nuclear DIS data show that fast hadrons with $|\boldsymbol{p}_h| \gg 1\,{\rm GeV}$ are not substantially attenuated in nuclei [22–27]; the soft neutron spectra produced by nuclear breakup in DIS likewise indicate the absence of strong FSI [25, 28]. Theoretical estimates of the hadron formation time show that such fast hadrons form mainly outside of the nucleus and cannot interact with hadronic cross sections; see Section 5.10 of Ref. [5] for an overview. The dominant FSI in tagged DIS on the deuteron therefore comes from "slow" hadrons with $|\boldsymbol{p}_h| \lesssim 1\,{\rm GeV}$ in the nucleon DIS final state. Such hadrons are formed inside the nucleus and can interact with the spectator with hadronic cross sections (see Fig. 1). In the terminology of DIS, the "fast" and "slow" part of the DIS final state on the nucleon correspond to the current and target fragmentation regions (see Sec. V). We note that the physical picture of FSI proposed here is consistent with the general QCD factorization theorem for target fragmentation in DIS, which is a rigorous asymptotic result and holds irrespective of the type of target (nucleon or nucleus) [29, 30]. FSI of the "fast" DIS hadrons with the nuclear remnant would amount to a violation of factorization for the nuclear target in the asymptotic regime. In contrast, FSI of the "slow" DIS hadrons with the nuclear remnant represent a particular soft-interaction contribution to the nuclear fracture function that is allowed by the factorization theorem.

We express this physical picture of FSI in a schematic model. We calculate the tagged DIS cross section on the

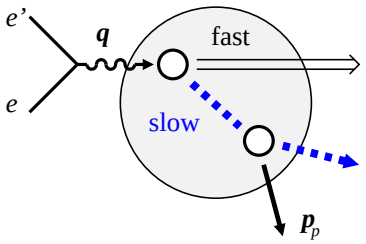

FIG. 1. Physical picture of FSI in electron–deuteron DIS with proton tagging, $e + d \to e' + p(p_p) + X$, in the deuteron rest frame. A slow hadron in the final state produced by DIS on the active neutron scatters from the spectator proton, changing its momentum compared to the IA. The fast component of the DIS final state does not interact strongly with the spectator.

deuteron using LF quantum mechanics, including the IA and FSI amplitudes. We use empirical hadron distributions, measured in ep/ed DIS, to describe the slow part of the hadronic final state produced on the nucleon in the deuteron. The interactions of the slow hadrons with the spectator are treated as on-shell scattering with an effective cross section. Off-shell effects can be absorbed into the effective cross section and the slow hadron distribution; they are physically indistinguishable from effects of the finite hadron formation time and can consistently be accounted for in this way. This model amounts to a minimal description of FSI based on the space-time evolution of the DIS process and empirical hadron distributions.

In the present study we use the apparatus of LF quantum mechanics to describe the initial-state nuclear structure and final-state interactions in tagged DIS. High-energy processes such as DIS effectively probe a strongly interacting system at fixed LF time $x^+ = x^0 + x^3$, along the direction defined by the reaction axis. In LF quantization one follows the time evolution of the system in x^+ and describes its structure by wave functions and densities at $x^+ =$ const. [31–35]. The scheme is unique in that it permits a composite description in which effects of the off-shellness of the constituents remain finite as the scattering energy becomes large [11]. It makes possible a composite description of nuclear structure in DIS in terms of nucleon degrees of freedom, which exhibits a close correspondence with non-relativistic nuclear structure (NN interactions, wave functions), satisfies sum rules (baryon number, LF momentum), and enables a smooth matching with nucleon structure (parton picture, QCD degrees of freedom) [1, 11]. It is important to understand that the structure thus described is "low-energy" nuclear structure, governed by interactions and degrees of freedom on the nuclear scale; it is only presented in a way that is appropriate for the initial state of high-energy processes. The application of LF quantum mechanics to nuclear high-energy processes is described in detail in Refs. [1, 11]; the elements used in the present calculation are summarized below.

Conservation of baryon number and LF momentum is an important consideration in describing nuclear DIS. The LF IA for the inclusive DIS structure functions correctly implements the baryon number and momentum sum rules for the deuteron, i.e., the baryon numbers of the p and n add up to the total baryon number of the deuteron when integrating over all configurations in the wave function, and the LF "plus" momenta of the p and n add up to the total momentum of the deuteron [11]. It means that at this level there are no non-nucleonic degrees of freedom and ensures that, when the nucleons are resolved into partons, the partonic sum rules for the deuteron are satisfied. In the tagged DIS structure functions one recovers these sum rules when integrating over the spectator recoil momentum. FSI in tagged DIS may distort the recoil momentum distribution but should not modify the sum rules for the recoil momentum–integrated structure functions. In our picture this can be accomplished by modeling the slow hadron–nucleon rescattering process as elastic scattering (no additional hadrons are produced) and implementing unitarity of the rescattering amplitude. In this sense our model of FSI in tagged DIS preserves the baryon number and momentum sum rules and is consistent with the standard LF treatment of the inclusive DIS structure functions.

The plan of the article is as follows. In Sec. II we present the kinematic variables and invariant structure functions in tagged DIS, introduce the collinear frame used in the LF description, and discuss the recoil momentum variables. In Sec. III we summarize the elements of LF quantum mechanics used in our calculations — the single-nucleon states, the deuteron LF wave function, and its rotationally symmetric representation. In Sec. IV we calculate the tagged DIS cross section in the IA and study its properties. We discuss the LF current components, compute the IA current and structure functions, introduce the LF spectral function, and discuss the non-relativistic limit and the analytic properties in t. In Sec. V we discuss the slow hadron distribution in DIS on the nucleon — the kinematic variables, structure functions, and the features of empirical distributions. In Sec. VI we calculate the FSI effects in tagged DIS in LF quantum mechanics and study their properties. The FSI effects are expressed in terms of a distorted spectral function. We formulate a factorized approximation using the fact that the range of the rescattering interaction is small compared to the deuteron size. We demonstrate the positivity of the cross section, investigate the recoil momentum dependence of the FSI effects, and discuss the analytic properties of the distorted spectral function. We also comment

on the role of unitarity of the rescattering process and the implementation of sum rules for the LF spectral function with FSI. In Sec. VII we discuss the strategy for neutron structure measurements in tagged DIS with EIC. A summary and outlook are given in Sec. VIII.

Technical material needed to reproduce the calculations is summarized in appendices. Appendix A describes a simple two-pole parametrization of the deuteron wave function with correct analytic properties, which we use in the numerical calculations. Appendix B contains the projection formulas for extracting the tagged structure functions from the deuteron tensor in the IA and with FSI. Appendix C summarizes our parametrization of the nucleon-nucleon cross section used in the numerical estimates of FSI effects. Appendix D describes the evaluation of the rescattering phase-space integral in LF coordinates.

The physical picture of FSI in tagged DIS proposed here is specific to the region of intermediate x as defined above, and our model should be used in this context only. In tagged DIS in the limit $x \to 1$ the minimal rest-frame momentum of the "slow" hadrons produced on the nucleon becomes large, as their LF momentum fractions are bounded by $1 - x$, and the interactions are suppressed by the hadron formation time (see Fig. 1). The framework developed in the present work could be extended to this region when supplied with empirical information about the formation time effects. (The work of Refs. [36–38] considers tagged DIS at large x in a subasymptotic domain of fixed energy and momentum transfer, where the limit $x \to 1$ corresponds to a small inelasticity $W^2 - M_N^2$, and the DIS final state is modeled as a superposition of baryonic resonances; this formulation is different from the asymptotic one presented here and not appropriate for collider energies.) In tagged DIS at small x ($\ll 0.01$), diffractive scattering on the nucleon becomes significant and gives rise to a new mechanism of FSI. In diffractive scattering the nucleon appears intact in the final state and recoils with a momentum $p_p \sim$ few 100 MeV. Because the diffractive nucleon retains its quantum numbers ("vacuum exchange") and emerges with a small recoil momentum, there is a significant amplitude for the final-state pn system to revert back to a deuteron bound state. In tagged DIS in this kinematics the outgoing pn scattering state must be properly orthogonalized to the deuteron bound state, which results in significant distortion. This new mechanism of FSI in tagged DIS on the deuteron at small x is closely related to shadowing in inclusive DIS and will be discussed elsewhere [21].

In the present work we consider unpolarized electron–deuteron DIS and calculate the FSI effects in the tagged cross section integrated over the azimuthal angle of the recoil momentum, as relevant for the extraction of the neutron structure functions F_{2n} and F_{Ln}. The extension to polarized electron-deuteron DIS with spectator tagging and azimuthal angle–dependent response functions will be left to a future study, as the number of structures in the cross section becomes very considerable [39]. A proper treatment of FSI in the polarized deuteron would require also empirical information on the spin dependence of the slow DIS hadron distributions, which is not available at present. We note that the schematic model of FSI proposed here could be applied also to the time–reversal–odd (T–odd) response functions in tagged DIS, which are zero in the IA and can be used for sensitive tests of the FSI dynamics.

To simplify the presentation we suppress the internal spin structure of the deuteron and present the IA and FSI expressions for an S–wave bound state. This allows us to leave aside for the moment the complications resulting from the treatment of spin in LF quantum mechanics (Melosh rotations, angular conditions) and focus on the aspects essential to FSI. The resulting expressions are a good approximation at recoil proton momenta $|\boldsymbol{p}_p| < 200\,\mathrm{MeV}$, where the S–wave dominates in the deuteron's nonrelativistic momentum density (see below), and which are of prime interest for neutron structure extraction. The expressions for the IA and FSI cross sections derived here can easily be generalized to account for the deuteron spin structure, by including the summation over LF helicity components [40].

FSI effects in DIS from nuclei and their kinematic dependence were studied in Refs. [41–44] using a detailed microscopic model of hadron production in DIS (string breaking, gluon radiation). In contrast to these studies we use a simple generic description of hadron production and consider specifically the region of intermediate x. FSI effects have also been studied extensively in quasi-elastic scattering from nuclei, including deuteron electrodisintegration $e + d \to e' + p + n$ [45]; see Ref. [46] for a review. There is an interesting formal analogy between FSI in quasi-elastic deuteron breakup at ∼1–2 GeV incident momenta and our picture of slow-hadron rescattering in DIS, and one can establish the correspondence between the formulas.

II. TAGGED DIS KINEMATICS

A. Kinematic variables

We begin by summarizing the kinematic variables and cross section formulas for inclusive electron scattering on the deuteron with an identified nucleon in the final state ("tagged DIS"). The kinematic factors are given in their exact form (no simplifications are made using the DIS limit) and expressed in terms of relativistic invariants, as suitable for collider experiments. The cross section formulas given in this section are general and make no assumption regarding composite nuclear structure; particular results based on such approximations will be presented in Secs. IV and VI.

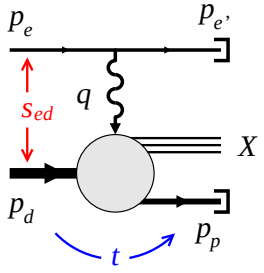

FIG. 2. Inclusive electron scattering from the deuteron with an identified proton in the deuteron fragmentation region, $e + d \to e' + p + X$ ("tagged DIS").

To be specific we consider the case that the identified nucleon is a proton; equivalent formulas can be written for the case of an identified neutron. Thus, we consider the scattering process (see Fig. 2)

$$e(p_e) + d(p_d) \to e'(p_{e'}) + p(p_p) + X, \tag{2.1}$$

where X denotes an unresolved hadronic final state. Here p_e and $p_{e'}$ are the 4–momenta of the initial and final electron, p_d is the 4–momentum of the deuteron, and p_p is the 4–momentum of the identified proton. The 4–momentum transfer to the nuclear system, calculated from the initial and final electron 4–momenta, is

$$q \equiv p_e - p_{e'}, \qquad Q^2 \equiv -q^2 > 0. \tag{2.2}$$

Invariants formed from the electron and deuteron 4–momenta are

$$s_{ed} = (p_e + p_d)^2, \tag{2.3}$$

$$W_d^2 = (q + p_d)^2, \tag{2.4}$$

which describe, respectively, the electron–deuteron and the virtual photon–deuteron squared CM energies. Useful scaling variables are

$$x_d \equiv \frac{-q^2}{2(p_d q)} = \frac{Q^2}{W_d^2 - M_d^2 + Q^2}, \tag{2.5}$$

$$y \equiv \frac{(p_d q)}{(p_d k)} = \frac{Q^2}{x_d(s_{ed} - M_d^2)}. \tag{2.6}$$

The variable x_d is the Bjorken variable for the nuclear target ($0 < x_d < 1$) and will be used in the kinematic formulas for the cross section, to facilitate comparison with the standard expressions for electron–proton scattering. In the description of composite deuteron structure we shall use the alternative variable

$$x \equiv 2x_d \qquad (0 < x < 2), \tag{2.7}$$

which corresponds to the effective Bjorken variable for scattering from a nucleon in the unbound nucleus (deuteron). The variable y describes the electron's fractional energy loss (or inelasticity) in the deuteron rest frame. The invariants and scaling variables formed with the recoil nucleon momentum p_p will be presented in Sec. II D below.

B. Cross section and structure functions

The invariant amplitude for the electroproduction of a final state $p + X$, including the detected proton p and a specified set of hadrons X, is in leading order of the electromagnetic coupling given by

$$\mathcal{M}[ed \to e'pX] = \frac{e^2}{q^2} \langle e', \boldsymbol{p}_{e'} | \hat{J}^\mu(0) | e, \boldsymbol{p}_e \rangle \, \langle p, \boldsymbol{p}_p; X | \hat{J}^\mu(0) | d, \boldsymbol{p}_d \rangle, \tag{2.8}$$

where e is the elementary charge, and the brackets denote the transition matrix elements of the electromagnetic 4–vector current $\hat{J}^\mu(0)$ between the initial and final electron and nuclear/hadronic states. All particle states (electron, deuteron, nucleon) are normalized according to the relativistic convention

$$\langle e, \boldsymbol{p}_{e2} | e, \boldsymbol{p}_{e1} \rangle = (2\pi)^3 \, 2E_e(\boldsymbol{p}_{e1}) \, \delta^{(3)}(\boldsymbol{p}_{e2} - \boldsymbol{p}_{e1}), \qquad \text{etc.} \tag{2.9}$$

The spin quantum numbers of the states are suppressed for brevity and will be specified below. The differential cross section for production of the specified hadronic state is [47]

$$d\sigma[ed \to e'pX] \;=\; (2\pi)^4\delta^{(4)}(p_e + p_d - p_{e'} - p_p - p_h)\;\frac{|\mathcal{M}|^2}{4I}\;d\Gamma_{e'}\;d\Gamma_p\;d\Gamma_X. \tag{2.10}$$

The invariant incident particle current is defined as (we neglect the electron mass)

$$I \equiv \sqrt{(p_e p_d)^2} \;\equiv\; \tfrac{1}{2}(s_{ed} - M_d^2). \tag{2.11}$$

The invariant phase space elements of the scattered electron and the identified proton are

$$d\Gamma_{e'} \;\equiv\; \frac{d^3p_{e'}}{(2\pi)^3 2E_{e'}}, \qquad E_{e'} \;=\; |\boldsymbol{p}_{e'}|, \tag{2.12}$$

$$d\Gamma_p \;\equiv\; \frac{d^3p_p}{(2\pi)^3 2E_p}, \qquad E_p \;=\; \sqrt{|\boldsymbol{p}_p|^2 + M_N^2}. \tag{2.13}$$

The phase space element of the multi–hadron state X can be defined analogously in terms of the hadron momenta, but its explicit form is not needed in the following. The cross section for tagged inclusive scattering is then given by integrating Eq. (2.10) over the phase space of the unidentified hadron state X and summing over all such states (we denote both operations together symbolically by $\sum_X$),

$$d\sigma[ed \to e'pX] \;=\; \sum_X (2\pi)^4\delta^{(4)}(p_e + p_d - p_{e'} - p_p - p_X)\;\frac{|\mathcal{M}|^2}{4I}\;d\Gamma_{e'}\;d\Gamma_p \tag{2.14}$$

$$\;=\; \frac{4\pi e^4}{4I(-q^2)^2}\;w_{\mu\nu}W_d^{\mu\nu}\;d\Gamma_{e'}\;d\Gamma_p. \tag{2.15}$$

The leptonic tensor is defined as

$$w^{\mu\nu} \;\equiv\; w^{\mu\nu}(p_{e'}, p_e) \;=\; \langle e', \boldsymbol{p}_{e'}|\hat{J}^\mu(0)|e, \boldsymbol{p}_e\rangle^*\;\langle e', \boldsymbol{p}_{e'}|\hat{J}^\nu(0)|e, \boldsymbol{p}_e\rangle. \tag{2.16}$$

In the case of scattering of an unpolarized electron beam (average over initial helicities) and unspecified polarization of the final electron (sum over final helicities) its explicit form is

$$w^{\mu\nu} \;=\; 4p_e^\mu p_e^\nu + q^2 g^{\mu\nu} \;+\; \text{terms} \propto q^\mu, q^\nu \tag{2.17}$$

The deuteron tensor is defined as (using $q = p_e - p_{e'}$)

$$W_d^{\mu\nu} \equiv W_d^{\mu\nu}(p_d, q, p_p)$$

$$= (4\pi)^{-1}\sum_X (2\pi)^4\;\delta^{(4)}(q + p_d - p_p - p_X)\;\langle pX|\hat{J}^\mu(0)|d\rangle^*\;\langle pX|\hat{J}^\nu(0)|d\rangle \tag{2.18}$$

$$= (4\pi)^{-1}\sum_h (2\pi)^4\;\delta^{(4)}(q + p_d - p_p - p_X)\;\langle d|\hat{J}^{\mu\dagger}(0)|pX\rangle\;\langle pX|\hat{J}^\nu(0)|d\rangle, \tag{2.19}$$

in which $J^{\mu\dagger} = J^\mu$ (hermiticity of the electromagnetic current operator). It obeys the transversality conditions $q_\mu W_d^{\mu\nu} = 0$ and $W_d^{\mu\nu}q_\nu = 0$ and can be expanded in tensors constructed from the 4–vectors p_d, q and p_p, and the invariant tensor $g^{\mu\nu}$. It is convenient to introduce the auxiliary 4–vectors

$$L^\mu \equiv p_d^\mu - \frac{(p_d q)q^\mu}{q^2}, \qquad (qL) \;=\; 0, \qquad L^2 \;>\; 0, \tag{2.20}$$

$$T^\mu \equiv p_p^\mu - \frac{(p_p q)q^\mu}{q^2} - \frac{(p_p L)L^\mu}{L^2}, \qquad (qT) \;=\; 0, \quad (LT) \;=\; 0, \qquad T^2 \;<\; 0. \tag{2.21}$$

Their particular meaning in a frame where p_d and q are collinear is explained in Sec. II C. We decompose the deuteron tensor as

$$W_d^{\mu\nu} = \left(g^{\mu\nu} - \frac{q^\mu q^\nu}{q^2}\right)\frac{F_{Ld}}{2} \;+\; \left(\frac{L^\mu L^\nu}{L^2} + \frac{q^\mu q^\nu}{q^2} - g^{\mu\nu}\right)\frac{F_{Td}}{2}$$

$$+\; \frac{T^\mu L^\nu + L^\mu T^\nu}{\sqrt{-T^2}\sqrt{L^2}}\;\frac{F_{LT,d}}{2} \;+\; \left(g^{\mu\nu} - \frac{L^\mu L^\nu}{L^2} - \frac{q^\mu q^\nu}{q^2} - \frac{2T^\mu T^\nu}{T^2}\right)\frac{F_{TT,d}}{2} \tag{2.22}$$

Here $F_{Ld}, F_{Td}, F_{LT,d}$ and $F_{TT,d}$ are invariant structure functions, depending on the kinematic invariants formed from the vectors q, p_d and p_p. The first and second tensor structures in Eq. (2.22) do not involve the identified proton momentum p_p are are present also in untagged (fully inclusive) scattering. Our definition of the longitudinal and transverse structure functions, F_{Ld} and F_{Td}, is identical to that of Ref. [48]. Their relation to the conventional functions F_{1d} and F_{2d} is

$$F_{Td} \;=\; \frac{(-q^2)L^2}{(p_d q)^2}\,\frac{F_{2d}}{x_d} \;=\; \left(1+\frac{4x_d^2M_d^2}{Q^2}\right)\,\frac{F_{2d}}{x_d}, \tag{2.23}$$

$$F_{Ld} \;=\; \frac{(-q^2)L^2}{(p_d q)^2}\,\frac{F_{2d}}{x_d} - 2F_{1d} \;=\; \frac{1}{x_d}\left[\left(1+\frac{4x_d^2M_d^2}{Q^2}\right)F_{2d} - 2x_d F_{1d}\right], \tag{2.24}$$

$$F_{Td} - F_{Ld} \;=\; 2F_{1d}. \tag{2.25}$$

The third and fourth tensor structures in Eq. (2.22) vanish when averaging over the orientation of the vector T in the plane orthogonal to L and q and are present only for fixed momentum p_p.

The contraction of the leptonic and deuteron tensors can be expressed in terms of the parameter

$$\epsilon \;\equiv\; \frac{w_{\mu\nu}\dfrac{L^\mu L^\nu}{L^2}}{w_{\mu\nu}\left(\dfrac{L^\mu L^\nu}{L^2}+\dfrac{q^\mu q^\nu}{q^2}-g^{\mu\nu}\right)} \;=\; \frac{1-y-\dfrac{x_d^2y^2M_d^2}{Q^2}}{1-y+y^2/2+\dfrac{x_d^2y^2M_d^2}{Q^2}}, \tag{2.26}$$

which can be interpreted as the ratio of the probabilities of longitudinal and transverse polarization of the virtual photon. To express the contractions of the p_p–dependent tensor structures in invariant form we expand the initial electron momentum as

$$p_e = \frac{(p_e L)L}{L^2} + \frac{(p_e q)q}{q^2} + \Delta, \qquad (\Delta L) \;=\; 0, \qquad (\Delta q) \;=\; 0, \tag{2.27}$$

$$(p_e T) = (\Delta T) \;=\; \sqrt{-\Delta^2}\sqrt{-T^2}\,\cos\phi_p. \tag{2.28}$$

The particular meaning of the angle ϕ_p in a collinear frame is described in Sec. II C. We obtain

$$w_{\mu\nu}W^{\mu\nu} \;=\; \frac{Q^2}{1-\epsilon}\left[\frac{1+\epsilon}{1-\epsilon}\,\frac{y^2}{(2-y)^2}\,F_{Td} \;-\; (1-\epsilon)\,F_{Ld} + \sqrt{2\epsilon(1+\epsilon)}\,\cos\phi_p\,F_{LT,d} \;+\; \epsilon\,\cos(2\phi_p)\,F_{TT,d}\right] \tag{2.29}$$

$$\;=\; \frac{Q^2}{1-\epsilon}\left[\frac{F_{2d}}{x_d} \;-\; (1-\epsilon)\,F_{Ld} \;+\; \ldots\right]. \tag{2.30}$$

The scattered electron phase space element can easily be expressed in terms of the invariants x_d and Q^2 and the azimuthal angle around the incident electron momentum direction, $\phi_{e'}$. Altogether, the differential cross section for tagged inclusive scattering with unpolarized beams and recoil nucleon, Eq. (2.15), becomes

$$\begin{aligned} d\sigma[ed\to e'pX] \;&=\; \frac{2\pi\alpha_{\rm em}^2 y^2}{Q^4(1-\epsilon)}\,dx_d\,dQ^2\,\frac{d\phi_{e'}}{2\pi} \\ &\times\; \left[\frac{F_{2d}}{x_d} \;-\; (1-\epsilon)F_{Ld} \;+\; \sqrt{2\epsilon(1+\epsilon)}\cos\phi_p F_{LT,d} \;+\; \epsilon\cos(2\phi_p)F_{TT,d}\right]\,d\Gamma_p, \end{aligned} \tag{2.31}$$

where $\alpha_{\rm em} \equiv e^2/(4\pi) \approx 1/137$ is the fine structure constant. The last two terms in the bracket drop out when the cross section is integrated over the recoil azimuthal angle ϕ_p. Specific forms of the recoil momentum phase space element are described in Sec. II D.

C. Collinear frames

In the theoretical description of tagged DIS we consider the process Eq. (2.1) in a frame where the deuteron momentum $\boldsymbol{p}_d$ and the momentum transfer $\boldsymbol{q}$ are collinear and define the z–axis of the coordinate system. This condition does not specify a unique frame, but rather a class of frames that are related by boosts along the z–axis ("collinear frames"). We specify the 4–momenta in this frame by their LF components

$$p^\pm \;\equiv\; p^0 \pm p^z, \qquad \boldsymbol{p}_T \;\equiv\; (p^x, p^y). \tag{2.32}$$

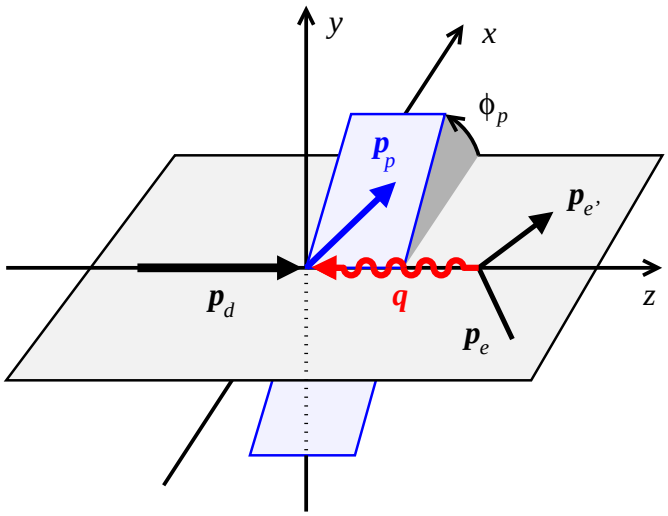

FIG. 3. Tagged DIS in the collinear frame, Eq. (2.33). The deuteron momentum p_d and the vector q are collinear and define the z–axis, with q pointing in the negative z–direction. The initial and final electron momenta lie in the xz plane and have positive x component. ϕ_p is the angle of the transverse (xy) component of the recoil momentum, measured relative to the positive x axis.

The LF components of p_d and q in the collinear frame are

$$\left.\begin{array}{lll} p_d^+ > 0 \ \text{(arbitrary)}, & p_d^- = \dfrac{M_d^2}{p_d^+}, & \boldsymbol{p}_{dT} = 0, \\ q^+ = -\xi_d p_d^+, & q^- = \dfrac{q^2}{q^+} = \dfrac{Q^2}{\xi_d p_d^+}, & \boldsymbol{q}_T = 0. \end{array}\right\} \tag{2.33}$$

The parameter ξ_d is fixed by the condition

$$2p_d q = p_d^+ q^- + p_d^- q^+ = \frac{Q^2}{x_d}, \tag{2.34}$$

the solution of which is

$$\xi_d = \frac{2x_d}{1 \pm \sqrt{1 + 4M_d^2 x_d^2/Q^2}} \qquad \text{(choose +)}. \tag{2.35}$$

We select the solution with the plus sign, which has the property that in the scaling limit $Q^2 \gg M_d^2$

$$\xi_d = x_d + O(M_d^2/Q^2). \tag{2.36}$$

With this choice the momentum transfer vector $\boldsymbol{q}$ points in the *negative* z–direction (see Fig. 3),

$$2q^z = q^+ - q^- = -\xi_d p_d^+ - \frac{Q^2}{\xi_d p_d^+} < 0. \tag{2.37}$$

The LF components of the longitudinal auxiliary 4–vectors L and T, Eqs. (2.20) and (2.21), are obtained as

$$\left.\begin{array}{lll} L^+ = \left(1 - \dfrac{\xi_d}{2x_d}\right) p_d^+, & L^- = \left(M_d^2 + \dfrac{Q^2}{\xi_d}\right) \dfrac{1}{p_d^+}, & \boldsymbol{L}_T = 0, \\ T^+ = 0, & T^- = 0, & \boldsymbol{T}_T = \boldsymbol{p}_{pT}. \end{array}\right\} \tag{2.38}$$

The vector L has only collinear components, while T has only transverse components and coincides with the recoil hadron transverse momentum in the collinear frame. Because the momentum transfer $\boldsymbol{q}$ is along the (negative) z–direction, the initial and final electron momenta have the same transverse components,

$$\boldsymbol{p}_{eT} = \boldsymbol{p}_{e'T} \qquad \text{(collinear frame)}, \tag{2.39}$$

such that they define a plane together with the z–axis (electron scattering plane). The recoil angle ϕ_p, defined in terms of invariants in Eq. (2.28), then is the azimuthal angle of $\boldsymbol{p}_p$, measured relative to the electron scattering plane. It is conventional to choose the electron transverse momenta in the x–direction, such that the electron scattering plane is defined by the xz plane. In this case the angle ϕ_p becomes the conventional azimuthal angle of $\boldsymbol{p}_p$ in the xy plane, $\cos\phi_p = p_p^x/|\boldsymbol{p}_{pT}|$ (see Fig. 3).

The deuteron plus momentum $p_d^+ > 0$ in the above formulas remains arbitrary and defines a particular member of the class of collinear frames. Longitudinal boosts (along the z–axis) can be performed simply by changing the value of p_d^+ in the above formulas. Note that the class of collinear frames contains several special cases of interest: (a) the target rest frame, $p_d^+ = M_d$; (b) the Breit frame, $p_d^+ = \sqrt{Q^2}/\xi_d$, in which $q^0 = (q^+ + q^-)/2 = 0$; (c) the center-of-mass frame of the virtual photon and the deuteron, $p_d^+ = \sqrt{Q^2 + \xi_d M_d^2}/\sqrt{\xi_d(1-\xi_d)}$, in which $q^z = (q^+ - q^-)/2 = -p_d^z = -(p_d^+ - p_d^-)/2$ and thus $\boldsymbol{q} = -\boldsymbol{p}_d$. For reference we note that the collinear frames used here are equivalent to the covariant formulation of the collinear expansion in terms of light–like vectors of Ref. [48].

D. Recoil momentum variables

The tagged structure functions of the deuteron in Eq. (2.22) depend on the usual DIS variables (e.g. W_d and Q^2) as well as the recoil nucleon momentum. The latter dependence involves two independent variables formed from p_p, related to the two invariants $(p_p p_d)$ and $(p_p q)$; the dependence on the third invariant $(p_p p_e)$ is encoded in the explicit ϕ_p dependence of the cross section. Here we describe several physically interesting choices of recoil momentum variables that are used in the subsequent calculations. We present their relation to the rest–frame recoil momentum, their kinematic limits, and the corresponding phase space elements. We assume isospin symmetry and define the nucleon mass as the average of the proton and neutron masses

$$M_N = (M_p + M_n)/2 \;=\; 0.9389\,\mathrm{GeV}. \tag{2.40}$$

The deuteron binding energy and mass are taken at their exact values

$$\epsilon_d \;=\; 2.2\,\mathrm{MeV}, \qquad M_d \;=\; M_p + M_n - \epsilon_d \;=\; 2M_N - \epsilon_d \;=\; 1.8756\,\mathrm{GeV}. \tag{2.41}$$

Note that the relation between the deuteron binding energy and mass is not affected when replacing the proton and neutron masses by their average.

In a collinear frame defined by Eqs. (2.33) the tagged structure functions can be regarded as functions of the LF plus momentum fraction of the recoil proton and the transverse momentum modulus of the recoil momentum,

$$\alpha_p \;\equiv\; \frac{2p_p^+}{p_d^+} \;=\; \frac{2(p_p^0 + p_p^z)}{p_d^0 + p_d^z}, \tag{2.42}$$

$$|\boldsymbol{p}_{pT}| \;\equiv\; \sqrt{(p_p^x)^2 + (p_p^y)^2}. \tag{2.43}$$

The definition of α_p in Eq.(2.42), as the fraction relative to $p_d^+/2$, is natural and leads to simple expressions in the nuclear structure calculations below. The kinematic limits of α_p are dictated by LF plus momentum conservation in the scattering process and given by

$$\alpha_p/2 \;<\; 1 - \xi_d. \tag{2.44}$$

The invariant phase space element in terms of α_p and $|\boldsymbol{p}_{pT}|$ takes the form

$$\frac{d^3p_p}{E_p} \;=\; \frac{d\alpha_p}{\alpha_p}\, d^2p_{pT}. \tag{2.45}$$

An important variable is the invariant momentum transfer between the initial–state deuteron and the final–state nucleon (see Fig. 2),

$$t \;\equiv\; (p_p - p_d)^2, \tag{2.46}$$

or the reduced variable

$$t' \;\equiv\; t - M_N^2. \tag{2.47}$$

The theoretical analysis of tagged DIS Eq. (2.1) relies essentially on the analytic properties of the cross section in t'; see Secs. IV and VI below. The invariant t' is related in a simple manner to the energy of the recoiling nucleon in the deuteron rest frame (we use "RF" to denote rest-frame energy and momentum),

$$t' \;=\; M_d^2 - 2M_d E_p(\mathrm{RF}), \qquad [E_p(\mathrm{RF}) \equiv \sqrt{|\boldsymbol{p}_p(\mathrm{RF})|^2 + M_N^2}]. \tag{2.48}$$

The kinematic limit of t' is attained at $\boldsymbol{p}_p(\mathrm{RF}) = 0$,

$$t' \;<\; t'_{\min} \;\equiv\; M_d^2 - 2M_d M_N \;=\; -M_d\epsilon_d \;=\; -0.0041\,\mathrm{GeV}^2. \tag{2.49}$$

Inside the physical region the rest–frame momentum is obtained from t' as

$$|\boldsymbol{p}_p(\mathrm{RF})|^2 = -\frac{t'}{2}\left(1 - \frac{t'}{2M_d^2}\right) \;+\; \frac{M_d^2}{4} - M_N^2. \tag{2.50}$$

A simpler relation is obtained if we neglect the $t'/(2M_d^2)$ term in the parenthesis; this approximation is well justified for typical values $|t'| \sim 0.1\,\mathrm{GeV}^2$ and becomes exact in the limit $t' \to 0$. Namely,

$$|\boldsymbol{p}_p(\mathrm{RF})|^2 \;\approx\; -\frac{t'}{2} \;+\; \frac{M_d^2}{4} - M_N^2 \;=\; -\frac{t'}{2} \;+\; \frac{t'_0}{2}, \tag{2.51}$$

$$t'_0 \;\equiv\; \frac{M_d^2}{2} - 2M_N^2 \;=\; -M_d\epsilon_d \;-\; \frac{\epsilon_d^2}{2} \;=\; -2M_N\epsilon_d \;+\; \frac{\epsilon_d^2}{2} \;=\; t'_{\min} \;+\; O(\epsilon_d^2). \tag{2.52}$$

The difference between t'_0 and the exact $t'_{\min}$, Eq. (2.49), is of the order $10^{-6}\,\mathrm{GeV}^2$ and negligible for all practical purposes. In this approximation the invariant t' is the negative of twice the squared rest frame recoil momentum, minus a fixed small amount proportional to the deuteron binding energy,

$$t' \;\approx\; -2\,|\boldsymbol{p}_p(\mathrm{RF})|^2 \;+\; t'_0. \tag{2.53}$$

The relation of the invariant t' to the collinear variables α_p and $|\boldsymbol{p}_{pT}|$ can easily be established using the fact that the deuteron rest frame is a special collinear frame ($p_d^+ = M_d$). Thus the rest-frame energy and z–momentum can be calculated in terms of the plus and minus LF components as

$$\left.\begin{matrix} E_p(\mathrm{RF}) \\ p_p^z(\mathrm{RF}) \end{matrix}\right\} \;=\; \frac{p_p^+ \pm p_p^-}{2} \;=\; \frac{\alpha_p M_d}{4} \pm \frac{|\boldsymbol{p}_{pT}|^2 + M_N^2}{\alpha_p M_d}, \tag{2.54}$$

and t' can be obtained from the above rest-frame formulas. Specifically, with Eq. (2.53) we obtain

$$t' \;=\; -2\,\left[|p_p^z(\mathrm{RF})|^2 \;+\; |\boldsymbol{p}_{pT}|^2\right] \;+\; t'_0. \tag{2.55}$$

In the theoretical analysis below we use a representation in which α_p and t' are independent variables. The physical region in these variables can easily be established from Eq. (2.55). For a given α_p the kinematic limit in t' is found by minimizing Eq. (2.55) with respect to $|\boldsymbol{p}_{pT}|$ and given by (see Fig. 4)

$$t' \;<\; -\frac{2M_d^2}{\alpha_p^2}\left(\frac{\alpha_p^2}{4} - \frac{M_N^2}{M_d^2}\right) \;+\; t'_0. \tag{2.56}$$

One sees that the minimum value of $-t'$ increases quadratically as α_p moves away from $2M_N/M_d \approx 1$. Conversely, for a given $t' < t'_0$ the allowed values of α_p are

$$\alpha_1 \;<\; \alpha_p \;<\; \alpha_2, \tag{2.57}$$

$$\alpha_{1,2} \;=\; \frac{2}{M_d}\left[E_p(\mathrm{RF}) \mp |\boldsymbol{p}_p(\mathrm{RF})|\right] \;=\; \frac{2}{M_d}\left[\sqrt{\frac{t'_0 - t'}{2} + M_N^2} \;\mp\; \sqrt{\frac{t'_0 - t'}{2}}\right]. \tag{2.58}$$

The invariant phase space element in this representation is given by [cf. Eq. (2.48)]

$$\frac{d^3p_p}{E_p} = \frac{M_d}{8E_p(\mathrm{RF})}\; d(-t')\; d\alpha_p\; d\phi_p, \tag{2.59}$$

$$E_p(\mathrm{RF}) = \sqrt{|\boldsymbol{p}_p(\mathrm{RF})|^2 + M_N^2} \;=\; \sqrt{\frac{t'_0 - t'}{2} + M_N^2}. \tag{2.60}$$

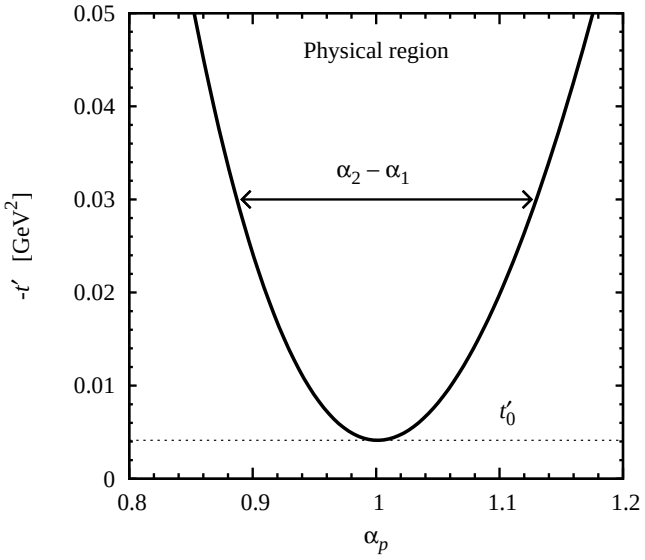

FIG. 4. Physical region of recoil proton momentum phase space in the variables α_p and t'.

Another physically interesting variable is the angle of the recoil momentum in the deuteron rest frame,

$$\cos\theta_p \;\; = \frac{p_p^z(\mathrm{RF})}{|\boldsymbol{p}_p(\mathrm{RF})|}. \tag{2.61}$$

For a given modulus $|\boldsymbol{p}_p(\mathrm{RF})|$ the angle is related to the LF fraction α_p as

$$\alpha_p \;\; = \;\; \frac{2}{M_d}\left(\sqrt{|\boldsymbol{p}_p(\mathrm{RF})|^2 + M_N^2} \;+\; |\boldsymbol{p}_p(\mathrm{RF})|\cos\theta_p\right). \tag{2.62}$$

The physical region for the angle θ_p is determined by the condition that $0 < \alpha_p < 2$, which implies

$$-1 \;\; < \;\; \cos\theta_p \;\; < \;\; \frac{M_d - \sqrt{|\boldsymbol{p}_p(\mathrm{RF})|^2 + M_N^2}}{|\boldsymbol{p}_p(\mathrm{RF})|} \tag{2.63}$$

The upper limit becomes less than unity only at $|\boldsymbol{p}_p(\mathrm{RF})| > (M_d^2 - M_N^2)/(2M_d) \approx 3M_N/4$, which is much larger than the recoil momenta considered here, so that effectively all angles are allowed in our kinematics.

III. LIGHT-FRONT QUANTUM MECHANICS

A. Single–nucleon states

In our theoretical calculations of the tagged DIS cross section we use methods of LF quantum mechanics. They permit a composite description of nuclear structure in high-energy processes in terms of nucleon degrees of freedom, which can be matched with deep-inelastic nucleon structure and preserves the partonic sum rules [1, 11]. In this section we summarize the description of nucleon single-particle states and the deuteron bound state in LF quantum mechanics and the correspondence with the non-relativistic theory of the deuteron. The LF quantization axis chosen as the z–axis in the collinear frame of Sec. II C. The specific dynamical considerations in the application to tagged DIS will be described in Sec. IV.

In LF quantum mechanics plane-wave nucleon states are characterized by their LF plus and transverse momenta, $p_N^+ = p_N^0 + p_N^z$ and $\boldsymbol{p}_{NT} = (p_N^x, p_N^y)$ [cf. Eq. (2.32)], while $p_N^- = p_N^0 - p_N^z$ plays the role of energy and is fixed by the mass-shell condition $p_N^2 = p_N^+ p_N^- - |\boldsymbol{p}_{NT}|^2 = M_N^2$,

$$|N, p_N\rangle \;\; \equiv \;\; |N, p_N^+, \boldsymbol{p}_{NT}\rangle, \qquad p_N^- \;\; = \;\; \frac{|\boldsymbol{p}_{NT}|^2 + M_N^2}{p_N^+}. \tag{3.1}$$

To simplify the notation we label the states by the 4–momentum p_N and display the individual plus and transverse components only if necessary. The relativistic normalization condition for the states is [cf. Eq. (2.9)]

$$\langle N, p'_N | N, p_N \rangle \;=\; (2\pi)^3\, 2p_N^+\, \delta(p_N^{+\prime} - p_N^+)\; \delta(\boldsymbol{p}'_{NT} - \boldsymbol{p}_{NT}). \tag{3.2}$$

The invariant phase space integral over the nucleon LF momentum is

$$\begin{aligned} \int d\Gamma_N\; (...) &= \int \frac{d^4 p_N}{(2\pi)^4}\; 2\pi\delta(p_N^2 - M_N^2)\; \theta(p_N^0)\; (...) \\ &= \int \frac{dp_N^+ d^2 p_{NT}}{(2\pi)^3 2p_N^+}\; \theta(p_N^+)\; (...) \qquad [p_N^- = (|\boldsymbol{p}_{NT}|^2 + M_N^2)/p_N^+] \qquad (3.3) \\ &\equiv \int [dp_N]\; (...). \qquad (3.4) \end{aligned}$$

The condition $p_N^+ > 0$ is satisfied for all physical nucleon momenta. The completeness of single–nucleon states can then be stated in the form

$$\int [dp_N]\; |N, p_N\rangle\langle N, p_N| \;=\; 1_N, \tag{3.5}$$

which is the unit operator in the single-nucleon space. For reference we note that for a general 4–momentum p (not on mass–shell), the four–dimensional integral and the four-dimensional delta function in LF components take the form

$$\int d^4 p\; (...) \;=\; \frac{1}{2}\int_{-\infty}^{\infty} dp^+ \int_{-\infty}^{\infty} dp^- \int d^2 p_T\; (...), \qquad \delta^{(4)}(p) \;=\; 2\delta(p^+)\delta(p^-)\delta^{(2)}(\boldsymbol{p}_T). \tag{3.6}$$

The formulas can easily be generalized to account for nucleon spin degrees of freedom. Other hadronic states are described in a similar fashion.

B. Deuteron wave function

In the LF description of high-energy processes nuclei are described as bound states of nucleons and, possibly, non-nucleonic degrees of freedom (Δ isobars, pions) [1, 11]. Theoretical arguments show that for the deuteron the nucleonic (pn) component dominates over a wide range of excitation energies [11] (see also Sec. I), and we limit ourselves to this component in the present study. The deuteron is described as a bound state with relativistic normalization of the center-of-mass motion [cf. Eq.(3.2)]

$$|d, p_d\rangle, \quad p_d^- = \frac{|\boldsymbol{p}_{dT}|^2 + M_d^2}{p_d^+}, \tag{3.7}$$

$$\langle d, p'_d | d, p_d\rangle = (2\pi)^3\, 2p_d^+\, \delta(p_d^{+\prime} - p_d^+)\, \delta^{(2)}(\boldsymbol{p}'_{dT} - \boldsymbol{p}_{dT}). \tag{3.8}$$

The expansion of the deuteron state in plane-wave nucleon states is described by the LF wave function (see Fig. 5)

$$\begin{aligned} \langle p, p_p; n, p_n | d, p_d\rangle &= (2\pi)^3\, 2p_d^+\, \delta(p_p^+ + p_n^+ - p_d^+)\, \delta^{(2)}(\boldsymbol{p}_{pT} + \boldsymbol{p}_{nT} - \boldsymbol{p}_{dT}) \\ &\quad \times (2\pi)^{3/2} \Psi_d(\alpha_p, \boldsymbol{p}_{pT} | \boldsymbol{p}_{dT}), \qquad (3.9) \end{aligned}$$

$$\alpha_p \equiv \frac{2p_p^+}{p_d^+}, \qquad \alpha_n \;\equiv\; \frac{2p_n^+}{p_d^+}. \tag{3.10}$$

The factor $(2\pi)^{3/2}$ is conventional. The function Ψ_d depends on the LF momentum fraction and the transverse momentum of the proton, α_p and $\boldsymbol{p}_{pT}$, and the deuteron transverse momentum $\boldsymbol{p}_{dT}$; it is independent of the total plus momentum p_d^+ because of longitudinal boost invariance [11, 34]. The delta functions in Eq. (3.9) require that

$$\alpha_p + \alpha_n \;=\; 2, \qquad \boldsymbol{p}_{pT} + \boldsymbol{p}_{nT} \;=\; \boldsymbol{p}_{dT}, \tag{3.11}$$

which in particular implies that

$$0 < \alpha_p, \alpha_n < 2. \tag{3.12}$$

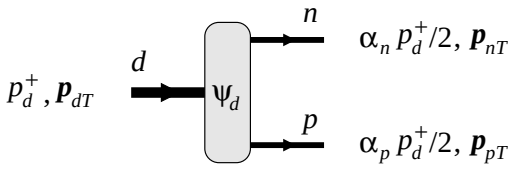

FIG. 5. Deuteron NN LF wave function.

In the present study we do not consider polarization phenomena at the deuteron or the nucleon level and omit the spin quantum numbers in the states and in the wave function. At this level the matrix element Eq. (3.9) is symmetric with respect to interchange of the proton and neutron, and the wave function satisfies

$$\Psi_d(\alpha_p, \boldsymbol{p}_{pT}|\boldsymbol{p}_{dT}) \;=\; \Psi_d(2-\alpha_p, \boldsymbol{p}_{dT}-\boldsymbol{p}_{pT}|\boldsymbol{p}_{dT}) \;=\; \Psi_d(\alpha_n, \boldsymbol{p}_{nT}|\boldsymbol{p}_{dT}). \tag{3.13}$$

The normalization of the deuteron wave function follows from the normalization condition for the deuteron state Eq. (3.8) and the completeness relation for the single-nucleon states Eq. (3.5). Inserting complete sets of single-nucleon intermediate states into Eq. (3.8) and integrating out the delta functions one obtains (we replace the arguments by α_N and $\boldsymbol{p}_{NT}$ for brevity)

$$\int \frac{d\alpha_p\; d^2p_{pT}}{\alpha_p(2-\alpha_p)}\; |\Psi_d(\alpha_p, \boldsymbol{p}_{pT}|\boldsymbol{p}_{dT})|^2 \;=\; 1. \tag{3.14}$$

In the calculations of deuteron structure in the collinear frame of Sec. II C we need the wave function at zero deuteron transverse momentum, which we denote by

$$\Psi_d(\alpha_p, \boldsymbol{p}_{pT}) \;\equiv\; \Psi_d(\alpha_p, \boldsymbol{p}_{pT}|\boldsymbol{p}_{dT}=0). \tag{3.15}$$

The symmetry relation Eq.(3.13) for this function takes the simple form

$$\Psi_d(\alpha_p, \boldsymbol{p}_{pT}) \;=\; \Psi_d(2-\alpha_p, -\boldsymbol{p}_{pT}) \;=\; \Psi_d(\alpha_n, -\boldsymbol{p}_{nT}). \tag{3.16}$$

The above formulas can easily be generalized to account for deuteron and nucleon spin. The summation over spin quantum numbers will be performed implicitly in the calculation of matrix elements below.

For modeling the actual form of the deuteron LF wave function it is natural to consider the connection of the LF formulation with the non-relativistic description of deuteron structure. In general this connection is rather complicated, because of the different symmetry groups of the dynamics in the two formulations. However, a simple connection can be established in the approximation where the deuteron's LF structure is restricted to the pn component, which we adopt here [1, 11]. One starts with the LF version of the Lippmann-Schwinger equation for the two-body wave function (or Weinberg equation [49]) and imposes the condition that the scattering-state solutions give rotationally invariant on-shell NN scattering amplitudes (angular conditions) [1, 11]. The resulting equation for bound states has a simple connection with the Schrödinger equation for the non-relativistic deuteron wave function, which one can use to construct an approximation of the LF wave function in terms of the non-relativistic wave function (see Sec. III C). Methods for direct solution of the LF two-body bound-state equation have been described in Refs. [50, 51]. For attempts to model deuteron LF structure beyond the pn component, and for approximation methods for heavier nuclei, we refer to Refs. [52, 53] and references therein.

C. Rotationally invariant representation

The LF wave function of a two-body bound state such as the deuteron can be expressed in a form that exhibits 3-dimensional rotational invariance [1, 11, 54]. This representation can be motivated by group-theoretical or dynamical considerations (see above) and is useful for several purposes: (a) it explains how rotational invariance is dynamically realized in LF quantum mechanics, where it is not manifest (angular conditions); (b) it enables an approximation of the LF wave function in terms of the 3-dimensional non-relativistic wave function; (c) it brings out the analytic properties of the LF wave function in the nucleon momentum.

The rotationally invariant momentum variable for the two-nucleon system can be introduced through an intuitive procedure, by identifying the pn configurations in the deuteron LF wave function with a free pn system in its center-of-mass frame [11]. One starts from a pn configuration in its center-of-mass frame, with the proton having LF momentum

α_p and $\boldsymbol{p}_{pT}$; calculates the invariant mass of the pn configuration; and equates the invariant mass with the squared energy of a free pn system with relative 3–momentum

$$\boldsymbol{k} \;\equiv\; (\boldsymbol{k}_T, k^z), \qquad \boldsymbol{k}_T \;=\; \boldsymbol{p}_T. \tag{3.17}$$

This leads to the equation

$$s_{pn} \;\equiv\; \frac{\boldsymbol{p}_{pT}^2 + M_N^2}{\frac{\alpha_p}{2}\left(1 - \frac{\alpha_p}{2}\right)} \;\stackrel{!}{=}\; 4E_N(\boldsymbol{k})^2 \;=\; 4\left(|\boldsymbol{k}|^2 + M_N^2\right). \tag{3.18}$$

One then determines the component k^z as function of α_p and $|\boldsymbol{p}_{pT}|$ by solving Eq. (3.18),

$$k^z \;=\; (\alpha_p - 1)\left[\frac{\boldsymbol{p}_{pT}^2 + M_N^2}{\alpha_p(2-\alpha_p)}\right]^{1/2}. \tag{3.19}$$

Equations (3.17) and (3.19) define the equivalent 3–momentum $\boldsymbol{k}$ in terms of the LF variables of the two-body system. The inverse relation is

$$\alpha_p \;=\; 1 + \frac{k^z}{E_N} \;=\; \frac{2(E_N + k^z)}{2E_N}, \qquad E_N \;\equiv\; \sqrt{|\boldsymbol{k}|^2 + M_N^2}. \tag{3.20}$$

Note that in this parametrization the nucleon plus momentum fraction is obtained by dividing $E_N + k^z$ by the *internal energy* of the pn system, $2E_N$, not by the *external mass* of the bound state, as in the kinematic variable Eq. (2.43). The invariant phase space elements in the two sets of variables are related as

$$\frac{d\alpha_p\, d^2p_{pT}}{\alpha_p(2-\alpha_p)} \;=\; \frac{d^3k}{\sqrt{|\boldsymbol{k}|^2 + M_N^2}} \;=\; \frac{d^3k}{E_N(\boldsymbol{k})}. \tag{3.21}$$

The rotationally invariant form of the deuteron LF wave function is then obtained by demanding that

$$\Psi_d(\alpha_p, \boldsymbol{p}_{pT}) \;=\; \text{function}(|\boldsymbol{k}|). \tag{3.22}$$

It was shown in Ref. [11] that this condition is sufficient to guarantee rotational invariance in two-body bound state calculations.

The rotationally symmetric form Eq. (3.22) suggests a natural approximation of the rest-frame deuteron LF wave function in terms of the non-relativistic wave function:

$$\Psi_d(\alpha_p, \boldsymbol{p}_{pT}) \;\stackrel{\text{app}}{=}\; \sqrt{E_N(\boldsymbol{k})}\;\; \widetilde{\Psi}_d(\boldsymbol{k}), \tag{3.23}$$

where $\widetilde{\Psi}_d$ denotes the non-relativistic wave function and the arguments are related by Eqs. (3.17) and (3.19). This approximation has the following properties: (a) it becomes exact at small momenta $|\boldsymbol{k}| \ll M_N$, where $E_N(\boldsymbol{k}) \approx M_N$ is constant and the relation between α_N and k^z becomes the standard non-relativistic approximation; (b) it has correct overall normalization, because the normalization integrals are related as [cf. Eq. (3.14)]

$$\int \frac{d\alpha_p\, d^2p_{pT}}{\alpha_p(2-\alpha_p)}\, |\Psi_d(\alpha_p, \boldsymbol{p}_{pT})|^2 \;=\; \int d^3k\, |\widetilde{\Psi}_d(\boldsymbol{k})|^2 \;=\; 1. \tag{3.24}$$

The rotationally invariant representation Eq. (3.22) is also sufficient for ensuring the correct analytic properties of the LF wave function at small relative momenta (nucleon pole). We can demonstrate this using the approximation Eq. (3.23), which becomes exact at small recoil momenta. On general grounds the non-relativistic deuteron wave function has a pole at small unphysical momenta of the form

$$\widetilde{\Psi}_d(\boldsymbol{k}) \;\sim\; \frac{\Gamma}{|\boldsymbol{k}|^2 + a^2} \qquad (|\boldsymbol{k}| \to a), \tag{3.25}$$

$$a^2 \;=\; M_N\epsilon_d - \frac{\epsilon_d^2}{4}. \tag{3.26}$$

The pole results from the free propagation of the nucleons outside the range of pn interaction and controls the large-distance behavior of the coordinate–space wave function. [In the Bethe–Peierls approximation the entire deuteron

wave function is given by Eq. (3.25).] By expressing $|\boldsymbol{k}^2|$ in Eq. (3.25) in terms of the LF momentum variables using Eq. (3.18), one easily sees that the pole corresponds to a pole in the invariant mass s_{pn} of the LF wave function,

$$\Psi_d(\alpha_p, \boldsymbol{p}_{pT}) \;\sim\; \frac{4(M_N^2 - a^2)^{1/4}\Gamma}{s_{pn} - M_d^2}. \tag{3.27}$$

The singularities Eq. (3.25) viz. Eq. (3.27) give rise to the nucleon pole in the deuteron spectral function and play an essential role in the analysis of tagged DIS (see below).

For practical calculations one can use Eq. (3.23) with a non-relativistic deuteron wave function obtained from realistic NN potentials [55]. At the low momenta of interest here ($|\boldsymbol{k}| \lesssim 200\,\mathrm{MeV}$) an excellent approximation to the realistic wave functions is provided by a simple two-pole parametrization, which implements the nucleon pole and has correct analytic properties (see Appendix A). We use this parametrization in the numerical calculations below.

IV. IMPULSE APPROXIMATION

A. LF current components

We now compute the cross section for tagged DIS on the deuteron using LF quantum mechanics. The basic considerations in treating nuclear structure in high-energy scattering are described in Refs. [1, 11] and summarized in Sec. I. In LF quantization the effects of the off-shellness of the constituents in a bound state remain finite as the scattering energy becomes large, which makes possible a composite description of the nucleus in terms of nucleon degrees of freedom (see below). We use the collinear frame of Sec. II C ($\boldsymbol{p}_{dT} = 0, \boldsymbol{q}_T = 0$), in which the initial nucleus and the DIS final state evolve along the same z–direction, as this permits a natural description of FSI with rotational invariance in the transverse plane. Non-collinear frames with $\boldsymbol{q}_T \neq 0$ can be used for LF calculations of the inclusive DIS cross section but are not suitable for FSI [1]. In the collinear frame the momentum transfer to the nucleus has LF component $q^+ < 0$, Eq. (2.33), so that the current cannot produce physical hadron states out of the vacuum, but can only couple to nucleons in the nuclear LF wave function.

In order to extract the tagged deuteron structure functions of Eq. (2.22) in the collinear frame we must calculate both + and T components of the nuclear tensor. It is well-known that in LF quantization the different components of the current operator have different status as to how they involve the interactions of the system. This is seen explicitly in the LF quantization of quantum field theories, where only two components of the spin-1/2 Dirac field are independent canonical degrees of freedom, while the other two are dependent and must be eliminated through the equations of motion [56, 57]. The "good" current J^+ is formed out of canonical degrees of freedom and free of interactions; the "bad" current $\boldsymbol{J}_T$ is formed out of canonical and dependent degrees of freedom and involves explicit interactions; the "worst" current J^- is formed entirely out of dependent degrees of freedom.[2] Following Refs. [1, 11] we calculate the J^+ and $\boldsymbol{J}_T$ matrix elements in our approach (IA and FSI); the J^- component can be eliminated through the transversality condition in the collinear frame (current conservation) and does not need to be considered explicitly,

$$q^\mu \langle B|J_\mu|A\rangle \;=\; \frac{q^+}{2}\langle B|J^-|A\rangle \;+\; \frac{q^-}{2}\langle B|J^+|A\rangle \;=\; 0. \tag{4.1}$$

The use of the component $\boldsymbol{J}_T$ for structure function calculations represents an approximation, whose accuracy cannot be established from first principles in our phenomenological approach. In inclusive DIS, comparison between a good-current calculation in a non-collinear frame and the good-and-bad-current calculation in the collinear frame shows that the two schemes give the same results in the DIS limit $(\mathrm{mass}^2)/W^2 \to 0$ [1]. This indicates that the collinear method should be reliable for the leading-twist tagged structure functions F_{2d} and F_{Ld} calculated in this work. A further test of the method will be performed in Sec. IV C. The applicability to higher-twist structure functions, which represent power-suppressed structure in the tagged cross section, remains to be investigated.

B. IA current

The starting point of the nuclear structure calculation is the IA. Its physical assumptions are: (a) the current operator is the sum of one–body nucleon currents; (b) the final state produced by the one–body nucleon current

[2] In the equivalent formulation based on equal-time quantization in the infinite–momentum frame $|\boldsymbol{p}| \to \infty$, the "good" components are those that tend to a finite limit as $|\boldsymbol{p}| \to \infty$ (in the non-covariant normalization of states), while the other components vanish.

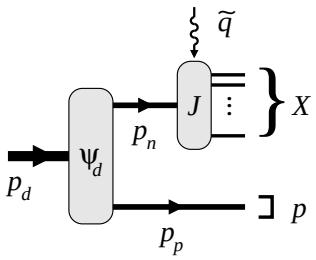

FIG. 6. Current matrix element of tagged DIS on the deuteron in the IA.

evolves independently of nuclear remnant (see Fig. 6) [58]. In the IA we consider the nuclear current matrix element in Eq. (2.19) in the collinear frame ($\boldsymbol{p}_{dT} = 0$) and insert plane-wave proton and neutron states between the deuteron state and the current operator. Taking the proton as the spectator, and the neutron as coupling to the current, we obtain (see Fig. 6)

$$\langle pX|\hat{J}^\mu(0)|d\rangle[\mathrm{IA}] \;=\; \int [dp_p] \int [dp_n]\; \langle X|\hat{J}^\mu(0)|n,p_n\rangle\; \langle p,p_p|p,p_{p1}\rangle\; \langle p,p_p;n,p_n|d,p_d\rangle \tag{4.2}$$

$$\;=\; (2\pi)^{3/2}\; \frac{p_d^+}{p_n^+}\; \langle X|\hat{J}^\mu(0)|n,p_n\rangle\; \Psi_d(\alpha_p,\boldsymbol{p}_{pT}) \qquad (p_n^+ = p_d^+ - p_p^+,\; \boldsymbol{p}_{nT} = -\boldsymbol{p}_{pT}). \tag{4.3}$$

The deuteron tensor Eq. (2.19) then becomes

$$W_d^{\mu\nu}(p_d,q;p_p) \;=\; \left(\frac{p_d^+}{p_n^+}\right)^2\; (2\pi)^3\; |\Psi_d(\alpha_p,\boldsymbol{p}_{pT})|^2$$

$$\times\; (4\pi)^{-1} \sum_X\; (2\pi)^4\; \delta^{(4)}(q + p_d - p_p - p_X)\; \langle n,p_n|\hat{J}^\mu(0)|X\rangle\; \langle X|\hat{J}^\nu(0)|n,p_n\rangle$$

$$(p_n^+ = p_d^+ - p_p^+,\; \boldsymbol{p}_{nT} = -\boldsymbol{p}_{pT}). \tag{4.4}$$

The expression on the second line has a form suggestive of the scattering tensor for inclusive scattering on the neutron. However, we must take into account that in LF quantum mechanics 4–momenta are not conserved, and that

$$p_d - p_p \;\neq\; p_n \qquad (\text{4-vectors}) \tag{4.5}$$

in the argument of the 4-dimensional delta function. This is because the LF energy of the neutron is determined by the mass shell condition

$$p_n^- \;=\; \frac{|\boldsymbol{p}_{nT}|^2 + M_N^2}{p_n^+} \;\neq\; p_d^- - p_p^-. \tag{4.6}$$

The expression in Eq. (4.4) can therefore not be regarded as the neutron scattering tensor with the original 4–momentum transfer q, which is fixed kinematically by the electron 4–momenta. To write it as a proper scattering tensor we define an effective 4–momentum transfer as

$$\widetilde{q} \;\equiv\; q + p_d - p_n - p_p, \qquad \text{or} \qquad p_n + \widetilde{q} \;=\; q + p_d - p_p$$

$$\left[p_n^+ = p_d^+ - p_p^+,\; \boldsymbol{p}_{nT} = -\boldsymbol{p}_{pT},\; p_n^- = (|\boldsymbol{p}_{nT}|^2 + M_N^2)/p_n^+\right]. \tag{4.7}$$

The vector $\widetilde{q}$ has the same plus and transverse components as the original q and differs only in its minus component, which is not conserved in LF quantum mechanics. The difference accounts for the fact that the pn configurations in the deuteron are off the LF energy shell and participate in the scattering process with shifted kinematics. With the effective momentum transfer Eq. (4.7) the deuteron tensor Eq. (4.4) can then be expressed in terms of the effective neutron tensor [we use $p_d^+/p_n^+ = 2/(2-\alpha_p)$]

$$W_d^{\mu\nu}(p_d,q,p_p) \;=\; \left(\frac{p_d^+}{p_n^+}\right)^2\; (2\pi)^3\; |\Psi_d(\alpha_p,\boldsymbol{p}_{pT})|^2\; W_n^{\mu\nu}(p_n,\widetilde{q}) \tag{4.8}$$

$$= \frac{4(2\pi)^3}{(2-\alpha_p)^2}\,|\Psi_d(\alpha_p,\boldsymbol{p}_{pT})|^2\;W_n^{\mu\nu}(p_n,\widetilde{q}) \tag{4.9}$$

$$W_n^{\mu\nu}(p_n,\widetilde{q}) \;\equiv\; (4\pi)^{-1}\sum_X (2\pi)^4\;\delta^{(4)}(\widetilde{q}+p_n-p_X)\;\langle n,p_n|J^\mu(0)|X\rangle\;\langle X|J^\nu(0)|n,p_n\rangle. \tag{4.10}$$

Equation (4.9) represents the "master formula" for tagged DIS in the LF IA and expresses the factorization of deuteron and nucleon structure.

The assignment of the active nucleon 4-momentum p_n as in Eq. (4.6), and of the 4-momentum transfer $\widetilde{q}$ as in Eq. (4.7), are dictated by LF quantum mechanics, in which the LF + and T momenta are conserved and the particles are on mass-shell, but the total LF energy of the intermediate states is different from that of the initial and final states. A crucial point is that in this scheme the non-conservation of 4-momentum does not give rise to any large invariants in the DIS limit $W^2\to\infty$, $Q^2\to\infty$, Q^2/W^2 fixed. The off-shellness of the minus component of the nucleon 4-momentum implied by Eq. (4.6) is

$$p_n^- - p_d^- + p_p^- \;=\; \frac{|\boldsymbol{p}_{pT}|^2+M_N^2}{p_n^+} - \frac{M_d^2}{p_d^+} + \frac{|\boldsymbol{p}_{pT}|^2+M_N^2}{p_p^+} \tag{4.11}$$

$$= \frac{1}{p_d^+}\left[\frac{4(|\boldsymbol{p}_{pT}|^2+M_N^2)}{\alpha_p(2-\alpha_p)} - M_d^2\right], \tag{4.12}$$

where we have used the explicit expressions for the LF momentum components in the collinear frame of Sec. II C. The plus component of the momentum transfer is $q^+ = -\xi_d p_d^+$, cf. Eq.(2.33). The variables $\alpha_p, |\boldsymbol{p}_{pT}|$ and ξ_d remain finite in the DIS limit, and p_d^+ is a finite boost parameter. One therefore has

$$2q(p_n-p_d+p_p) \;=\; q^+(p_n^- - p_d^- + p_p^-) \;=\; O\left\{|\boldsymbol{p}_{pT}|^2, (\text{mass})^2\right\}, \tag{4.13}$$

i.e., the invariant remains finite and does not grow as W^2 or Q^2. (Note that individually $qp_d\sim W^2$ and $qp_n\sim W^2$, because p_d and p_n have non-zero plus components.) It implies that the effects caused by the LF energy off-shellness are power-suppressed as $\sim |\boldsymbol{p}_{pT}|^2/W^2$ or $\sim (\text{mass})^2/W^2$ in the DIS limit. This circumstance is unique about LF quantization and is the reason for the use this approach in high-energy scattering.

C. Structure functions

Expressions for the tagged deuteron structure functions are obtained from Eq. (4.9) by substituting the specific form of the neutron tensor and projecting the tensor equation on the structures of Eq. (2.22). The decomposition of the neutron tensor is analogous to that of the deuteron tensor Eq. (2.22), but with the target 4–momentum given by p_n, and the 4–momentum transfer given by $\widetilde{q}$,

$$W_n^{\mu\nu}(p_n,\widetilde{q}) = \left(g^{\mu\nu} - \frac{\widetilde{q}^\mu\widetilde{q}^\nu}{\widetilde{q}^2}\right)\frac{F_{Ln}(\widetilde{x},\widetilde{Q}^2)}{2} \;+\; \left(\frac{\widetilde{L}_n^\mu\widetilde{L}_n^\nu}{\widetilde{L}_n^2} + \frac{\widetilde{q}^\mu\widetilde{q}^\nu}{\widetilde{q}^2} - g^{\mu\nu}\right)\frac{F_{Tn}(\widetilde{x},\widetilde{Q}^2)}{2}, \tag{4.14}$$

$$F_{Tn} = \frac{(-\widetilde{q}^2)L_n^2}{(p_n\widetilde{q})^2}\;\frac{F_{2n}}{\widetilde{x}} \;=\; \left(1+\frac{4\widetilde{x}^2M_N^2}{\widetilde{Q}^2}\right)\;\frac{F_{2n}}{\widetilde{x}}, \tag{4.15}$$

$$\widetilde{L}_n^\mu \equiv p_n^\mu - \frac{(p_n\widetilde{q})\widetilde{q}^\mu}{\widetilde{q}^2}, \qquad \widetilde{x} \;\equiv\; \frac{-\widetilde{q}^2}{2(p_n\widetilde{q})}, \qquad \widetilde{Q}^2 \;\equiv\; -\widetilde{q}^2. \tag{4.16}$$

Equations for the structure functions can then be derived by considering the + and T tensor components in the collinear frame (see Appendix B). They take on a simple form in the DIS limit, where one can neglect terms of the order $|\boldsymbol{p}_{pT}|^2/W^2$ and $(\text{mass})^2/W^2$, so that off-shell effects are suppressed [cf. Eq. (4.13)]. In particular, in this limit

$$\widetilde{Q}^2 \;=\; Q^2, \qquad \widetilde{x} \;=\; \frac{x}{2-\alpha_p}, \tag{4.17}$$

up to power corrections, i.e., the nucleon structure functions are evaluated at the kinematically given Q^2, and at an effective value of x that accounts for the longitudinal motion of the nucleons in the bound state. Altogether we obtain

$$F_{2d}(x,Q^2;\alpha_p,p_{pT}) \;=\; \frac{|\Psi_d(\alpha_p,\boldsymbol{p}_{pT})|^2}{2-\alpha_p}\;F_{2n}\left(\widetilde{x},Q^2\right), \tag{4.18}$$

$$F_{Ld}(x,Q^2;\alpha_p,p_{pT}) \;=\; \frac{2\,|\Psi_d(\alpha_p,\boldsymbol{p}_{pT})|^2}{(2-\alpha_p)^2}\;F_{Ln}\left(\widetilde{x},Q^2\right). \tag{4.19}$$

These formulas express the deuteron DIS structure functions with tagged proton in terms of the deuteron LF momentum density and the active neutron inclusive structure functions. The case of tagged neutron and active proton is described by the same formulas with the proton and neutron labels interchanged.

Our calculation in the collinear frame uses both good and bad LF current components to identify the structure functions (cf. Sec. IV A). The results for the bad current component in the LF IA are generally sensitive to the energy off-shellness (4-momentum nonconservation) in the intermediate state. These effects are related to those of explicit interactions in the bad current component operators. In a complete dynamical theory both could be treated consistently starting from the microscopic interaction. To assess their influence within our phenomenological approach we perform a simple test, following Ref. [1]. We evaluate Eq. (4.9) with the neutron tensor $W_n^{\mu\nu}$ taken at the off-mass-shell 4-momentum $\widetilde{p}_n \equiv p_d - p_p$ with $\widetilde{p}_n^2 \neq M_N^2$, as would by obtained from the external 4-momenta using 4-momentum conservation, and at the original momentum transfer q ("virtual nucleon"). We compare the results with those of the LF prescription, where $W_n^{\mu\nu}$ is evaluated at p_n and $\widetilde{q}$, Eqs. (4.6) and (4.7). The differences in the leading-twist tagged structure functions F_{2d} and F_{Ld} turn out to be of the order $|\boldsymbol{p}_{pT}|^2/W^2$ and $(\text{mass})^2/W^2$ and are thus power-suppressed in the DIS limit [cf. Eq. (4.13)]. This suggests that our collinear LF calculation is safe in the DIS limit.

In addition to the kinematic off-shell effects discussed so far, nuclear binding causes dynamical modifications of the structure of the nucleon, which manifest themselves e.g. in the suppression of the nuclear structure functions at $x > 0.3$ compared to the sum of the corresponding nucleon structure functions (EMC effect). Theoretical analysis shows that to first order in the nuclear binding these modifications are proportional to the LF energy off-shellness of the nuclear configurations (or the nucleon virtuality in the virtual nucleon formulation), which in turn is proportional to the non-relativistic kinetic energy of the nucleons [1, 59]. The modifications are therefore much smaller in the deuteron than in heavy nuclei. Simple scaling arguments suggest that in average configurations in the deuteron the EMC-like modifications should be at the level of $\sim 2-3\%$. They are reduced further when selecting configurations with proton recoil momenta less than the typical nucleon momentum in the deuteron (the median momentum is $\sim 70\,\text{MeV}$; see Fig. 17 and Appendix A). The modifications can be eliminated entirely by performing on-shell extrapolation in the recoil momentum, which effectively turns the deuteron into a free pn system (see Sec. IV F).

D. Spectral function

The IA for the deuteron tensor in tagged DIS, Eq. (4.9), is conveniently expressed in terms of the deuteron spectral function, defined as

$$S_d(\alpha_p,\boldsymbol{p}_{pT}) \equiv \frac{|\Psi_d(\alpha_p,\boldsymbol{p}_{pT})|^2}{2-\alpha_p}. \tag{4.20}$$

It is a function of the LF momentum variables of the recoil proton and satisfies the sum rules

$$\int_0^2 \frac{d\alpha_p}{\alpha_p}\int d^2p_{pT}\;S_d(\alpha_p,\boldsymbol{p}_{pT}) = \int \frac{d\alpha_p\,d^2p_{TR}}{\alpha_p(2-\alpha_p)}\,|\Psi_d(\alpha_p,\boldsymbol{p}_{pT})|^2 \;=\; 1, \tag{4.21}$$

$$\begin{aligned}\int_0^2 \frac{d\alpha_p}{\alpha_p}\int d^2p_{pT}\;(2-\alpha_p)\;S_d(\alpha_p,\boldsymbol{p}_{pT}) &= \int \frac{d\alpha_p\,d^2p_{pT}}{\alpha_p(2-\alpha_p)}\;\;(2-\alpha_p)\,|\Psi_d(\alpha_p,\boldsymbol{p}_{pT})|^2\\ &= \int \frac{d\alpha_p\,d^2p_{pT}}{\alpha_p(2-\alpha_p)}\;\;\alpha_p\,|\Psi_d(\alpha_p,\boldsymbol{p}_{pT})|^2\\ &= \int \frac{d\alpha_p\,d^2p_{pT}}{\alpha_p(2-\alpha_p)}\,|\Psi_d(\alpha_p,\boldsymbol{p}_{pT})|^2 \;=\; 1.\end{aligned} \tag{4.22}$$

The first sum rule, Eq. (4.21), follows from the normalization condition of the deuteron LF wave function, Eq. (3.14), and reflects the total number of nucleons in the bound state (nucleon number sum rule). The second sum rule, Eq. (4.22), follows from the symmetry of the two-body LF wave function in the transverse rest frame, Eq. (3.16), and expresses the conservation of the LF plus momentum (momentum sum rule). The physical implications of these sum rules will be explained in the following. In terms of the spectral function the IA result for the tagged structure

functions, Eqs. (4.18) and (4.19), are now expressed as

$$F_{2d}(x,Q^2;\alpha_p,p_{pT}) = S_d(\alpha_p,\boldsymbol{p}_{pT})\; F_{2n}\left(\widetilde{x},Q^2\right), \tag{4.23}$$

$$F_{Ld}(x,Q^2;\alpha_p,p_{pT}) = \frac{2\,S_d(\alpha_p,\boldsymbol{p}_{pT})}{2-\alpha_p}\; F_{Ln}\left(\widetilde{x},Q^2\right). \tag{4.24}$$

It is instructive to consider the integral of the tagged deuteron structure function over the recoil momentum

$$F_{2d}^{\rm int}(x,Q^2) \;\equiv\; \int_0^{2-x}\frac{d\alpha_p}{\alpha_p}\int d^2p_{pT}\; F_{2d}(x,Q^2;\alpha_p,p_{pT}). \tag{4.25}$$

The restriction $\alpha_p < 2-x$ results because the recoil proton plus momentum cannot exceed the total plus momentum of the DIS final state. Notice that this integral over the LF variables corresponds to the integral over the invariant recoil momentum phase space, Eq. (2.45). With the IA expression Eq. (4.23) the integrated structure function becomes

$$F_{2d}^{\rm int}(x,Q^2) \equiv \int_0^{2-x}\frac{d\alpha_p}{\alpha_p}\int d^2p_{pT}\; S_d(\alpha_p,\boldsymbol{p}_{pT})\; F_{2n}(\widetilde{x},Q^2) \tag{4.26}$$

$$= \int_0^{2-x}\frac{d\alpha_p}{\alpha_p(2-\alpha_p)}\int d^2p_{pT}\; |\Psi_d(\alpha_p,\boldsymbol{p}_{pT})|^2\; F_{2n}(\widetilde{x},Q^2) \tag{4.27}$$

$$[\widetilde{x} = x/(2-\alpha_p)].$$

Equation (4.28) has several interesting properties. First, using the symmetry of the LF wave function, Eq. (3.16), the integral can equivalently be expressed as an integral over the active neutron fraction $\alpha_n = 2-\alpha_p$, whereupon it takes the form of a standard partonic convolution formula,

$$F_{2d}^{\rm int}(x,Q^2) = \int_x^2\frac{d\alpha_n}{\alpha_n}\int d^2p_{nT}\; |\Psi_d(\alpha_n,\boldsymbol{p}_{nT})|^2\; F_{2n}(\widetilde{x},Q^2) \qquad (\widetilde{x}\equiv x/\alpha_n). \tag{4.28}$$

Second, using the momentum sum rule for the spectral function, Eq. (4.22), and changing the order of the integrations, one easily shows that

$$\int_0^2 dx\; F_{2d}^{\rm int}(x,Q^2) \;=\; \int_0^1 d\widetilde{x}\; F_{2n}(\widetilde{x},Q^2). \tag{4.29}$$

A similar formula applies to the case of tagged neutron and active proton. Together, they imply that the LF momentum sum rule for the deuteron is satisfied exactly in the IA if one adds the contributions from proton and neutron tagging, i.e., from scattering on the active neutron and proton,

$$\int_0^2 dx\;\left[F_{2d}^{\rm int}(p\text{ tagged}) + F_{2d}^{\rm int}(n\text{ tagged})\right](x,Q^2) \;=\; \int_0^1 d\widetilde{x}\;\left[F_{2n}+F_{2p}\right](\widetilde{x},Q^2). \tag{4.30}$$

Third, for non-exceptional values of x the integral over α_p in Eq. (4.28) is dominated by the region $\alpha_p \sim 1$, so that one can neglect the variation of $\widetilde{x} = x/(2-\alpha_p)$ under the integral and evaluate the structure function at $\alpha_p = 1$ (peaking approximation),

$$F_{2d}^{\rm int}(x,Q^2) \;\approx\; F_{2n}(x,Q^2)\int_0^2\frac{d\alpha_p}{\alpha_p}\int d^2p_{pT}\; S_d(\alpha_p,\boldsymbol{p}_{pT}) \;=\; F_{2n}(x,Q^2). \tag{4.31}$$

In the second step we have used the number sum rule for the spectral function, Eq. (4.21). Again a similar formula applies to the case of tagged neutron and active proton. Thus the sum of proton-tagged and neutron-tagged deuteron structure functions in the peaking approximation reduces to the sum of the free neutron and proton structure functions, as it should be.

Some comments are in order regarding our definition of the spectral function Eq. (4.20). In the IA for a complex nucleus ($A > 2$) the spectral function describes the probability for removing a nucleon, leaving the $A-1$ remnant system R in a state with given momentum $\boldsymbol{p}_R$ and total energy E_R, which includes the energy of the excitation and/or internal motion of the system. In the IA for the deuteron ($A = 2$), assuming that it can be described as an pn system (neglecting $NN\pi$ and $\Delta\Delta$ components), the recoiling system is a single nucleon, and its energy is fixed by the energy-momentum relation (there is no excitation or internal motion), so that the spectral function depends on

the momentum variables only. In fact, the proton-tagged spectral function defined by Eq. (4.20) is related in a simple way to the neutron LF momentum density in the deuteron [11], cf. Eq. (3.16),

$$S_d(\alpha_p, \boldsymbol{p}_{pT}) = \frac{\alpha_p}{\alpha_n}\, \rho_d(\alpha_n, \boldsymbol{p}_{nT}), \tag{4.32}$$

$$\rho_d(\alpha_n, \boldsymbol{p}_{nT}) \equiv \frac{|\Psi_d(\alpha_n, \boldsymbol{p}_{nT})|^2}{2-\alpha_n} \;=\; \frac{|\Psi_d(\alpha_p, \boldsymbol{p}_{pT})|^2}{\alpha_p} \tag{4.33}$$

$$(\alpha_n = 2-\alpha_p,\ \boldsymbol{p}_{nT} = -\boldsymbol{p}_{pT}).$$

The density is regarded as a function of the neutron LF momentum variables and satisfies the normalization condition

$$\int \frac{d\alpha_n}{\alpha_n} \int d^2p_{nT}\; \rho_d(\alpha_n, \boldsymbol{p}_{nT}) \;=\; 1. \tag{4.34}$$

In this sense we could express the IA result (and the distortion effects due to FSI considered below) as well in terms of the active neutron density. We choose to express them in terms of the spectral function Eq. (4.20), as this function depends on the observable recoil proton momentum.

E. Nonrelativistic limit

A remarkable property of the IA in LF quantum mechanics is that it coincides with the non-relativistic approximation in the limit of small proton recoil momentum in the deuteron rest frame. This coincidence is not trivial, as the LF expression Eq. (4.9) involves a wave function and a flux factor that refer explicitly to the direction of the quantization axis set by the high-energy process. To demonstrate it, we consider the function

$$\frac{2\, S_d(\alpha_p, \boldsymbol{p}_{pT})}{2-\alpha_p} \;=\; \frac{2\,|\Psi_d(\alpha_p, \boldsymbol{p}_{pT})|^2}{(2-\alpha_p)^2} \;=\; \frac{2E_N(\boldsymbol{k})\,|\widetilde{\Psi}_d(\boldsymbol{k})|^2}{(2-\alpha_p)^2} \tag{4.35}$$

in the deuteron rest frame, where the LF variables α_p and $\boldsymbol{p}_{pT}$ and the equivalent 3–momentum variable $\boldsymbol{k}$ (see Sec. III C) are given in terms of the proton recoil momentum $\boldsymbol{p}_p$, and expand the function in powers of the recoil momentum,

$$|\boldsymbol{p}_p|,\ p_p^z \;\ll\; M_N. \tag{4.36}$$

To simplify the expressions we also expand in the deuteron binding energy $\epsilon_d = 2M_N - M_d$, counting $\epsilon_d M_N = O(p_p^2)$, which allows us to study the deuteron wave function at momenta near the nucleon pole Eq. (3.27). The proton LF momentum fraction in the rest frame is given by

$$\frac{\alpha_p}{2} \;=\; \frac{\sqrt{|\boldsymbol{p}_p|^2 + M_N^2} + p_p^z}{M_d} \;=\; \frac{\sqrt{|\boldsymbol{p}_p|^2 + M_N^2} + p_p^z}{2M_N - \epsilon_d} \tag{4.37}$$

and can be expanded to the necessary order. The flux factor in Eq. (4.35) becomes

$$2-\alpha_p \;=\; 1 - \frac{p_p^z}{M_N} \;+\; O(p_p^2). \tag{4.38}$$

The modulus $|\boldsymbol{k}|$ is defined by Eq. (3.18), and the expansion gives

$$|\boldsymbol{k}|^2 + a^2 \;=\; (|\boldsymbol{p}_p|^2 + a^2)\left(1 + \frac{p^z}{M_N}\right) \;+\; O(p_p^3) \qquad (a^2 \equiv \epsilon M_N). \tag{4.39}$$

Combining them to form the function of Eq. (4.35) we obtain

$$\frac{2\,|\Psi_d(\alpha_p, \boldsymbol{p}_{pT})|^2}{(2-\alpha_p)^2} \;=\; \frac{2E_N(\boldsymbol{k})\,|\widetilde{\Psi}_d(\boldsymbol{k})|^2}{(2-\alpha_p)^2}$$

$$\sim\; \frac{2M_N\,\Gamma^2}{(2-\alpha_p)^2(|\boldsymbol{k}|^2 + a^2)^2}$$

$$= \frac{2M_N\Gamma^2}{(1-p_p^z/M_N)^2\,(1+p_p^z/M_N)^2\,(|\boldsymbol{p}_p|^2+a^2)^2} \;+\; O(p_p^2)$$

$$= \frac{2M_N\Gamma^2}{(|\boldsymbol{p}_p|^2+a^2)^2} \;+\; O(p_p^2)$$

$$= 2M_N\,|\widetilde{\Psi}(\boldsymbol{p}_p)|^2 \;+\; O(p_p^2). \tag{4.40}$$

Both the flux factor Eq. (4.38) and the wave function argument Eq. (4.39) involve corrections linear in p_p^z, which refer explicitly to the LF direction and break rotational symmetry. In the function Eq. (4.40), however, the linear corrections cancel, and the first corrections are quadratic in the recoil momentum components. This means that rotational invariance is effectively restored in the LF formulation at small recoil momenta. It implies that the results of the LF IA are numerically close to those of the conventional non-relativistic IA at recoil momenta $|\boldsymbol{p}_p|, p_p^z \ll M_N$. It also ensures proper analyticity of the LF expressions in t' (see Sec. IV F).

F. Analytic properties

We now want to study the analytic properties of the IA spectral function in the invariant momentum transfer t'. For this purpose it is natural to use as independent variables t' and the proton LF fraction α_p; the relation of these variables to α_p and $\boldsymbol{p}_{pT}$ is given by Eq. (2.55). The analytic properties of the spectral function are governed by the nucleon pole of the deuteron LF wave function, Eq. (3.27). The invariant mass difference in Eq. (3.27) is expressed in terms of α_p and t' as

$$s_{pn} - M_d^2 \;=\; \frac{-2t'}{2-\alpha_p}. \tag{4.41}$$

One sees that the LF spectral function Eq. (4.20) in the limit $t' \to 0$ at fixed α_p behaves as

$$S_d(\alpha_p, \boldsymbol{p}_{pT}) \;\sim\; \frac{R}{(t')^2} \;+\; \text{terms } O(t'^{-1}) \qquad (t' \to 0,\ \alpha_p \text{ fixed}), \tag{4.42}$$

$$R \;\equiv\; R(\alpha_p) \;=\; 4\sqrt{M_N^2 - a^2}\,\Gamma^2(2-\alpha_p). \tag{4.43}$$

The spectral function has a pole at $t' = 0$, whose residue depends on α_p and is calculable in terms of the residue of the pole of the 3–dimensional deuteron wave function, Γ. We note that (a) the nucleon pole is a general feature and relies only on rotational invariance and the analytic properties of the rest–frame wave function; (b) the pole in the spectral function is reproduced by the relativistically invariant formulation of high-energy scattering on the deuteron (Feynman diagrams, virtual nucleon approximation), where it corresponds to "nucleon exchange" between the deuteron and the electromagnetic current; (c) the pole Eq. (4.42) represents the leading singularity in the limit $t' \to$ and is contained in the IA cross section; FSI modify only subleading singularities in t', as was proven in general in Ref. [15] and will be demonstrated explicitly using the specific model of FSI derived in Sec. VI.

In the limit $t' \to 0$ the invariant mass difference in deuteron LF wave function tends to zero, Eq. (4.41). This implies that the LF energy off–shellness of the pn system in the IA vanishes [cf. Eq. (4.6) and (4.7)]

$$p_d^+(\widetilde{q}^- - q^-) \;=\; p_d^+(p_d^- - p_n^- - p_p^-) \;=\; -(s_{pn} - 4M_N^2) \;\to 0. \tag{4.44}$$

The kinematic shift in the 4–momentum transfer, $\widetilde{q} - q$, Eq. (4.7), therefore disappears at the pole, and the IA effectively describes the scattering from a free on-shell neutron.

The analytic properties of the LF spectral function suggest a natural method for extracting the free neutron structure functions from proton-tagged DIS measurements on the deuteron. One measures the proton-tagged structure function at fixed Q^2 as a function of x and the recoil proton momentum $|\boldsymbol{p}_p|$. One then tabulates the tagged structure function data in α_p and t', which extends over the physical region $t' < t'_{\rm min}$. The free neutron structure function is then obtained by multiplying the tagged structure function data by $(t')^2/R$ (i.e., extracting the pole factor of the spectral function) and extrapolating the resulting data to $t' \to 0$ (on-shell extrapolation). The procedure gives the residue of the tagged structure function at the pole (with the residue of the spectral function removed), which by definition is the free neutron structure function. Nuclear binding and FSI only modify the tagged structure function at $t' \neq 0$ but drop out at the pole, so that the procedure is exact in principle. In practice its accuracy is determined by the variation of the tagged structure function in t' away from the pole. This question will be addressed with the specific model of FSI developed in Sec. VI.

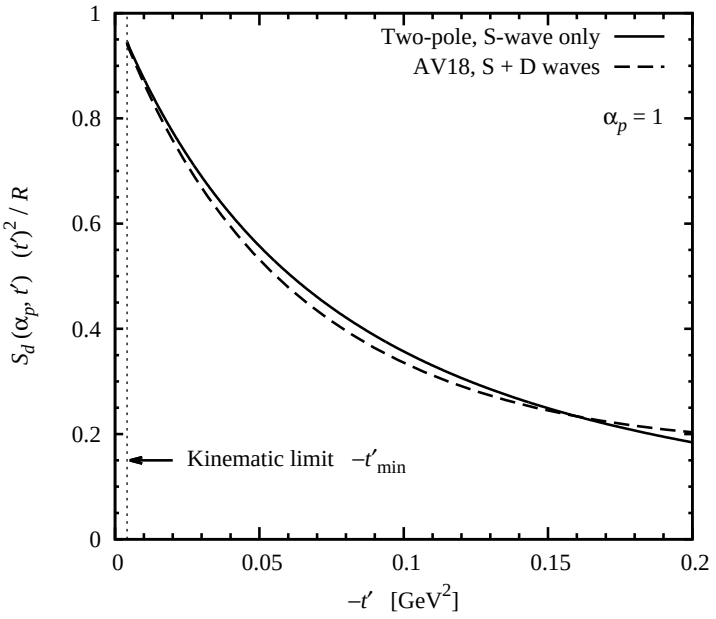

FIG. 7. The deuteron spectral function in the IA, S_d[IA], with the pole factor $R/(t')^2$ extracted, as function of t', for $\alpha_p = 1$. Solid line: Two–pole parametrization of deuteron wave function, Eq. (A1) (S–wave only). Dashed line: AV18 wave function (S + D waves) [55]. The momentum densities are shown in Fig. 17a.

Figure 7 shows the t' dependence of the IA spectral function after extraction of the pole factor $R/(t')^2$. One sees that the dependence is smooth over a broad region $|t'| \lesssim 0.1\,\mathrm{GeV}^2$, suggesting that a polynomial fit would permit accurate extrapolation to $t' = 0$. (The minimum value $|t'_{\rm min}|$ is indicated on the graph.) The plot shows the IA spectral functions obtained with two different deuteron wave functions — the two-pole parametrization of Appendix A (S wave only), and the AV18 wave function (S + D waves) [55]; the differences are very small over the t' range shown here.

V. FINAL–STATE HADRON DISTRIBUTIONS

A. Kinematic variables

FSI in tagged DIS arise from interactions of the spectator nucleon with "slow" hadrons produced by the DIS process on the active nucleon (rest frame momenta $|\boldsymbol{p}_h| \lesssim 1\,\mathrm{GeV}$, or target fragmentation region; see Sec. I). In order to calculate these effects we need to study the properties of the slow hadron distributions in DIS on the nucleon and parametrize them for our purposes. In this section we discuss the kinematic variables characterizing the final–state hadron distributions, the conditional structure functions, and the basic features of experimental distributions.

For the theoretical description of DIS on the nucleon ($N = p, n$) we use a frame where the nucleon momentum $\boldsymbol{p}_N$ and the momentum transfer $\boldsymbol{q}$ are collinear and define the z–axis of the coordinate system (cf. Sec. II C).[3] In such a frame the LF components of the nucleon 4–momentum p_N and the 4–momentum transfer q are

$$\left.\begin{aligned} p_N^+ &> 0 \ \text{(arbitrary)}, \qquad & p_N^- &= \frac{M_N^2}{p_N^+}, \qquad & \boldsymbol{p}_{NT} &= 0, \\ q^+ &= -\xi p_N^+, & q^- &= \frac{Q^2}{\xi p_N^+}, & \boldsymbol{q}_T &= 0, \end{aligned}\right\} \tag{5.1}$$

[3] In the calculation of FSI in tagged DIS on the deuteron below we shall neglect the effect of the active nucleon's transverse momentum on the final-state hadron spectrum, so that the z–axis axis of the virtual photon-nucleon frame coincides with that of the virtual photon-deuteron frame.

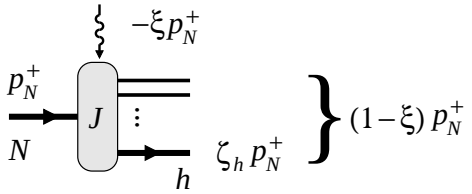

FIG. 8. Current matrix element in DIS on the nucleon with an identified hadron h in the nucleon fragmentation region, $eN \to e' + h + X'$. The LF plus momenta of the final state are expressed as fractions of p_N^+.

where p_N^+ is arbitrary and defines the particular frame, and the variable ξ is determined by

$$\xi \;=\; \frac{2x}{1+\sqrt{1+4M_N^2x^2/Q^2}} \;=\; x \,+\, O(M_N^2/Q^2) \qquad (Q^2 \gg M_N^2). \tag{5.2}$$

With this choice of components the momentum transfer vector $\boldsymbol{q}$ points in the *negative* z–direction, $2q^z = q^+ - q^- < 0$.

An identified hadron h in the DIS final state is characterized by its LF momentum $p_h^+ \equiv \zeta_h p_N^+$ and transverse momentum $\boldsymbol{p}_{hT}$ (see Fig. 8). Because the hadron LF momentum cannot exceed the total LF momentum of the DIS final state, $p_N^+ + q^+ = (1-\xi)p_N^+$, the hadron fraction ζ_h is restricted to

$$0 \;<\; \zeta_h \;<\; 1-\xi. \tag{5.3}$$

In particular, values $\zeta_h \sim 1$ become kinematically accessible only for $x \sim \xi \ll 1$.

It is instructive to consider the hadron momentum distribution in the nucleon rest frame in terms of the ordinary momentum variables. The connection with the LF momentum distribution can established easily, because the nucleon rest frame is a special collinear frame with $p_N^+ = M_N$. The fraction ζ_h is related to the 3–component of the hadron rest frame momentum, p_h^z, by

$$\zeta_h = \frac{\sqrt{(p_h^z)^2 + |\boldsymbol{p}_{hT}|^2 + M_h^2} + p_h^z}{M_N}, \tag{5.4}$$

$$p_h^z = -\frac{|\boldsymbol{p}_{hT}|^2 + M_h^2 - \zeta_h^2 M_N^2}{2\zeta_h M_N}. \tag{5.5}$$

One observes: (a) If $M_h \geq M_N$ (e.g., if the identified hadron is a nucleon) the hadron z–momentum is negative, i.e., along the direction of the $\boldsymbol{q}$–vector. Such hadrons always go "forward" in the rest frame, meaning in the direction of the $\boldsymbol{q}$–vector. The momentum distribution is a cone opening in the negative z–direction. (b) If $M_h < M_N$ (e.g., if the identified hadron is a pion) the hadron z–momentum can be positive for sufficiently small $|\boldsymbol{p}_{hT}|$, i.e., opposite to the direction of the $\boldsymbol{q}$–vector. Such hadrons can go "backwards" in the nucleon rest frame.

Figure 9 shows the momentum distribution of nucleons ($M_h = M_N$) in the nucleon fragmentation region for fixed values of ζ_h. One sees that small longitudinal momenta $p_h^z \to 0$ correspond to LF fractions $\zeta_h \to 1$, and that the cones are shifted to larger longitudinal momenta as ζ_h deviates from unity. Note that ζ_h is kinematically restricted by Eq. (5.3). Figure 10 shows the minimal 3–momentum of nucleons in the nucleon fragmentation region as a function of ξ. The minimal value of the 3–momentum is attained for $\boldsymbol{p}_{hT} = 0$ [see Eq. (5.5) and Fig. 9] and given by

$$|\boldsymbol{p}_h|(\min) \;=\; \frac{\xi(1-\xi/2)M_N}{1-\xi} \qquad (h = N). \tag{5.6}$$

One sees that nucleons with $|\boldsymbol{p}_h| \lesssim 1\,\mathrm{GeV}^2$ appear only if $x \sim \xi \ll 1$. Note that Eq. (5.6) gives only the *kinematic limit*, and that the *average* values of the nucleon momenta in the fragmentation region are substantially larger, because the phase space opens with transverse momentum.

The LF variables ζ_h and $\boldsymbol{p}_{hT}$ can be related to other variables used to characterize experimental hadron distributions in DIS. One commonly used variable is the fraction of the rest-frame energy transfer carried by the hadron,

$$z_h \;\equiv\; \frac{E_h}{\nu}, \qquad \nu \;=\; \frac{Q^2}{2M_N x} \;=\; \frac{Q^2}{2M_N\xi}\left(1 - \frac{\xi^2 M_N^2}{Q^2}\right). \tag{5.7}$$

Using Eq. (5.4) and setting

$$p_h^z \;=\; -\sqrt{E_h^2 - M_{hT}^2}, \qquad M_{hT}^2 \;\equiv\; |\boldsymbol{p}_{hT}|^2 + M_h^2, \tag{5.8}$$

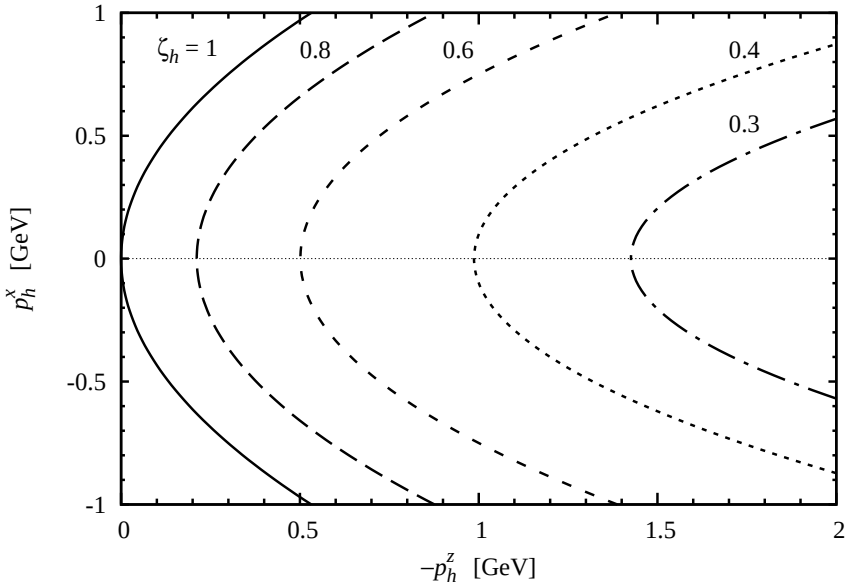

FIG. 9. Momentum distributions of nucleons ($M_h = M_N$) in the nucleon fragmentation region in DIS, $eN \to e' + h + X$. The contours show the allowed values of p_h^z and p_h^x (with $p_h^y = 0$, so that $|\boldsymbol{p}_{hT}| = |p_h^x|$) for given constant values of ζ_h. The contours thus describe the intersection of the allowed 3-momentum cones with the transverse x–plane.

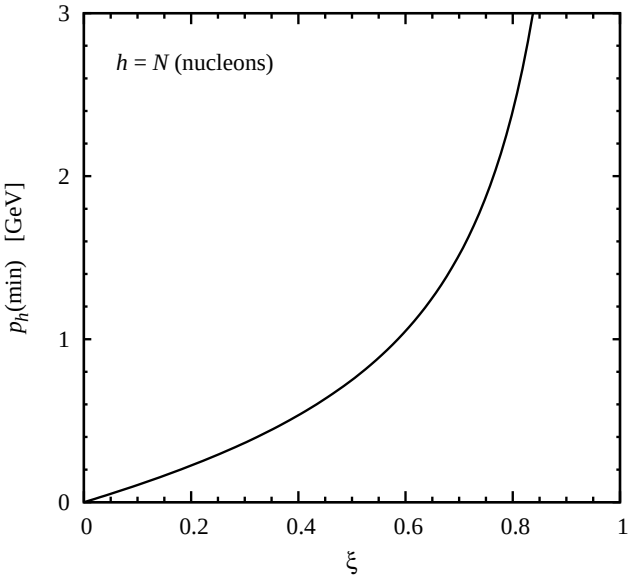

FIG. 10. Minimal 3–momentum $|\boldsymbol{p}_h|$(min) of nucleons ($M_h = M_N$) in the nucleon fragmentation region in DIS, Eq. (5.6), as a function of the variable $\xi = x + O(M_N^2/Q^2)$, Eq. (5.2).

one obtains

$$\zeta_h = \frac{z\nu - \sqrt{(z\nu)^2 - M_{hT}^2}}{M_N} \approx \frac{M_{hT}^2}{2z\nu M_N} = \frac{xM_{hT}^2}{zQ^2} \qquad (z\nu \gg M_{hT}), \tag{5.9}$$

$$z_h = \frac{\zeta_h^2 M_N^2 + M_{hT}^2}{2\zeta_h M_N \nu}. \tag{5.10}$$

One sees that LF fractions $\zeta_h = O(1)$ correspond to parametrically small energy fractions $z = O(M_{hT}/\nu) \ll 1$ in the nucleon rest frame (slow hadrons). Another commonly used variable is the hadron's longitudinal momentum in the

center–of–mass (CM) frame of the virtual photon–nucleon collision, in which $\boldsymbol{q} + \boldsymbol{p}_N = 0$. It is usually expressed in terms of the Feynman scaling variable [4]

$$x_{\rm F} \;\equiv\; -\frac{p_h^z}{p_{h,\rm max}^z}. \tag{5.11}$$

The connection with the LF variables is established by noting that the CM frame is the special collinear frame with

$$p_N^+ \;=\; \sqrt{\frac{Q^2 + \xi M_N^2}{\xi(1-\xi)}}. \tag{5.12}$$

The hadron longitudinal CM momentum is

$$p_h^z \;=\; \frac{p_h^+ + p_h^-}{2} \;=\; \frac{\zeta_h^2 (p_N^+)^2 - M_{hT}^2}{2\zeta_h p_N^+}. \tag{5.13}$$

The maximum (positive) value is attained for $\zeta_h = 1 - \xi$ and $\boldsymbol{p}_{hT} = 0$,

$$p_{h,\rm max}^z \;=\; \frac{(1-\xi)^2 (p_N^+)^2 - M_h^2}{2(1-\xi) p_N^+}. \tag{5.14}$$

The scaling variable is thus obtained as

$$x_{\rm F} = -\frac{(1-\xi)\,[\zeta_h^2 (p_N^+)^2 - M_{hT}^2]}{\zeta_h\,[(1-\xi)^2 (p_N^+)^2 - M_h^2]} \;\approx\; -\frac{\zeta_h}{1-\xi} \qquad (\zeta_h p_N^+ \gg M_{hT}). \tag{5.15}$$

The latter condition is fulfilled if $Q^2 \gg M_{hT}^2$ (DIS limit) and $\zeta_h = O(1)$. One concludes that $-x_{\rm F}$ in the nucleon fragmentation region (from -1 to approximately -0.5) can be identified directly with the normalized hadron LF fraction $\zeta_h/(1-\xi)$. We use this relation in our analysis of experimental slow hadron spectra below.

B. Multiplicity distributions

The hadronic tensor and differential cross section for DIS on the nucleon with an identified final-state hadron h are described by expressions analogous to those for DIS on the deuteron with an identified nucleon in Sec. II B; see Eqs. (2.19) and (2.31). The hadronic tensor is parametrized by conditional nucleon structure functions

$$F_{2N,h}(x, Q^2; \zeta_h, \boldsymbol{p}_{hT}), \qquad etc., \tag{5.16}$$

which depend on the identified hadron's LF momentum fraction ζ_h and transverse momentum $\boldsymbol{p}_{hT}$. It is convenient to extract the inclusive structure functions and write the conditional structure functions in the form

$$F_{2N,h}(x, Q^2; \zeta_h, \boldsymbol{p}_{hT}) = F_{2N}(x, Q^2)\; D_h(x, Q^2; \zeta_h, \boldsymbol{p}_{hT}), \qquad etc. \tag{5.17}$$

The the function D_h describes the normalized differential multiplicity distribution of the hadron h, i.e., the differential number of hadrons dN_h per DIS event observed in a phase space element $d\Gamma_h$:

$$\frac{dN_h}{N_{\rm incl}} \;=\; D_h\, d\Gamma_h, \qquad d\Gamma_h \;=\; \frac{d\zeta_h\, d^2 p_{hT}}{2(2\pi)^3 \zeta_h}. \tag{5.18}$$

As such it can be directly extracted from the experimental multiplicity distributions. In particular, the p_{hT}–integrated LF momentum distribution of the hadron is

$$\frac{1}{N_{\rm incl}} \frac{dN_h}{d\zeta_h} = \frac{1}{2(2\pi)^3 \zeta_h} \int d^2 p_{hT}\; D_h. \tag{5.19}$$

It can be identified with the $x_{\rm F}$ distribution in the nucleon fragmentation region, cf. Eq. (5.15). Note the factor $1/\zeta_h$ on the right-hand side, which results from the definition of the invariant phase space element Eq. (5.18).

---

[4] The variable $x_{\rm F}$ in electroproduction is conventionally defined such that hadrons moving in virtual photon direction have $x_{\rm F} > 0$, and hadrons moving in the target direction have $x_{\rm F} < 0$. In our convention $q^z < 0$ and $p_N^z > 0$; hence the minus sign in Eq. (5.11).

C. Experimental distributions

Measurements of hadron multiplicity distributions in the target fragmentation region in DIS on the nucleon have been reported by several fixed-target experiments using electron beams (Cornell Synchrotron [60]) and muon beams (CERN EMC [61–63], FNAL E665 [24]), as well as at the HERA electron-proton collider [64–67]. Slow hadron distributions were also measured in neutrino-proton DIS experiments [68–70]. While the kinematic coverage is far from complete, these data roughly cover the x–region of interest for our study and allow us to infer the basic features of the multiplicity distributions. Unfortunately many data are not separated according to hadron species, as few dedicated studies of the target fragmentation region have been performed so far. We now briefly review the main features of the data and their theoretical interpretation.

The multiplicity distributions of hadrons with $x_{\rm F} \lesssim -0.2$ are approximately independent of Q^2 for fixed x. Scaling of the distributions is observed in all quoted electron and muon experiments, covering the valence region $x > 0.2$ [60], the region $x \lesssim 0.1$ [24, 61–63], and the small–x region $x < 10^{-2}$ [64–67]. This behavior is consistent with theoretical expectations based on QCD factorization of the conditional DIS cross sections in the target fragmentation region [29, 30]. The multiplicity distributions in the target fragmentation region show only weak variation with x in the region $x \lesssim 0.1$. This indicates that the hadronization of the target remnant is largely independent of the dynamics producing the parton distributions in the nucleon in this region of x (sea quarks, gluons).

The $x_{\rm F}$ distributions of protons (integrated over transverse momentum) in DIS on the proton are approximately flat for $x_{\rm F} < -0.3$. A value of $(1/N_{\rm incl})\, dN_p/dx_{\rm F} \sim 0.5 - 0.6$ at $x_{\rm F} = (-0.7, -0.3)$ was measured by EMC at $\langle x \rangle = 0.1$ [62]. A value $(1/N_{\rm incl})\, dN_p/dx_{\rm F} \sim 0.4$ at $x_{\rm F} = (-0.8, -0.4)$ was obtained by the HERA experiments at $x \lesssim 0.01$ [64, 67]. (At larger negative $x_{\rm F}$ diffraction gives rise to a distinct contribution to the proton spectrum at HERA; this mechanism is marginal in the kinematic region considered here.) The $x_{\rm F}$ distribution of neutrons measured in DIS on the proton at HERA [65, 66] is also flat and has a value of $(1/N_{\rm incl})\, dN_p/dx_{\rm F} \sim 0.2$ at $x_{\rm F} = (-0.8, -0.4)$. The sum of proton and neutron multiplicity distributions is thus $(1/N_{\rm incl})\, dN_{p+n}/dx_{\rm F} \sim 0.6$ at $x_{\rm F} = (-0.8, -0.4)$. That this value is significantly less than 1 shows that part of the baryon number is transported to smaller $x_{\rm F}$ and materializes outside the target region. We note that both the flatness of the distributions and the baryon number transport are reproduced by string models of the fragmentation mechanism.

The transverse momentum distributions of protons and neutrons in the target fragmentation region drop steeply with $p_{T,h}$ and can be approximated by Gaussian distributions $\sim \exp(-B_h p_{hT}^2)$ $(h = p, n)$, where the slope B_h determines the average squared transverse momentum as $\langle p_{hT}^2 \rangle = B_h^{-1}$. The empirical slope for protons is $B_p \sim 4\,{\rm GeV}^{-2}$ at $x > 0.2$ (Cornell) [60] and $B_p = 6$–8 ${\rm GeV}^{-2}$ at $x < 10^{-2}$ (HERA) [64, 67]. A values $B_p \sim 6$ ${\rm GeV}^{-2}$ was also observed in neutrino DIS at $W^2 < 50\,{\rm GeV}^2$ [68].

The multiplicity distribution of charged pions shows very different behavior from that of protons and neutrons. The $x_{\rm F}$ distribution of pions are significantly smaller than those of protons at $x_{\rm F} < -0.3$ but rise strongly at $x_{\rm F} > -0.3$ [62]. Pion production thus happens mainly in the central region of the DIS process and is governed by other dynamical mechanisms than target fragmentation.

D. Implications for FSI

The experimental results described in Sec. V C characterize the slow hadron distributions causing FSI in tagged DIS on the deuteron. We now want to summarize the implications and formulate a simple parametrization of the slow hadron distribution for our subsequent calculations.

The dominant hadrons produced in electron-nucleon DIS at $\zeta_h > 0.2$ are protons and neutrons emerging from the hadronization of the remnant of the active nucleon. These protons and neutrons can interact with the spectator nucleon with the large NN cross section of ~ 40 mb at momenta $|\boldsymbol{p}_h| \sim 1$–$2$ GeV (see Fig. 9 and Appendix C). We therefore suppose that the dominant FSI in tagged DIS at $x \sim 0.1 - 0.5$ arises from such protons and neutrons in the target fragmentation region of the active nucleon. FSI induced by pions could in principle be treated within the same picture but are expected to be small.

If the active nucleon in the deuteron is the proton (i.e., if the neutron is tagged), the multiplicity distributions of slow nucleons (protons plus neutrons) can be inferred directly from the proton DIS data. If the active nucleon is a neutron (proton tagged), we suppose that at $x \sim 0.1$ the distribution of slow nucleons (protons plus neutrons) is approximately the same as in DIS on the proton, because the deep-inelastic process occurs mainly on singlet sea quarks produced by gluon radiation and does not change the flavor structure of the baryon remnant system (we neglect the effect of the flavor asymmetry of sea quarks in this context). Since furthermore the nucleon-nucleon cross section at momenta $\sim$ few GeV is approximately the same for pp, pn and nn scattering (see Appendix C), the FSI effect is the same for deuteron DIS with active proton or active neutron. These approximations permit a model-independent

estimate of FSI effects at $x \sim 0.1$ and will be used in our subsequent calculations. The physical picture of FSI and the formulas derived in the following are valid also at larger x ($\lesssim 0.5$), where the scattering primarily occurs mainly on valence quarks; in this region they should be evaluated with a detailed model of the quark flavor dependence of the slow hadron multiplicity distributions.

In our numerical studies of FSI in tagged deuteron DIS we use a simple parametrization of the multiplicity distribution of slow protons and neutrons, D_h ($h = p, n$), which reflects the basic features of the experimental distributions and offers sufficient flexibility to study the dependence of FSI on the slow hadron distribution. We parametrize the distribution in the form

$$D_h(x, Q^2; \zeta_h, p_{hT}) = [2(2\pi)^3]\ \zeta_h\ f_h(\zeta_h)\ g_h(p_{hT}) \qquad (h = p, n). \tag{5.20}$$

The function $f_h(\zeta_h)$ describes the ζ_h distribution and can be identified with the p_{hT}–integrated multiplicity distribution Eq. (5.19). We choose it such that

$$f_h(\zeta_h) \sim c_h \ = \ \text{const} \qquad (1 > \zeta_h \gtrsim \zeta_0), \tag{5.21}$$

$$f_h(\zeta_h) \to 0 \qquad\qquad (\zeta_h \to 0). \tag{5.22}$$

The constant c_h can be inferred from the experimental proton/neutron ζ_h (or $x_{\rm F}$) distributions in the "flat" region. For the sum of proton and neutron distributions it is

$$\sum_{h=p,n} c_h \ = c_p + c_n \ = \ 0.6 - 0.8. \tag{5.23}$$

The cutoff at $\zeta_h \to 0$ limits the distribution to slow hadrons in the nucleon rest frame, which are fully formed inside the deuteron and interact with the spectator with the NN cross section. A value $\zeta_0 \sim 0.2$ corresponds to rest-frame momenta $|\boldsymbol{p}_h| \lesssim 2$ GeV (see Fig. 9). A simple choice for $f_h(\zeta_h)$ is

$$f_h(\zeta_h) \ \ = \ \ \frac{c_h(\zeta_h/\zeta_0)^n}{1 + (\zeta_h/\zeta_0)^n}, \tag{5.24}$$

where we choose $n = 3$–5; the results are not sensitive to the details of the cutoff. The function $g_h(p_{hT})$ describes the normalized p_{hT} distribution of the protons/neutrons and is modeled by a Gaussian,

$$g_h(p_{hT}) \ = \ \frac{B_h}{\pi} \exp(-B_h p_{hT}^2), \qquad \int d^2p_{hT}\ g_h(p_{hT}) \ = \ 1, \tag{5.25}$$

with an empirical slope

$$B_h \ = \ 6 - 8\,\text{GeV}^{-2} \qquad (h = p, n). \tag{5.26}$$

As explained above, this distribution is used for the slow protons/neutrons in DIS on either the proton or neutron in the deuteron.

In our treatment of FSI we describe the interactions of the slow protons/neutrons with the spectator nucleon as on-shell rescattering with an effective interaction. Off-shell effects are physically related to effects of the finite hadron formation time and can be modeled as a modification of the on-shell effective interaction and the slow proton/neutron distribution. The on-shell effective interaction (scattering amplitude) can be determined from the NN total and elastic cross section data. The main features of the data and and a simple parametrization of the amplitude at incident momenta $|\boldsymbol{p}_h| \lesssim 2\,\text{GeV}$ are described in Appendix C.

VI. FINAL–STATE INTERACTIONS

A. FSI and IA currents

We now proceed to calculate the tagged DIS cross section including FSI between the spectator nucleon and the slow hadrons (protons/neutrons) emerging from the fragmentation of the active nucleon, in the physical picture described in Secs. I and V D. The calculation is performed in LF quantum mechanics in the collinear frame $\boldsymbol{p}_{dT} = 0$ as in Sec. IV and identifies corrections to the IA current and the deuteron tensor resulting from FSI.

To properly account for the configurations in which FSI can and cannot occur, we separate the multi-hadron states X produced in DIS on the nucleon into two classes:

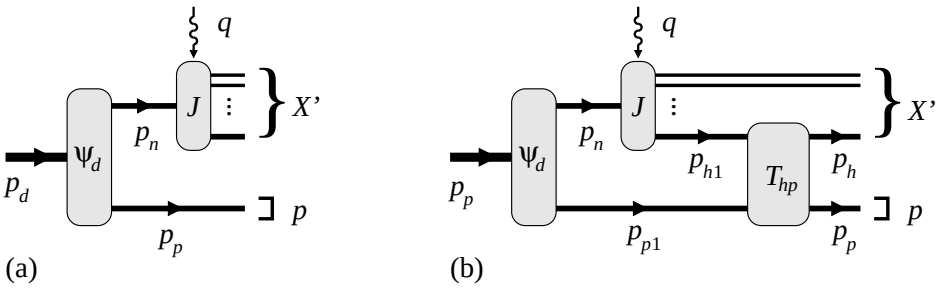

FIG. 11. Current matrix elements in tagged DIS on the deuteron. (a) IA current. (b) FSI between a slow DIS hadron h and the spectator.

(a) Multi-hadron states not containing a slow hadron capable of inducing FSI, which we denote by X_0.

(b) Multi-hadron states containing a slow hadron h capable of inducing FSI, which we denote by X_1. Their state vectors are of the form

$$|X_1\rangle \;=\; |h, X'\rangle \;\equiv\; |h\rangle|X'\rangle, \tag{6.1}$$

where X' is the product state of the remaining hadrons. The summation over these states is performed as

$$\sum_{X_1} \;\equiv\; \int d\Gamma_h \sum_{X'}. \tag{6.2}$$

By construction the classes X_0 and X_1 then exhaust all possible multi-hadron states, and the summation over all states becomes

$$\sum_{X} = \sum_{X_0} + \sum_{X_1}. \tag{6.3}$$

The separation is possible because the average slow hadron multiplicity is < 1 (cf. Sec. V D); i.e., we can assume that the final state contains zero or one slow hadrons, but not more.

We now consider tagged DIS on the deuteron separately for final states X_0 and X_1,

$$e + d \;\to\; e' + p + (X_0 \text{ or } X_1). \tag{6.4}$$

For final states of type X_0 FSI cannot occur, and the transition current is identical to that obtained in the IA, Eqs. (4.2) and (4.3),

$$\langle pX_0|\hat{J}^\mu(0)|d\rangle \;=\; \langle pX_0|\hat{J}^\mu(0)|d\rangle[\text{IA}]. \tag{6.5}$$

For final states of type X_1 the transition current is computed by inserting plane-wave nucleon and slow hadron intermediate states into the current matrix element (cf. Fig. 11),

$$\begin{aligned}\langle pX_1|\hat{J}^\mu(0)|d\rangle \;&\equiv\; \langle phX'|\hat{J}^\mu(0)|d\rangle \\ &= \int [dp_n] \int [dp_{p1}] \int [dp_{h1}]\; \langle p, p_p; h, p_h|p, p_{p1}; h, p_{h1}\rangle \\ &\times\; \langle X'; h, p_{h1}|\hat{J}^\mu(0)|n, p_n\rangle\; \langle p, p_{p1}; n, p_n|d, p_d\rangle. \end{aligned} \tag{6.6}$$

FSI between the slow hadron and the spectator are now incorporated by taking the hadron–spectator final state not as a product state (as is done in the IA) but as the scattering state generated by interactions between them. The boundary conditions for the scattering state correspond to the incoming–wave solution [71],

$$\langle p, p_p; h, p_h| \;\to\; {}_{\text{in}}\langle p, p_p; h, p_h|. \tag{6.7}$$

Following standard practice in nuclear physics we can express the wave function of this scattering state in terms of the effective interaction operator $\hat{T}$ (or T–matrix) corresponding to the interaction,

$${}_{\text{in}}\langle p, p_p; h, p_h|p, p_{p1}; h, p_{h1}\rangle \;=\; \langle p, p_p; h, p_h|p, p_{p1}; h, p_{h1}\rangle \;-\; \frac{\langle p, p_p; h, p_h|\,\hat{T}\,|p, p_{p1}; h, p_{h1}\rangle}{\frac{1}{2}(p_p^- + p_h^- - p_{p1}^- - p_{h1}^- + i0)}. \tag{6.8}$$

Equation (6.8) represents the LF analogue of the Lippmann–Schwinger equation in non-relativistic quantum mechanics. The denominator is the difference of LF energies between the initial and final states (the LF Hamiltonian in our convention is $\hat{H}_{\rm LF} = \frac{1}{2}\hat{P}^-_{\rm tot}$; see Appendix 1 of Ref. [72]). In the context of a time-dependent formulation Eq. (6.8) can be regarded as the matrix element of the LF time evolution operator corresponding to the hadron–spectator interaction between LF time $x^+ = 0$ (when the current creates the state h) and $x^+ \to +\infty$ (when the interactions are switched off),

$$ {}_{\rm in}\langle p, p_p; h, p_h | p, p_{p1}; h, p_{h1}\rangle \;=\; \langle p, p_p; h, p_h |\, \hat{U}(\infty, 0)\, | p, p_{p1}; h, p_{h1}\rangle. \tag{6.9}$$

This representation makes it obvious that the scattering state obeys incoming-wave boundary conditions.[5]

The effective interaction operator in Eq. (6.8) conserves the total LF momentum of the states. Using translational invariance, we can write the matrix element in the numerator of Eq. (6.8) in the form

$$\begin{aligned}\langle p, p_p; h, p_h |\, \hat{T}\, | p, p_{p1}; h, p_{h1}\rangle \;&=\; (2\pi)^3\, \delta(p_p^+ + p_h^+ - p_{p1}^+ - p_{h1}^+)\, \delta^{(2)}(\boldsymbol{p}_{pT} + \boldsymbol{p}_{hT} - \boldsymbol{p}_{p1T} - \boldsymbol{p}_{h1T}) \\ &\times\; T(p_p, p_h; p_{p1}, p_{h1}),\end{aligned} \tag{6.10}$$

where no assumption is made about the LF energies of the initial and final states. The on-shell part of the scattering term in Eq. (6.8), in which the total final LF energy is equal to initial one, is obtained by retaining the pole term of the energy denominator,

$$\left.\frac{\langle p, p_p; h, p_h |\, \hat{T}\, | p, p_{p1}; h, p_{h1}\rangle}{\frac{1}{2}(p_p^- + p_h^- - p_{p1}^- - p_{h1}^- - i0)}\right|_{\rm on-shell}$$

$$= i\,(2\pi)\,\delta(p_p^- + p_h^- - p_{p1}^- - p_{h1}^-)\,\langle p, p_p; h, p_h |\, \hat{T}\, | p, p_{p1}; h, p_{h1}\rangle \tag{6.11}$$

$$= i\,(2\pi)^4\,\delta(p_p^- + p_h^- - p_{p1}^- - p_{h1}^-)\,\delta(p_p^+ + p_h^+ - p_{p1}^+ - p_{h1}^+)\,\delta^{(2)}(\boldsymbol{p}_{pT} + \boldsymbol{p}_{hT} - \boldsymbol{p}_{p1T} - \boldsymbol{p}_{h1T})\,T \tag{6.12}$$

$$= i\,(2\pi)^4\,\delta^{(4)}(p_p + p_h - p_{p1} - p_{h1})\,\frac{T}{2}. \tag{6.13}$$

Here T is the on-shell matrix element of effective interaction, which coincides with the invariant amplitude of the physical $ph \to ph$ scattering process,

$$T(p_p, p_h; p_{p1}, p_{h1}) = \mathcal{M}(s_{ph}, t_{ph}), \tag{6.14}$$

$$s_{ph} \;\equiv\; (p_{p1} + p_{h1})^2 = (p_p + p_h)^2, \tag{6.15}$$

$$t_{ph} \;\equiv\; (p_{p1} - p_p)^2 = (p_{h1} - p_h)^2. \tag{6.16}$$

Equations (6.8)–(6.16) allow us to express the FSI matrix element in terms of the physical $ph \to ph$ amplitude within our scheme of approximations. The factor 1/2 in Eq. (6.13) accounts for the fact that the interaction in the matrix element is present only from $x^+ = 0$ to ∞ (i.e, "half the time"), while in the scattering process it is present from $x^+ = -\infty$ to ∞. We note that the same factor 1/2 is obtained in an equivalent calculation of the FSI effect in the current matrix element using invariant perturbation theory, where it appears from the Cutkosky rules for the on-shell part of the Feynman diagram.

We can now derive from Eq. (6.6) the explicit expressions for the transition current to X_1 states. The $d \to pn$ matrix element in Eq. (6.6) is expressed in terms of the deuteron LF wave function Eq. (3.9). The FSI matrix element is substituted by Eq. (6.8). The non-interaction term on the R.H.S. results in an expression of the same form as the IA result, Eq. (4.3). The interaction term is expressed in terms of the on-shell scattering amplitude using Eqs. (6.13) and (6.14). Altogether the transition current to X_1 states, Eq. (6.6), can be written as the sum of an IA and an FSI term,

$$\langle pX_1|\hat{J}^\mu(0)|d\rangle \;\equiv\; \langle phX'|\hat{J}^\mu(0)|d\rangle \;=\; \langle \ldots\rangle\,[\mathrm{IA}] \;+\; \langle \ldots\rangle\,[\mathrm{FSI}] \tag{6.17}$$

$$\langle phX'|\hat{J}^\mu(0)|d\rangle\,[\mathrm{IA}] \;=\; \frac{p_d^+}{p_n^+}\,\langle h, p_h; X'|\hat{J}^\mu(0)|n, p_n\rangle\,(2\pi)^{3/2}\,\Psi_d(\alpha_p, \boldsymbol{p}_{pT})$$

---

[5] The formal operator generating a two-body scattering state from the product states [cf. Eq. (6.8)] is known as the Møller operator and can be defined in a general context. Its representation as the limit of a time evolution operator depends on asymptotic conditions; for a discussion see Refs. [73–75].

$$[p_n^+ = p_d^+ - p_p^+,\ \boldsymbol{p}_{nT} = -\boldsymbol{p}_{pT}], \tag{6.18}$$

$$\begin{aligned}\langle phX'|\hat{J}^\mu(0)|d\rangle\,[\mathrm{FSI}] = \int [dp_{p1}]\,\frac{p_d^+}{p_n^+}\,\langle h, p_{h1}; X'|\hat{J}^\mu(0)|n, p_n\rangle\,(2\pi)^{3/2}\,\Psi_d(\alpha_{p1}, \boldsymbol{p}_{p1T}) \\ \times\ \frac{2\pi}{p_{h1}^+}\,\delta(p_p^- + p_h^- - p_{p1}^- - p_{h1}^-)\,\frac{i}{2}\,\mathcal{M}(s_{ph}, t_{ph})\end{aligned}$$

$$\begin{aligned}&[p_n^+ = p_d^+ - p_{p1}^+,\ \boldsymbol{p}_{nT} = -\boldsymbol{p}_{p1T};\\ &p_{h1}^+ = p_h^+ + p_p^+ - p_{p1}^+,\ \boldsymbol{p}_{h1T} = \boldsymbol{p}_{hT} + \boldsymbol{p}_{pT} - \boldsymbol{p}_{p1T}],\end{aligned} \tag{6.19}$$

where s_{ph} and t_{ph} are given by Eqs. (6.16) and (6.16).

B. Distorted spectral function

The deuteron tensor for tagged DIS in the presence of FSI is obtained as the product of the current matrix element and its complex conjugate, summed over all final states X, Eq. (2.19). In accordance with the distinction between final states with zero and one slow hadron, X_0 and X_1, we now write this sum as

$$\begin{aligned}W_d^{\mu\nu} \ &= \ \sum_{X_0}\langle d|\hat{J}^\mu(0)|pX_0\rangle\ \langle pX_0|\hat{J}^\nu(0)|d\rangle \\ &+\ \sum_{X_1}\langle d|\hat{J}^\mu(0)|pX_1\rangle\ \langle pX_1|\hat{J}^\nu(0)|d\rangle,\end{aligned} \tag{6.20}$$

and substitute the expressions Eq. (6.5) and Eqs. (6.17)–(6.19) for the different current matrix elements. It is easy to see that in Eq. (6.20) the sum over states X_0 (for which the current is always of IA form), and the part of the sum over states X_1 involving the IA term of the currents (in which no FSI takes place), reproduce the original IA result for the deuteron tensor, Eq. (4.4),

$$\begin{aligned}&\sum_{X_0}\langle d|\hat{J}^\mu(0)|pX_0\rangle[\mathrm{IA}]\ \langle pX_0|\hat{J}^\nu(0)|d\rangle[\mathrm{IA}] \\ +\ &\sum_{X_1}\langle d|\hat{J}^\mu(0)|pX_1\rangle[\mathrm{IA}]\ \langle pX_1|\hat{J}^\nu(0)|d\rangle[\mathrm{IA}] \\ =\ &\sum_{X}\langle d|\hat{J}^\mu(0)|pX\rangle[\mathrm{IA}]\ \langle pX|\hat{J}^\nu(0)|d\rangle[\mathrm{IA}] \ \ =\ \ W_d^{\mu\nu}[\mathrm{IA}].\end{aligned} \tag{6.21}$$

Here we have used that the sum over states X_0 and X_1 exhausts the full set of inclusive final states X, Eq. (6.3).

Corrections to the IA tensor arise from the FSI terms in the currents in the sum over states X_1 in Eq. (6.20). These corrections come in two types: (a) the products of the FSI term of one current and the IA term of the other (linear FSI); (b) the product of the FSI terms from both currents (quadratic FSI).

Consider the linear FSI correction arising from the product of the FSI current Eq. (6.19) and the complex conjugate IA current Eq. (6.18). Because of the momentum integral in the FSI current, the momentum of the active neutron in the FSI current, p_n^+ and $\boldsymbol{p}_{nT}$, is generally different from that in the IA current. The corresponding neutron current matrix elements can therefore not generally be combined to form the neutron tensor (which is diagonal in the neutron momentum), as was done for the IA in Eq. (4.4). An important simplification arises from the fact that the characteristic momenta in deuteron wave function are much smaller than in nucleon current matrix element. The latter is therefore not affected by the small shift of the active neutron momentum caused by the FSI integral and can be evaluated at the nominal active neutron momentum defined by the IA.

A similar simplification can be made regarding the slow hadron momentum in the neutron current matrix element. Under the FSI integral the slow hadron produced by the nucleon current has momentum p_{h1}^+ and $\boldsymbol{p}_{h1T}$, which differs from the momentum it has in the IA, p_h^+ and $\boldsymbol{p}_{hT}$, by the momentum transfer through the rescattering process. Assuming that this momentum transfer is much smaller than the typical slow hadron momentum, we can evaluate the nucleon current at the nominal slow hadron momentum defined by the IA. Together, the two approximations imply that the nucleon current matrix elements are evaluated at the *same nucleon and slow hadron momenta* in both the FSI and IA, so that their product can be replaced by the nucleon tensor.

With these simplifications we can write the FSI term of the current matrix element, Eq. (6.19), in the form

$$\langle phX'|\hat{J}^\mu(0)|d\rangle\,[\mathrm{FSI}] \;=\; \frac{p_d^+}{p_n^+}\,\langle h,p_h;X'|\hat{J}^\mu(0)|n,p_n\rangle\,(2\pi)^{3/2}\,iI_d,$$
$$[p_n^+ = p_d^+ - p_p^+,\; \boldsymbol{p}_{nT} = -\boldsymbol{p}_{pT}], \tag{6.22}$$

$$I_d \equiv I_d(\alpha_p,\boldsymbol{p}_{pT},\alpha_h,\boldsymbol{p}_{hT}) \;\equiv\; \int [dp_{p1}]\;\frac{2\pi}{p_{h1}^+}\,\delta(p_p^- + p_h^- - p_{p1}^- - p_{h1}^-)\,\frac{1}{2}\,\Psi_d(\alpha_{p1},\boldsymbol{p}_{p1T})\,\mathcal{M}(s_{ph},t_{ph})$$
$$[p_{h1}^+ = p_h^+ + p_p^+ - p_{p1}^+,\; \boldsymbol{p}_{h1T} = \boldsymbol{p}_{hT} + \boldsymbol{p}_{pT} - \boldsymbol{p}_{p1T}]. \tag{6.23}$$

The function I_d represents the integral of the deuteron LF wave function and the rescattering amplitude over the phase space available for the rescattering process, defined by the LF momenta of the final–state particles. Note that we have extracted the factor of i from the rescattering integral and exhibit it explicitly in Eq. (6.22). The complete deuteron tensor emerging from the IA and FSI current matrix elements, Eqs. (6.17) and (6.22), including the pure IA contribution Eq. (6.21), is then obtained as

$$W_d^{\mu\nu} \;\equiv\; W_d^{\mu\nu}(p_d,q,p_p) \;=\; W_d^{\mu\nu}[\mathrm{IA}] \;+\; W_d^{\mu\nu}[\mathrm{FSI}] \;+\; W_d^{\mu\nu}[\mathrm{FSI}^2], \tag{6.24}$$

$$W_d^{\mu\nu}[\mathrm{IA}] \;=\; (2\pi)^3\,\left(\frac{p_d^+}{p_n^+}\right)^2\,|\Psi_d|^2\,W_n^{\mu\nu}(p_n,\widetilde{q}), \tag{6.25}$$

$$W_d^{\mu\nu}[\mathrm{FSI}] \;=\; (2\pi)^3\,\left(\frac{p_d^+}{p_n^+}\right)^2\,\sum_h\,\int_{\mathrm{phas}}[dp_h]\,(-2)\,\mathrm{Im}\,[\Psi_d I_d]\;W_{n,h}^{\mu\nu}(p_n,\widetilde{q},p_h), \tag{6.26}$$

$$W_d^{\mu\nu}[\mathrm{FSI}^2] \;=\; (2\pi)^3\,\left(\frac{p_d^+}{p_n^+}\right)^2\,\sum_h\,\int_{\mathrm{phas}}[dp_h]\,|I_d|^2\;W_{n,h}^{\mu\nu}(p_n,\widetilde{q},p_h) \tag{6.27}$$
$$[p_n^+ = p_d^+ - p_p^+,\; \boldsymbol{p}_{nT} = 0].$$

The linear and quadratic FSI terms include integration over the phase space of the unobserved slow hadron h; the physical limits of the phase space are denoted by "phas" and will be specified below. In addition, they include the summation over the relevant slow hadron species h. From Eqs. (6.25)–(6.27) expressions for the tagged deuteron structure functions can be obtained by performing suitable projections (see Appendix B). The operations are the same as in the IA calculation in Sec. IV D. When applying the projections, the conditional neutron tensor produces the conditional neutron structure functions,

$$W_{n,h}^{\mu\nu}(p_n,\widetilde{q},p_h) \;\to\; F_{2n,h}(\widetilde{x},Q^2;\zeta_h,p_{hT}) \;=\; F_{2n}(\widetilde{x},Q^2)D_h(\widetilde{x},Q^2;\zeta_h,p_{hT}) \quad \text{etc.}$$
$$[\widetilde{x} = x/(2-\alpha_p)]. \tag{6.28}$$

The tagged deuteron structure functions can be expressed in a form analogous to the IA, Eq. (4.20), in terms of a "distorted" spectral function,

$$F_{2d}(x,Q^2;\alpha_p,p_{pT}) \;=\; S_d(\alpha_p,\boldsymbol{p}_{pT})[\mathrm{dist}]\;F_{2n}\left(\widetilde{x},Q^2\right), \tag{6.29}$$

$$S_d[\mathrm{dist}] \;\equiv\; S_d[\mathrm{IA}] \;+\; S_d[\mathrm{FSI}] \;+\; S_d[\mathrm{FSI}^2]. \tag{6.30}$$

The explicit expressions of the terms are

$$S_d[\mathrm{IA}] \;=\; \frac{|\Psi_d|^2}{2-\alpha_p}, \tag{6.31}$$

$$S_d[\mathrm{FSI}] \;=\; \frac{1}{2-\alpha_p}\,\sum_h\,\int_{\mathrm{phas}}[dp_h]\,(-2)\,\mathrm{Im}\,[\Psi_d I_d]\;D_h, \tag{6.32}$$

$$S_d[\mathrm{FSI}^2] \;=\; \frac{1}{2-\alpha_p}\,\sum_h\,\int_{\mathrm{phas}}[dp_h]\,|I_d|^2\;D_h. \tag{6.33}$$

It remains to determine the kinematic limits of the phase space integral over the final-state slow hadron LF momentum in Eqs. (6.32) and (6.33), or Eqs. (6.26) and (6.27). We work in a collinear frame (cf. Sec. II C) and parametrize the LF plus momentum of the slow hadron and the recoil nucleon as fractions of $p_d^+/2$ [cf. Eq. (D8)],

$$p_h^+ \;=\; \frac{\alpha_h p_d^+}{2}, \qquad p_p^+ \;=\; \frac{\alpha_p p_d^+}{2}. \tag{6.34}$$

On general grounds the plus momentum fractions of the slow hadron and the recoil nucleon in the final state of DIS on the deuteron are bounded by [cf. Sec. V A and Eq. (5.3); we approximate $\xi_d \approx x_d$ and set $x_d = x/2$, cf. Eq. (2.7)]

$$0 \;<\; \alpha_h + \alpha_p \;<\; 2(1 - x_d) \;=\; 2 - x. \tag{6.35}$$

For given α_p, the phase space integral over the slow hadron momentum is therefore restricted to

$$\alpha_h \;<\; 2 - \alpha_p - x. \tag{6.36}$$

The LF momentum fraction of the slow hadron with respect to the active nucleon is

$$\zeta_h \;=\; \frac{p_h^+}{p_d^+ - p_p^+} \;=\; \frac{\alpha_h}{2 - \alpha_p}. \tag{6.37}$$

From Eq. (6.36) it follows that

$$\zeta_h \;=\; \frac{\alpha_h}{2 - \alpha_p} \;<\; 1 - \frac{x}{2 - \alpha_p} \;=\; 1 - \widetilde{x}, \tag{6.38}$$

as it should be for the DIS final state on the nucleon, cf. Eq. (5.3). Thus ζ_h is has the correct kinematic limits within our scheme of approximations.

The expressions of Eqs. (6.25)–(6.27) and (6.31)–(6.33) were derived neglecting spin degrees of freedom (deuteron as S–wave bound state, nucleon spins averaged over). They can easily be generalized to account for spin, by including the summation over the nucleon spins and the S– and D–wave components of the deuteron wave function. In this case an interference contribution to the FSI appears only if the spectator protons in the final state of the IA and FSI amplitudes have the same spin projection. This can happen either if they had the same spin in the inital deuteron wave function (S–wave or D–wave) and the proton spin was preserved in the rescattering process, or if they had different spins (S–D–wave interference) and the proton spin was flipped during the rescattering process (more complex trajectories, in which the spin of the active neutron in the two amplitudes is different, are also possible). Such S–D–wave interference effects are small at rest frame momenta $|\boldsymbol{p}_p| < 200\,\mathrm{MeV}$, where the deuteron's nonrelativistic momentum density is dominated by the S–wave (see Fig. 17).

C. Factorized approximation

In the rescattering integral Eq. (6.23) and the spectral function Eqs. (6.31)–(6.33), the deuteron wave function is evaluated at physical nucleon momenta, away from the singularities. Furthermore, since we neglect polarization degrees of freedom, the wave function does not contain any complex factors associated with spin dependence (cf. Sec. III C). The deuteron wave function can therefore be taken as explicitly real. The expression in the integrand of Eq. (6.32) can thus be simplified as

$$-2\,\mathrm{Im}\,[\Psi_d I_d] \;\;\to\;\; -2\,\Psi_d\,\mathrm{Im}\,[I_d]. \tag{6.39}$$

The phase of the rescattering integral Eq. (6.23) is determined by the phase of the rescattering amplitude,

$$\left.\begin{matrix}\mathrm{Re}\,I_d \\ \mathrm{Im}\,I_d\end{matrix}\right\} \;=\; \int [dp_{p1}]\;\frac{2\pi}{p_{h1}^+}\,\delta(p_p^- + p_h^- - p_{p1}^- - p_{h1}^-)\,\frac{1}{2}\,\Psi_d \left\{\begin{matrix}\mathrm{Re}\,\mathcal{M}(s_{ph}, t_{ph}) \\ \mathrm{Im}\,\mathcal{M}(s_{ph}, t_{ph})\end{matrix}\right\}, \tag{6.40}$$

where the momentum assignments are the same as in Eq. (6.23).

The evaluation of the rescattering integral of Eq. (6.23) or Eq. (6.40) is described in Appendix D. There we solve the constraint of the LF-energy-conserving delta function and determine the kinematic limits of the intermediate spectator nucleon LF variables ζ_{h1} and $\boldsymbol{p}_{h1T}$. We also show that the integral can be represented in a manifestly relativistically

invariant form, which is useful for comparing the LF formulation of FSI with the relativistically invariant formulation (virtual nucleon formulation) used in quasi–elastic high–energy scattering on the deuteron.

In the rescattering integral the deuteron wave function is convoluted with the proton–hadron (ph) elastic scattering amplitude. At the recoil momenta considered here ($p_p \lesssim 200\,\mathrm{MeV}$ in the deuteron rest frame), the integral is dominated by average proton momenta in the deuteron wave function. In this region the momentum dependence of the deuteron wave function is much steeper than that of the ph amplitude, because the deuteron size is much larger than the range of the hN interaction,

$$\text{deuteron size} \;\gg\; \text{range of hadron–nucleon interaction.} \tag{6.41}$$

This circumstance allows us to neglect the dependence of the ph scattering amplitude on the initial nucleon momentum p_{p1} in the rescattering integral (we do, however, retain the dependence of the scattering amplitude on the final p_p). The invariant momentum transfer in the ph scattering amplitude becomes

$$t_{ph} \;\to\; (p_d/2 - p_p)^2 \;=\; t' \,+\, O(\epsilon_d M_N), \tag{6.42}$$

and we replace the elastic amplitude in Eq. (6.40) by

$$\mathcal{M}(s_{ph}, t_{ph}) \;\to\; \mathcal{M}(s_{ph}, t'). \tag{6.43}$$

The rescattering integral then factorizes as

$$\left.\begin{matrix}\mathrm{Re}\, I_d \\ \mathrm{Im}\, I_d\end{matrix}\right\} \;=\; \frac{1}{2}\,\Phi_d \;\times\; \left\{\begin{matrix}\mathrm{Re}\,\mathcal{M}(s_{ph}, t') \\ \mathrm{Im}\,\mathcal{M}(s_{ph}, t')\end{matrix}\right\},$$

$$\Phi_d \;\equiv\; \int [dp_{p1}]\;\frac{2\pi}{p^+_{h1}}\;\delta(p^-_p + p^-_h - p^-_{p1} - p^-_{h1})\;\;\Psi_d(\alpha_{p1}, \boldsymbol{p}_{p1T}). \tag{6.44}$$

The function Φ_d represents the integral of the deuteron wave function over the phase space defined by the rescattering process, but is independent of the rescattering amplitude. It can be computed in closed form and permits a very efficient evaluation of the rescattering integral. In this approximation the parts of the distorted spectral function, Eqs. (6.31)–(6.33), become

$$S_d[\mathrm{IA}] = \frac{|\Psi_d|^2}{2 - \alpha_p}, \tag{6.45}$$

$$S_d[\mathrm{FSI}] = \frac{\Psi_d}{2 - \alpha_p}\;\sum_h\;\int_{\mathrm{phas}} [dp_h]\;\Phi_d\;[-\mathrm{Im}\,\mathcal{M}]\;D_h, \tag{6.46}$$

$$S_d[\mathrm{FSI}^2] = \frac{1}{2 - \alpha_p}\;\sum_h\;\int_{\mathrm{phas}} [dp_h]\;\Phi_d^2\;\frac{1}{4}[(\mathrm{Re}\,\mathcal{M})^2 + (\mathrm{Im}\,\mathcal{M})^2]\;D_h. \tag{6.47}$$

Figure 12 shows the numerical results for the FSI term in the distorted spectral function obtained with the exact integral Eq. (6.32) and the factorized approximation Eq. (6.46), in typical kinematics (the choice of parameters is explained below). One sees that the factorized formula provides an excellent approximation to the exact integral in our kinematics.

D. Positivity properties

Some comments are in order regarding the sign of the FSI correction and the positivity of the spectral function. The imaginary part of the elastic rescattering amplitude is related to the total proton–hadron cross section at the given energy by the optical theorem (cf. Appendix C for the case that the hadron is a nucleon, $h = p, n$), and therefore satisfies

$$\mathrm{Im}\,\mathcal{M}(s_{ph},\, t_{ph} = 0) \;>\; 0. \tag{6.48}$$

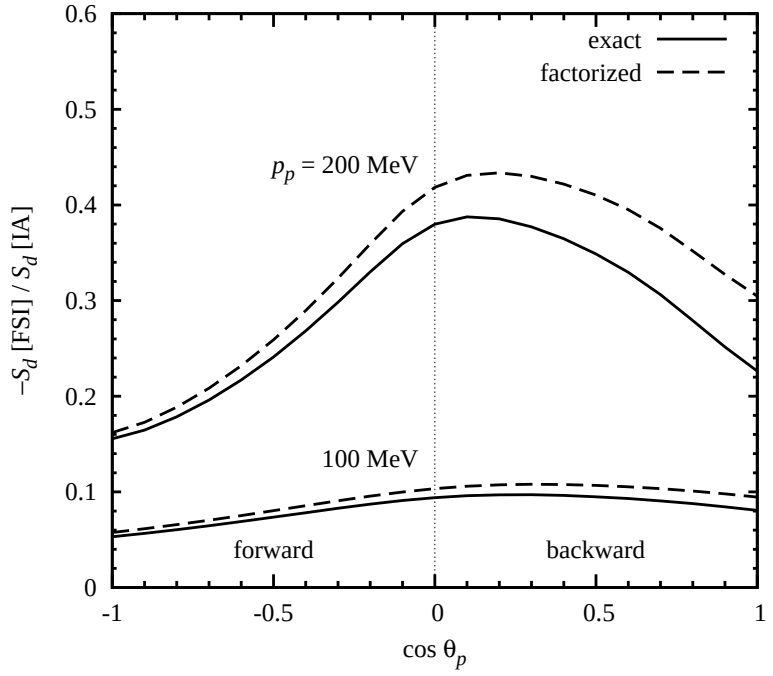

FIG. 12. Comparison of exact result and the factorized approximation for the distorted linear FSI term of the distorted deuteron spectral function, Eqs. (6.32) and (6.46). The plot shows the ratio $-S_d[\mathrm{FSI}]/S_d[\mathrm{IA}]$ as a function of the cosine of the recoil momentum angle in the deuteron rest frame, $\cos\theta_p$, for two values of the recoil momentum modulus $p_p \equiv |\boldsymbol{p}_p|$, as indicated on the plot. Model parameters are described in the text.

As a result, the contribution to the spectral function that arises from the interference of FSI and IA amplitudes and is linear in the FSI amplitude, Eq. (6.32), is explicitly negative

$$S_d[\mathrm{FSI}] \;<\; 0. \tag{6.49}$$

In contrast, the contribution that arises from the square of the FSI amplitude, Eq. (6.33), is explicitly positive,

$$S_d[\mathrm{FSI}^2] \;>\; 0. \tag{6.50}$$

These findings have a simple interpretation in terms of conventional quantum–mechanical scattering theory. The linear term in the FSI amplitude represents the loss of flux due to absorption of the outgoing hadron–nucleon wave at a given value of the final nucleon momentum. The quadratic term represents the gain in cross section due to scattering of the outgoing wave into a configuration with the given value of the final nucleon momentum. In the language of wave optics, the two effects can be referred to as "absorption" and "refraction." One expects that absorption is the dominant effect at low recoil momenta, while refraction becomes dominant at large recoil momenta. This expectation is borne out by the numerical results described below.

The total distorted spectral function must be positive,

$$S_d[\mathrm{dist}] \;>\; 0. \tag{6.51}$$

as it represents the physical cross section for tagged DIS on the deuteron. In our scheme this is ensured by the fact that the hadronic tensor (i.e., the cross section) is calculated as the square of the current matrix element with the outgoing distorted wave. The further approximations made in the distorted spectral function do not change this basic property. Because the linear term in the FSI amplitude is negative, Eq. (6.49), both the linear and quadratic terms are needed to ensure positivity of the overall spectral function. This is again demonstrated by the numerical results.

E. Recoil momentum dependence

We now evaluate the distorted spectral function numerically and study the magnitude of the distortion and its kinematic dependence on the recoil proton momentum. The parameters of the slow-hadron distribution and the

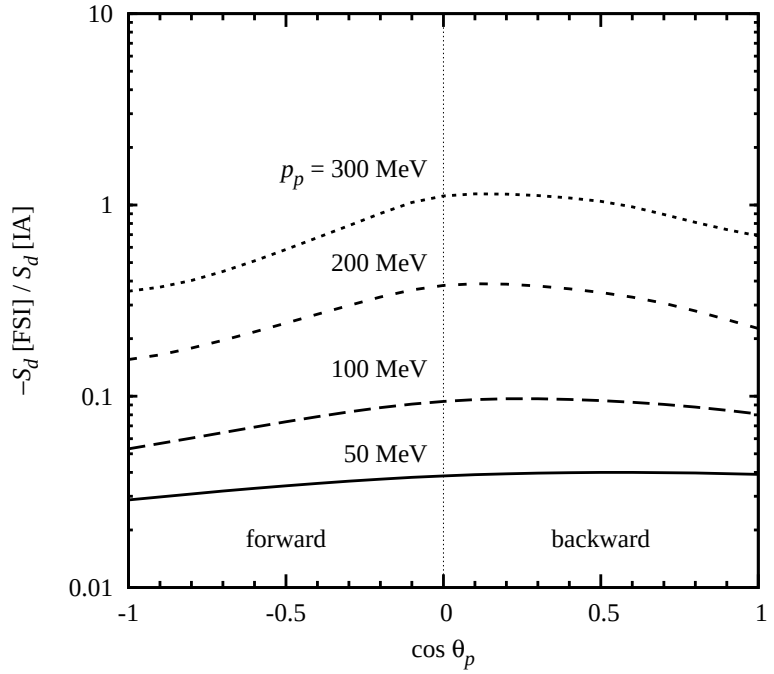

FIG. 13. The ratio of the FSI and IA deuteron spectral functions, $-S_d[\mathrm{FSI}]/S_d[\mathrm{IA}]$, Eqs. (6.31) and (6.32), as a function of the cosine of the recoil momentum angle in the deuteron rest frame, $\cos\theta_p$, for several values of the recoil momentum modulus $p_p \equiv |\boldsymbol{p}_p|$, as indicated on the plot. Note that the ratio shown here includes only the term linear in the FSI amplitude, not the quadratic one. Model parameters are described in the text.

rescattering amplitude are described in Sec. V D and Appendix C. Throughout we consider a value of $x \sim \xi \sim 0.1$, which is so small that it does not significantly restrict the slow hadron momentum, so that the integration can be carried out over the full range $0 < \zeta_h < 1$ [cf. Eq. (5.3) and Figs. 9 and 10]; the calculations can easily be extended to larger values of x.

The spectral function can be studied as a function of any of the recoil momentum variables described in Sec. II D. The most transparent representation is obtained using as independent variables the modulus and angle of the recoil momentum in the deuteron rest frame (which is a special collinear frame, cf. Sec. II D),

$$p_p \equiv |\boldsymbol{p}_p(\mathrm{RF})|, \qquad \cos\theta_p = \frac{p_p^z(\mathrm{RF})}{|\boldsymbol{p}_p(\mathrm{RF})|}. \tag{6.52}$$

Their relation to the variables t' and α_p is given by Eqs. (2.53) and (2.62).

Figure 13 shows the ratio of the linear FSI term in the distorted spectral function, $S_d[\mathrm{FSI}]$, Eq. (6.32), to the IA term, $S_d[\mathrm{IA}]$, Eq. (6.31), as a function of $\cos\theta_p$, for several values of p_p. This ratio describes the relative correction to the IA arising from the linear FSI term. Note that $S_d[\mathrm{FSI}] < 0$, and the ratio is plotted with a minus sign in order to display it on a logarithmic scale. The following features are apparent:

- The correction from the linear FSI term increases in magnitude with the recoil momentum, from a few percent at $p_p \sim 50\,\mathrm{MeV}$ to $O(1)$ at $\sim 200\,\mathrm{MeV}$.
- The correction is isotropic at low p_T and becomes peaked at $\cos\theta_p \sim 0$ at larger momenta, corresponding to the nucleon emerging at approximately $\theta_p \sim \pi/2 = 90\,\mathrm{deg}$ in the deuteron rest frame.

Figure 14 shows the ratio of the entire distorted spectral function, $S_d[\mathrm{dist}]$, including the IA, FSI and FSI^2 terms, Eqs. (6.30)–(6.33), to the IA spectral function $S_d[\mathrm{IA}]$. In other words, it shows the factor by which the IA spectral function is modified by the entire FSI effect. The following features are apparent:

- At low recoil momenta $p_p \lesssim 300\,\mathrm{MeV}$ the linear FSI term dominates and the FSI effect is mainly absorptive, reducing the spectral function relative to the IA. In this region the distorted spectral function has a minimum at $\cos\theta_p \sim 0$.

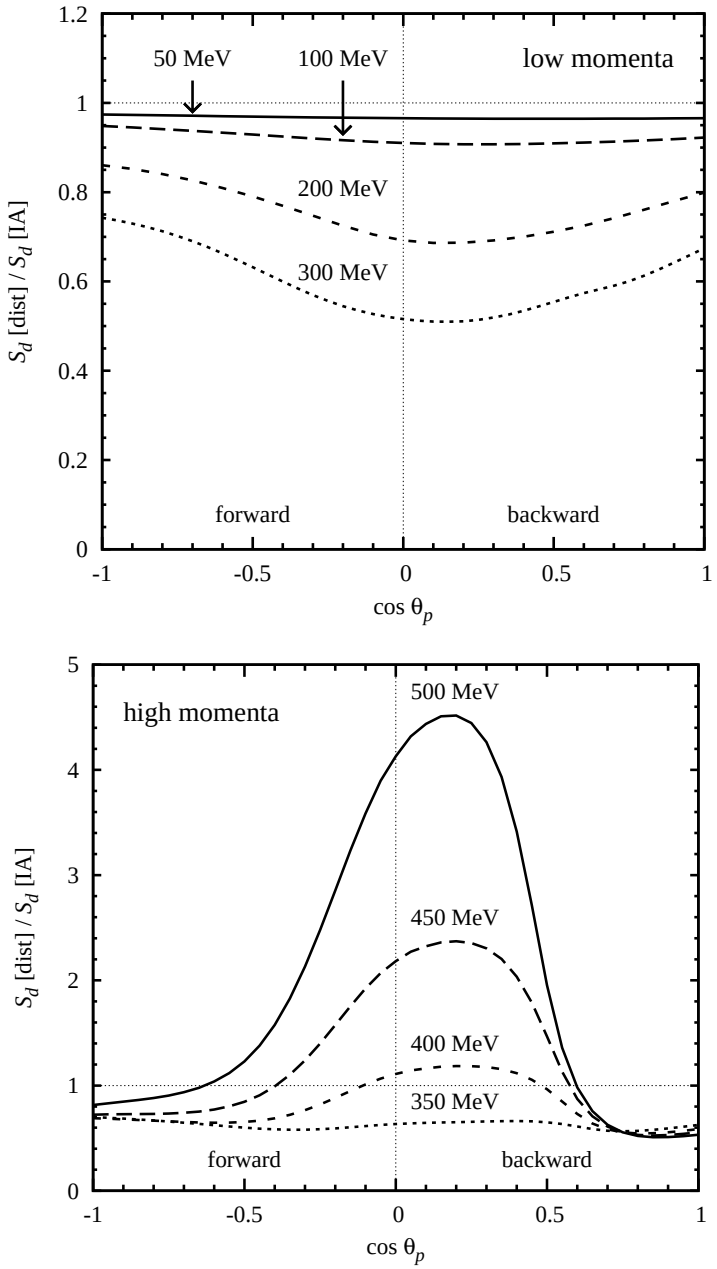

FIG. 14. The ratio of the distorted spectral function to the IA spectral function, $S_d[\text{dist}]/S_d[\text{IA}]$, Eqs. (6.30)–(6.33), as a function of the cosine of the recoil momentum angle in the deuteron rest frame, $\cos\theta_p$, for several values of the recoil momentum modulus $p_p \equiv |\boldsymbol{p}_p|$. The upper and lower plot show low and high values of the recoil momentum, as indicated on the plots. The distorted spectral function includes the IA, FSI and FSI^2 terms. Model parameters are described in the text.

- At higher recoil momenta $p_p \gtrsim 300\,\text{MeV}$ the FSI^2 term becomes dominant at forward and sideways angles, $\cos\theta_p < 0.7$, resulting in a large positive correction relative to the IA. The distorted spectral function now shows a maximum at $\cos\theta_p \sim 0$. The transition between the low- and high-momentum regimes is rather sudden.
- At backward angles $\cos\theta_p > 0.7$ the FSI^2 term is suppressed, so that the FSI remains absorptive even at large recoil momenta. The spectral function in this region shows little variation with the recoil momentum at $p_p \gtrsim 300\,\text{MeV}$. Overall this results in a forward–backward asymmetry of the spectral function at large momenta.
- The distorted spectral function is positive for all recoil momenta $\boldsymbol{p}_p$, as required on general grounds, cf. Eq. (6.51).

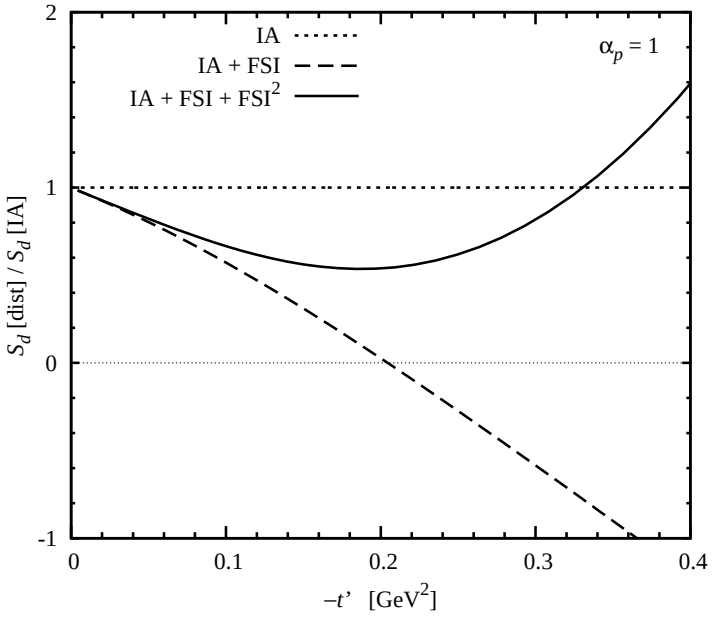

FIG. 15. The ratio of the distorted spectral function to the IA spectral function, $S_d[\text{dist}]/S_d[\text{IA}]$, Eqs. (6.30)–(6.33), as a function of $-t'$, for a fixed value $\alpha_p = 1$. The plot shows separately the IA, IA + FSI, and IA + FSI + FSI^2 results.

The observed dependencies are naturally explained by considering the kinematics of the scattering process in the rest frame. At low recoil momenta the main rescattering effect is always at $\theta_p \sim 90\,\text{deg}$, because the only way in which the forward–moving DIS hadron with momenta $\sim 1\,\text{GeV}$ could transfer a momentum of the order $p_p \sim 100\,\text{MeV}$ to the spectator proton is by pushing it sideways. At larger recoil momenta $p_p \gtrsim 300\,\text{MeV}$ is becomes increasingly possible for the forward–going DIS hadron to push the spectator forward, resulting in an enhancement of the spectral function in the forward region. In contrast, the backward region is protected from this effect, as it is kinematically impossible for the forward-going DIS hadron to push the spectator backwards.

The results shown in Fig. 13 and 14 are close to those obtained in Ref. [45] for the distorted spectral function of quasi-elastic deuteron breakup $d(e,e'p)n$ at intermediate energies $\sim$ few GeV in the Glauber approximation. This is natural, as our distorted spectral function also describes quasi-elastic breakup, if the tagged DIS structure function of the nucleon is replaced by its elastic structure function (i.e., by the square of the nucleon elastic form factor) at $\sim$ few GeV. Note that the present calculation includes only the S–wave of the deuteron bound state; if the D–wave were included the results of Fig. 13 and 14 at low recoil momenta $p_p < 200\,\text{MeV}$ would be practically unchanged, and at higher recoil momenta the pattern would still be the same [45].

Figure 15 shows the distorted spectral function as a function of the invariant momentum transfer t' and the recoil LF fraction α_p, as used in neutron structure extraction and on-shell extrapolation. The plot again shows the ratio $S_d[\text{dist}]/S_d[\text{IA}]$, Eqs. (6.30)–(6.33), and gives separately the results for the IA, the sum IA + FSI, and the sum IA + FSI + FSI^2 (total). One sees that

- For $|t'| \lesssim 0.1\,\text{GeV}^2$ the correction arises mainly from the linear FSI term and is negative.
- For $|t'| \gtrsim 0.2\,\text{GeV}^2$ the FSI^2 term dominates and causes a steep rise of the spectral function.
- The distorted spectral function is again positive for all t'.

F. Analytic properties

We must also investigate the effect of FSI on the analytic properties of the spectral function in t'. The IA current matrix element contains the nucleon pole of the deuteron wave function at $t' = 0$, which causes the IA spectral function to behave as $\sim R/(t')^2$ in the limit $t' \to 0$ (see Sec. IV F). It is easy to see that the FSI contribution to the current matrix element is non-singular in the limit $t' \to 0$. This follows from the fact that the rescattering integral I_d, Eq. (6.23) [or Φ_d in the factorized approximation, Eq. (6.44)] is a smooth function of the recoil momentum in the

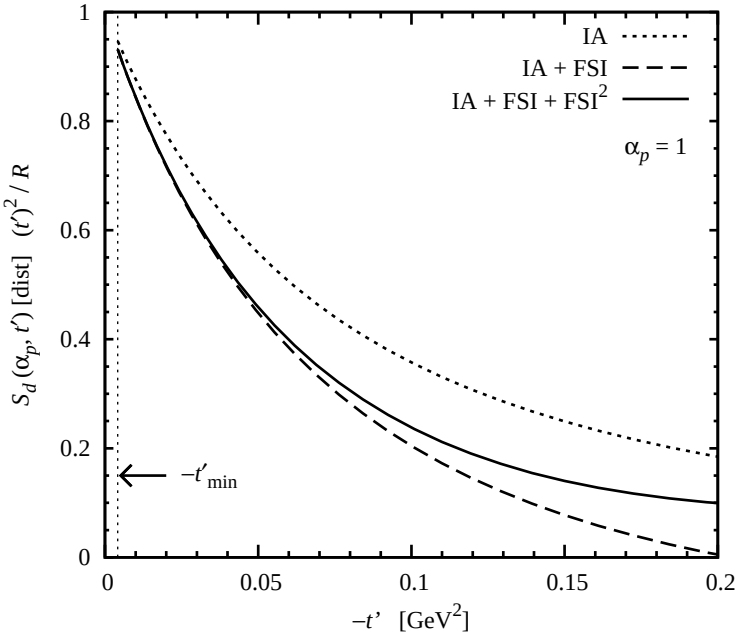

FIG. 16. The distorted spectral function S_d[dist], Eqs. (6.30)–(6.33), with the pole factor $R/(t')^2$ extracted, as function of t', for $\alpha_p = 1$. (cf. Fig. 7). The plot shows separately the IA, IA + FSI, and IA + FSI + FSI^2 results.

physical region $|\boldsymbol{p}_p(\mathrm{RF})| > 0$ (or $t' < t'_0$), remains regular at $|\boldsymbol{p}_p(\mathrm{RF})| = 0$, and can thus be continued to the unpysical point $|\boldsymbol{p}_p(\mathrm{RF})|^2 = t'_0 = -M_N\epsilon_d + \epsilon^2/4$ (or $t' = 0$) without encountering singularities of the deuteron wave function. In the invariant formulation using Feynman graphs, it follows from the fact that the nucleon pole arises from the nucleon tree graph, while the loop graphs describing FSI can at most modify the subleading behavior. A formal proof of this "no-loop theorem" was given in Ref. [15].

Figure 16 shows the distorted deuteron spectral function with the pole factor removed. The plot shows separately the IA, the sum IA + FSI, and the sum IA + FSI + FSI^2 (total). One sees that

- The FSI correction vanishes when approaching the pole.
- The FSI^2 correction vanishes even faster than the FSI one.
- The magnitude of the FSI correction is $\sim 1/2$ of the IA at $|t'| \sim 0.1\,\mathrm{GeV}^2$, decreasing approximately linearly with $|t'|$.

The fact that FSI does not modify the nucleon pole singularity of the IA spectral function is of central importance for the extraction of neutron structure from tagged DIS on the deuteron with proton tagging. It implies that FSI can be eliminated in a model-independent manner through the on-shell extrapolation procedure described in Sec. IV F. FSI modifies the measured tagged structure at $t' < t'_0$ but drops out when performing the extrapolation to $t' = 0$ [15].

G. Sum rules and unitarity

Important physical requirements of the deuteron spectral function are the nucleon number and LF momentum sum rules, Eqs. (4.21) and (4.22). They express the fact that the initial state consists of two nucleons and does not involve non-nucleonic degrees of freedom. The interactions summarized by the deuteron wave function distribute the LF momentum among the two nucleons but do not change the baryon number or the overall LF momentum of the system. The IA result for the spectral function satisfies both sum rules, and we would like them to be satisfied in the presence of FSI as well. We now want to discuss how this is accomplished within our model of FSI.

The nucleon number sum rule Eq. (4.21) demands that the integral of the distorted spectral function over the recoil proton momentum $(\alpha_p, \boldsymbol{p}_{pT})$ satisfy

$$\int \frac{d\alpha_p}{\alpha_p} \int d^2p_{pT}\; S_d(\alpha_p, \boldsymbol{p}_{pT})[\mathrm{dist}]$$

$$= 2(2\pi)^3 \int d\Gamma_p \; S_d(\alpha_p, \boldsymbol{p}_{pT})[\text{dist}] \;=\; 1. \tag{6.53}$$

Since the IA spectral function alone already satisfies the sum rule, Eq. (6.53) requires that the integral over the total FSI correction (linear and quadratic) be zero,

$$\int d\Gamma_p \; S_d(\alpha_p, \boldsymbol{p}_{pT})[\text{FSI} + \text{FSI}^2] \;=\; 0. \tag{6.54}$$

Equations (6.53) viz. (6.54) are realized in our formulation if the scattering process between the slow hadron and the spectator proton is elastic, i.e., if it only redistributes the momentum between the particles but preserves the overall flux. This is achieved if the operator converting the plane-wave state into the scattering state [the time evolution operator of Eq. (6.9)] is unitary in the two-particle space of the slow hadron and spectator nucleon,

$$\hat{U}^\dagger(\infty, 0)\, \hat{U}(\infty, 0) \;=\; 1. \tag{6.55}$$

In general the operator $\hat{U}(\infty, 0)$ would have matrix elements between states of different LF energy, so that the unitarity condition Eq. (6.55) would involve summation over two-particle intermediate states of arbitrary LF energy. In the on-shell approximation of Eq. (6.13) we effectively restrict the operator to have only energy-conserving matrix elements. In this approximation Eq. (6.55) is realized if the effective interaction satisfies the condition (here p_{h1}, p_{h2} and p_{p1}, p_{p2} denote arbitrary on-shell hadron and nucleon 4–momenta satisfying $p_{h2} + p_{p2} = p_{h1} + p_{p1}$)

$$\begin{aligned} &\tfrac{1}{2} T(p_{p2}, p_{h2}; p_{p1}, p_{h1}) - \tfrac{1}{2} T^*(p_{p2}, p_{h2}; p_{p1}, p_{h1}) \\ &= i \int d\Gamma_h \int d\Gamma_p \; (2\pi)^4 \delta^{(4)}(p_p + p_h - p_{p1} - p_{h1}) \\ &\times \tfrac{1}{4} \; T^*(p_{p2}, p_{h2}; p_p, p_h) \; T(p_p, p_h; p_{p1}, p_{h1}). \end{aligned} \tag{6.56}$$

Equation (6.56) has the form of the standard unitarity relation for the T–matrix, but with T replaced by $T/2$, corresponding to the fact that in Eqs. (6.8), (6.9), and (6.13) the T matrix appears with a factor $1/2$ relative to the standard definition of the S–matrix. If the interaction is chosen such as to satisfy Eq. (6.56), one can show that the linear and quadratic FSI term in the distorted spectral function, Eqs. (6.32) and (6.33), indeed obey Eq. (6.54). The proof involves converting the momentum integrals to a form such that Eq. (6.56) can be applied; we shall not present the details here.

The unitarity condition Eq. (6.56) has to be understood within our scheme of approximations based on the hierarchy Eq. (6.41). Our FSI calculation describes correction to the IA spectral function for recoil momenta of the order of the inverse deuteron size and are meaningful in this parametric region only. The unitarity condition Eq. (6.56) involves momenta of the order of the inverse range of the nucleon-nucleon interaction, which lie outside the region where we consider the rescattering process. We can therefore assume that unitarity is realized by contributions from parametrically large recoil momenta, where we can not — and do not need to — model the rescattering amplitude. In other words, we suppose that any change of flux in the low-momentum region in which we are interested will be compensated by a change in the high-momentum region which we cannot control. In this spirit we have parametrized the rescattering amplitude at low momenta without explicitly implementing the unitarity condition Eq. (6.56); see Appendix C.

The LF momentum sum rule Eq. (4.22) follows from the nucleon number sum rule Eq. (4.21) if the function $(2 - \alpha_p) S_d(\alpha_p, p_{pT})$ is symmetric under $\alpha_p \to 2 - \alpha_p$, which amounts to interchange of the LF momenta of the active nucleon and the spectator. The IA result embodies this symmetry exactly thanks to the symmetry of the deuteron LF wave function. The FSI correction does not satisfy it exactly, as the rescattering integral I_d in Eqs. (6.32) and (6.33) is generally not symmetric under $\alpha_p \to 2 - \alpha_p$. However, the symmetry of the spectral function is still achieved within the parametric approximation based on Eq. (6.41), as the variation of I_d in α_p around $\alpha_p = 1$ is much slower than that of ψ_d, so that I_d can effectively be regarded as a constant for the purpose of the reflection symmetry, and the symmetry of Eqs. (6.32) is again brought about by that of the deuteron wave function. In this sense also the momentum sum rule of the spectral function is preserved by the FSI within our scheme of approximations. Note that our physical picture of FSI applies only in a limited range of x, so that it is not possible to test the momentum sum rule for the deuteron structure function, Eq. (4.29), within our model.

VII. NEUTRON STRUCTURE EXTRACTION

Our findings regarding the momentum and angular dependence of FSI have implications for the extraction of neutron structure functions from deuteron DIS data with proton tagging. A full assessment of the strategy requires

an estimate of the uncertainties of the tagged structure function measurements and should be made with realistic pseudodata. Nevertheless, some general conclusions can be drawn already at this level.

The preferred method for extracting the free neutron structure function is the on-shell extrapolation in t' at fixed α_p (see Sec. IV F). The procedure eliminates modifications due to nuclear binding as well as FSI. The accuracy of the extrapolation depends on several factors: (a) the uncertainties of the tagged structure function data; (b) the smoothness of the t' dependence of the spectral function after removing the pole factor, which is determined by the FSI; (c) the distance between the physical region and the on-shell point, which depends on the recoil fraction α_p.

If accurate measurements of the tagged structure functions can be made down to rest-frame recoil momenta $p_p(\mathrm{RF}) \sim$ few 10 MeV, one may perform the on-shell extrapolation in t' at LF fractions $\alpha_p \approx 1$, where one can come closest to the pole in t' (see Fig. 4). In this situation our model predicts that the FSI corrections have smooth t' dependence, and a magnitude of $< 10\%$ of the IA at the lowest t' values, so that they are reliably eliminated by the extrapolation procedure. Since there are no singularities in t' between t'_0 and 0 the extrapolation can be performed using a polynomial fit to the t' dependence of the tagged structure function data [15].

If accurate measurements of the tagged structure functions are only possible at larger recoil momenta $p_p(\mathrm{RF}) \sim$ 100–200 MeV, one may instead focus on the backward region $\alpha_p > 1$ (or $\cos\theta_p > 0$), where our model predicts that FSI are relatively small; see Figs. 14 and 15. FSI are also suppressed in the forward region, $\alpha_p > 1$, but the predictions there are more model-dependent. In this case there is a trade-off between coming as close as possible to the pole (which favors $\alpha_p = 1$) and minimizing FSI (which favors $\alpha_p = 1$). While our model predicts that the t' dependence is smooth even in the presence of FSI, the distances from the pole are such that the magnitude of the correction is substantial ($\sim 50\%$ of the IA at $t' = 0.1$ GeV^2; see Fig. 16). In this situation one may no longer rely on polynomial extrapolation but fit the data with a more complex parametrization of the spectral function based on the expected functional form of the FSI correction.

VIII. SUMMARY AND OUTLOOK

In this work we have presented a theoretical framework for the analysis of DIS on the deuteron with spectator nucleon tagging. Nuclear and nucleonic structure are separated using the apparatus of LF quantum mechanics appropriate for high-energy scattering processes. The IA determines the basic dependence of the tagged cross section on the recoil momentum and its analytic properties (nucleon pole). In the region of intermediate x (roughly $0.1 < x < 0.5$) FSI arise mainly from the interaction of the spectator with slow hadrons produced in the fragmentation of the active nucleon (rest frame momenta $|\boldsymbol{p}_h| \sim 1$ GeV). We have described this effect in a schematic model using empirical slow-hadron distributions (protons, neutrons) and the nucleon-nucleon scattering amplitude. Our treatment is based on a hierarchy of dynamical scales (deuteron size $\gg$ range of rescattering) and gives rise to a self-consistent physical picture. The main conclusions regarding FSI in tagged DIS can be summarized as follows:

- *Absorption and refraction.* The rescattering between the slow DIS hadrons and the spectator nucleon involves absorptive interactions (linear in the imaginary part of amplitude, dominant at recoil momenta $|\boldsymbol{p}|_p < 200$ MeV) and refractive interactions (quadratic in real and imaginary parts, dominant at higher momenta). The net effect is to reduce the flux of spectator nucleons at low momenta and increase it at higher momenta.

- *Angular dependence.* The FSI effect on the recoil momentum distribution is approximately isotropic in the deuteron rest frame at momenta $|\boldsymbol{p}_p| < 100$ MeV. At higher momenta it becomes angle-dependent, with the strongest effect occurring in the direction approximately perpendicular to the $\boldsymbol{q}$–vector (sideways direction).

- *Analyticity in t'.* The FSI correction to the IA spectral function vanishes at the nucleon pole $t' \to 0$ (relative to the IA) and exhibits a smooth dependence on t' up to $|t'| \sim 0.1$ GeV^2. It can be eliminated through on-shell extrapolation $t' \to 0$.

- *Relative magnitude.* The FSI correction reduces the IA spectral function by $\sim 50\%$ at $|t'| \sim 0.1$ GeV^2. The effect becomes proportionately smaller as $|t'|$ decreases.

Our results show that the extraction of free neutron structure through on-shell extrapolation are possible if accurate measurements of the recoil momentum dependence can be performed in the region $|t'| \ll 0.1$ GeV^2 (or $|\boldsymbol{p}_p| \ll 200$ MeV). The analytic structure of the FSI correction and its moderate size indicate that the nucleon pole residue can be extracted reliably even in the presence of experimental errors. We emphasize that the extrapolation eliminates not only Fermi motion but also nuclear binding effects, as the phase space for interactions vanishes at the on-shell point. Measurements of tagged DIS over a wide kinematic range will become possible at a future EIC with suitable forward detectors. Simulations of neutron structure extraction through on-shell extrapolation using the IA cross section model suggest that the procedure is feasible under realistic conditions [76, 77]. The dominant systematic uncertainty in the

tagged structure function results from the uncertainty in the transverse recoil momentum $\boldsymbol{p}_{pT}$, as caused by the finite detector resolution and the intrinsic momentum spread of the deuteron beam [78]. These simulations can now be updated to include FSI effects in the cross section model; results will be reported elsewhere.

Tagged DIS on the deuteron has also been proposed as a tool to explore the dynamical origin of the nuclear modification of the nucleon's partonic structure. The idea is that the observed recoil momentum effectively controls the spatial size of the *pn* configuration in the deuteron, which makes is possible to study nuclear modifications of the nucleon structure functions in configurations of defined size ("tagged EMC effect") [1, 44, 79, 80]. The main challenge in such measurements is to separate initial-state modifications of the partonic structure from FSI effects. Our model provides an a-priori estimate of the size of the FSI effect and can be used to assess the sensitivity of such measurements to a putative nuclear modification of nucleon structure. In particular, the results of Fig. 14 show that in the backward region $\cos\theta_p > 0.7$ the FSI effect is practically independent of the modulus of the recoil momentum for values $|\boldsymbol{p}_p| \gtrsim 300$ MeV. An observed variation of the tagged structure function with $|\boldsymbol{p}_p|$ in this region could therefore be ascribed to initial-state modifications. The formulation of a practical procedure for tagged EMC effect studies at the EIC based on these findings should be the object of future work.

In applications to neutron structure and the EMC effect one aims to eliminate or minimize the FSI effects in tagged DIS. The same measurements could be used to study the FSI as an object in iteslf, by going to kinematics where the effects are maximal (recoil angles $-0.2 < \cos\theta_p < 0.4$; see Fig. 14) and verifying their strong kinematic dependence. Such measurements on the deuteron would help to understand better the pattern of nuclear breakup in DIS on heavier nuclei (e.g., slow neutron rates and angular distributions), which in turn would assist other studies of hard processes in nuclei (centrality dependence, hadronization and jets in nuclei) [5].

In the present study of FSI in tagged DIS we considered the case of unpolarized electron and deuteron and made several simplifying assumptions about deuteron structure, the DIS hadron spectrum, and the nature of the rescattering process. The treatment could be refined in several aspects while remaining within the same physical picture:

- *Spin degrees of freedom and polarization.* The spin degrees of freedom of the deuteron and the nucleons could be incorporated in the LF quantum-mechanical description without essential difficulties. A connection between the deuteron's NN LF wave function and the non-relativistic wave function along the lines of Sec. III C and Eq. (3.23) can be derived including spin; it involves relativistic spin rotations describing the transition from three-dimensional spin to LF helicities. The deuteron now includes S– and D–wave states ($L = 0$ and 2), giving rise to a rich structure. Expressions for the helicity representation of the deuteron NN LF wave function are given in Ref. [40], and the tagged DIS structure functions in the IA for the polarized deuteron can be obtained by substituting the unpolarized deuteron LF momentum density in Eq. (4.32) by the corresponding polarized density given there. A detailed treatment of polarized deuteron LF structure and double-polarized tagged DIS will be presented in Ref. [39]. When describing FSI in polarized tagged DIS one must account also for (a) the dependence of the slow hadron distribution on the spin of the active nucleon (there are presently few data on target fragmentation in polarized nucleon DIS); (b) the spin dependence of the rescattering amplitude; (c) contributions to the cross section resulting from the interference of amplitudes with different initial spin states (S–D wave interference). The correlation between the nucleon spin and its momentum in the deuteron, combined with a spin dependence of the slow hadron distribution and the rescattering in FSI, could give rise to pronounced spin-orbit effects in tagged DIS on the polarized deuteron. Electron polarization would bring into play the nucleon spin structure functions and enable spin-spin and further spin-orbit effects in tagged DIS.

- *Inelastic rescattering.* In the present calculation we implement FSI through elastic rescattering of slow hadrons (protons, neutrons) on the spectator. This scheme allows us to describe FSI in the hadronic tensor at the probabilistic level (because the same hadrons appear in the current matrix element with and without FSI) and preserve the nucleon number sum rule through elastic unitarity. It is clear that certain inelastic channels are open at the momenta $|\boldsymbol{p}_h| \sim 1$ GeV considered here and can have sizable cross section, for example, production of Δ isobars in nucleon-nucleon collisions. Including such channels in the FSI calculation is possible in theory but very difficult in practice. It requires a coupled-channel formalism, in which one considers all stable hadrons appearing in the final state (in the example of Δ excitation, this would be two nucleons and one pion) and implements all possible interactions between them. One would also need to know the amplitudes for the "direct" production of these hadrons through fragmentation of the active nucleon, which interfere with those of "indirect" production in the rescattering process. It is not obvious whether these amplitudes could be extracted from the DIS hadron multiplicities without further modeling.

- *Rescattering of pions.* We have focused here on FSI induced by the rescattering of slow protons and neutrons in the DIS final state, as these are the dominant hadrons at $x_{\rm F} < -0.3$ and have large cross sections for rescattering on the spectator nucleon. FSI could also arise from the rescattering of pions, whose multiplicity rises strongly at $x_{\rm F} > -0.3$. This effect could be calculated with the same formalism as used here (the formulas for the

rescattering integral in Appendix D are given for a general slow hadron mass). The pion–nucleon amplitude at pion momenta $|\boldsymbol{p}_h| \sim 1$ GeV is well constrained by data. One interesting aspect of pions is that they can emerge in the backward direction of the DIS process, i.e., opposite to the $\boldsymbol{q}$–vector [see Sec. V A and Eq. (5.5)], and therefore push the spectator in the backward direction. It would be worth investigating pion–induced FSI in a separate study.

The physical picture of FSI developed here refers to the kinematic region of intermediate $0.1 \lesssim x \lesssim 0.5$. In this region the slow hadron distributions are approximately independent of x, while diffractive hadron production is not yet important. Tagged DIS experiments can of course be performed also at larger or smaller values of x, with various scientific objectives. It is worthwhile summarizing what changes in the physical picture of FSI are expected in these regions.

- *FSI and diffraction at small x.* At $x \ll 0.1$ diffractive DIS becomes a distinctive source of slow nucleons in the target fragmentation region. The $x_{\rm F}$ spectra of protons in DIS on the proton measured at HERA show a diffractive peak near $x_{\rm F} = -1$ with an integrated multiplicity of ~ 0.1; see Ref. [81] for a review. Physically this effect is explained by a color-singlet exchange between the electromagnetic current and the nucleon, such that the DIS process leaves the nucleon intact and recoiling with a momentum $\sim$ few 100 MeV. If such diffractive production happens in tagged DIS on the deuteron, there is a significant probability for the diffractive nucleon and the spectator to recombine and form the deuteron, as they have the same spin-isospin quantum numbers and similar momenta as the original proton-neutron pair in the deuteron wave function. In measurements of tagged DIS at small x one selects the channel where this recombination does not happen and a proton-neutron scattering state is produced instead of the deuteron. In this situation it is essential that the wave function of the scattering state is constructed such that it is orthogonal to the deuteron, i.e., that it is obtained as the solution of the dynamical equation with the same effective interaction as gives the deuteron bound state, cf. Eqs. (6.9) and (6.8). It also requires that off-shell energies are allowed in the rescattering process. A detailed treatment of FSI in tagged DIS at small x will be presented in a forthcoming article [21].

- *FSI and in tagged DIS at large x.* In DIS on the nucleon at $x \gtrsim 0.5$ the distribution of hadrons in the target fragmentation region differs substantially from that at lower x. The reason is that the hadron LC fraction is kinematically restricted to $\zeta_h < 1-\xi \approx 1-x$, such that only small values of ζ_h are allowed at $x \to 1$. Physically speaking the DIS process almost "empties" the nucleon of LF momentum, and the produced hadrons have to share the small rest. These hadrons therefore have large momenta in the target rest frame, cf. Eq. (5.5) and Figs. 9 and 10, and their interactions with the spectator are suppressed by the formation time. Our picture therefore suggests that FSI may be suppressed in tagged DIS at large x. However, since $F_{2n} \ll F_{2p}$ at $x \to 1$, even small FSI would have a large relative effect on the extracted neutron structure function. The $x \to 1$ limit of tagged DIS therefore requires a dedicated study.

Appendix A: Deuteron wave function

In this appendix we describe a simple two–pole parametrization of the non-relativistic deuteron wave function (S–wave only, no D–wave), which has the correct analytic properties at small momenta and provides an excellent approximation to realistic wave functions over the range of momenta considered here. It is of the form (see e.g. Ref. [82])

$$\widetilde{\Psi}_d(\boldsymbol{k})_{\rm two-pole} \;=\; \frac{1}{\sqrt{c}} \left(\frac{1}{|\boldsymbol{k}|^2 + a^2} - \frac{1}{|\boldsymbol{k}|^2 + b^2} \right), \tag{A1}$$

$$\int d^3k \, |\widetilde{\Psi}_d(\boldsymbol{k})_{\rm two-pole}|^2 \;=\; 1, \qquad c \;=\; \frac{\pi^2 (a-b)^2}{ab(a+b)}, \tag{A2}$$

where the parameter a^2 is determined by the position of the nucleon pole [cf. Eq. (3.26)],

$$a^2 = M_N \epsilon_d - \frac{\epsilon_d^2}{4} \;=\; \frac{t_0'}{2}, \tag{A3}$$

and b^2 is determined empirically from the average deuteron size. The numerical values are

$$a \;=\; 0.0456\,{\rm GeV} \qquad [\text{from Eq. (A3)}], \qquad\qquad b \;=\; 0.2719\,{\rm GeV} \qquad (\text{empirically}). \tag{A4}$$

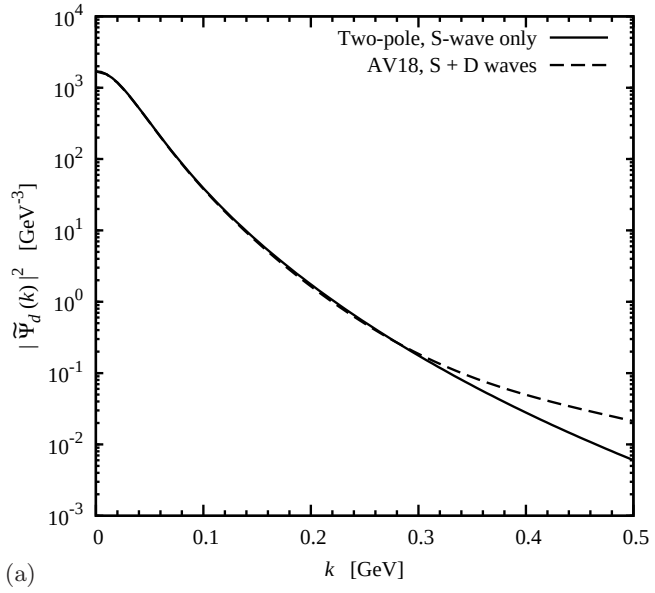

(a)

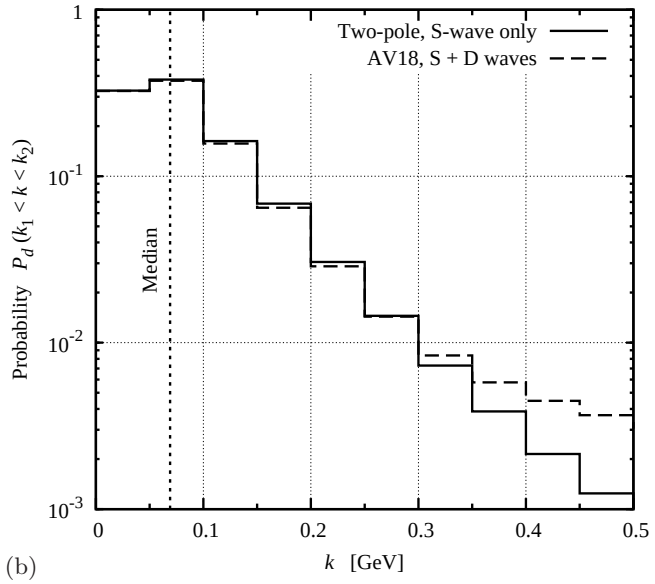

(b)

FIG. 17. (a) Momentum density of the non-relativistic deuteron wave function, $|\widetilde{\Psi}_d(\boldsymbol{k})|^2$, as a function of $k \equiv |\boldsymbol{k}|$. Solid line: Two–pole parametrization, Eq. (A1) (S–wave only). Dashed line: Wave function obtained with the AV18 NN potential (S + D waves) [55]. (b) Probability to find nucleon with momentum $k_1 < k < k_2$, Eq. (A5), for $k_{1,2}$ in steps of 50 MeV. The constant values shown at $k_1 < k < k_2$ give the value of $P_d(k_1 < k < k_2)$ for that range. The median momentum is indicated by a vertical line.

Figure 17a compares the momentum density $|\widetilde{\Psi}_d(\boldsymbol{k})|^2$ obtained with the two–pole parametrization, Eq. (A1), with that of the deuteron wave function obtained with the AV18 NN potential [55]. One sees that the two–pole form provides a completely adequate description of the momentum density over a wide range of momenta $|\boldsymbol{k}| < 0.3\,\mathrm{GeV}$. The discrepancy at larger momenta is due to the fact that the two–pole form contains only the S–wave, while the AV18 wave function includes the D–wave components, which becomes dominant at larger momenta.

Figure 17b shows the integral of the deuteron momentum density over finite intervals $k_1 < |\boldsymbol{k}| < k_2$, corresponding to the probability to find a nucleon with momentum in that range,

$$P_d(k_1 < |\boldsymbol{k}| < k_2) \;=\; \int d^3k\; \theta(k_1 < |\boldsymbol{k}| < k_2)\; |\widetilde{\Psi}_d(\boldsymbol{k})|^2 \;=\; 4\pi \int_{k_1}^{k_2} dk\; k^2\; |\widetilde{\Psi}_d(\boldsymbol{k})|^2. \tag{A5}$$

The result with the two-pole wave function is again compared with AV18. The histogram gives an intuitive picture of the momentum distribution of nucleons in the deuteron and enables simple estimates of the contribution of different momentum regions to observables. The median of the momentum distribution is 68 MeV for the two-pole wave function (69 MeV for AV18). Note that the median nucleon momentum in the deuteron is considerably larger than the "binding momentum" defined as $\sqrt{M_N \epsilon_d} = 45\,\mathrm{MeV}$; the different values illustrate the presence of multiple dynamical scales in the deuteron wave function.

Appendix B: Projection formulas

In this appendix we derive the explicit expressions of the proton-tagged deuteron structure functions in terms of the deuteron LF momentum density and the inclusive neutron structure functions, Eqs. (4.18) and (4.19), starting from the "master formula" for the scattering tensors in the collinear frame, Eq. (4.9). The same derivation can be used with the distorted spectral function in the presence of FSI. We write Eq. (4.9) in schematic form as

$$W_d^{\mu\nu}(p_d, q, p_p) \;=\; [...]\; W_n^{\mu\nu}(p_n, \widetilde{q}), \qquad [...] \;\equiv\; [2(2\pi)^3]\, \frac{2\,|\Psi_d(\alpha_p, \boldsymbol{p}_{pT})|^2}{(2-\alpha_p)^2}, \tag{B1}$$

and substitute the deuteron tensor parametrized by Eq. (2.22), and the neutron tensor parametrized by Eq. (4.14). We consider the deuteron tensor averaged over the transverse direction of the recoil momentum, in which only the structures with F_{Ld} and F_{Td} are present. Equations for the structure functions can be obtained by taking specific components of the tensor equation Eq. (B1) in the collinear frame (see Sec. II C). From the longitudinal component $\mu\nu = ++$ we obtain

$$F_{Ld} \;=\; [...]\; \frac{L_d^2}{(L_d^+)^2}\; \left\{ -\frac{(\widetilde{q}^+)^2}{\widetilde{q}^2}\; F_{Ln} \;+\; \left[\frac{(\widetilde{L}_n^+)^2}{\widetilde{L}_n^2} + \frac{(\widetilde{q}^+)^2}{\widetilde{q}^2} \right]\; F_{Tn} \right\} \tag{B2}$$

$$\;=\; [...]\; \frac{L_d^2}{(L_d^+)^2}\; \left[\frac{(\widetilde{q}^+)^2}{\widetilde{q}^2}\; (F_{Tn} - F_{Ln}) \;+\; \frac{(\widetilde{L}_n^+)^2}{\widetilde{L}_n^2}\; F_{Tn} \right]. \tag{B3}$$

From the transverse components $\mu\nu = ij, (i, j = x, y)$ we obtain

$$F_{Td} - F_{Ld} \;=\; [...]\; \left[F_{Tn} - F_{Ln} \;+\; \frac{|\widetilde{\boldsymbol{L}}_{nT}|^2}{2\widetilde{L}_n^2} F_{Tn} \right]. \tag{B4}$$

Here we have used that, after averaging over the direction of the transverse recoil momentum, rotational symmetry allows us to replace

$$\widetilde{L}_{nT}^i \widetilde{L}_{nT}^j \;\to\; \delta^{ij} |\widetilde{\boldsymbol{L}}_{nT}|^2/2. \tag{B5}$$

Explicit expressions for the structure functions are obtained from Eqs. (B3) and (B4) by substituting the specific expressions for the vector components in the collinear frame (see Sec. II C). The deuteron vector L_d is given by Eq. (2.38), and the nucleon vector components in the IA are

$$\widetilde{q}^+ \;=\; q^+, \qquad \widetilde{\boldsymbol{L}}_{nT} \;=\; -\boldsymbol{p}_{pT}. \tag{B6}$$

The exact expressions for the structure functions are complicated and not instructive. We quote only the expressions in the scaling limit $Q^2 \gg M_N^2, |\boldsymbol{p}_{pT}^2|$, where

$$-\frac{L_d^2 (\widetilde{q}^+)^2}{(L_d^+)^2 \widetilde{q}^2} \;\to\; 1, \qquad \frac{L_d^2 (\widetilde{L}_n^+)^2}{(L_d^+)^2 \widetilde{L}_n^2} \;\to\; 1, \qquad \frac{|\widetilde{\boldsymbol{L}}_{nT}|^2}{2\widetilde{L}_n^2} \;=\; O\left(\frac{|\boldsymbol{p}_{pT}|^2}{Q^2} \right). \tag{B7}$$

In this limit the L and T deuteron structure functions are obtained as

$$F_{Ld} \;=\; [...]\, F_{Ln}, \tag{B8}$$

$$F_{Td} \;=\; [...]\, F_{Tn}. \tag{B9}$$

Reverting to the long form of Eq. (B1) and writing the arguments of the structure functions, this is

$$F_{Ld}(x,Q^2) \;=\; [2(2\pi)^3]\,\frac{2\,|\Psi_d(\alpha_p,\boldsymbol{p}_{pT})|^2}{(2-\alpha_p)^2}\;F_{Ln}(\widetilde{x},Q^2), \tag{B10}$$

$$F_{Td}(x,Q^2) \;=\; [2(2\pi)^3]\,\frac{2\,|\Psi_d(\alpha_p,\boldsymbol{p}_{pT})|^2}{(2-\alpha_p)^2}\;F_{Tn}(\widetilde{x},Q^2), \tag{B11}$$

The corresponding formula for the deuteron structure function $F_{2d} = x_d F_{Td}$, Eq. (2.23), is

$$F_{2d}(x,Q^2) \;=\; [2(2\pi)^3]\,\frac{|\Psi_d(\alpha_p,\boldsymbol{p}_{pT})|^2}{2-\alpha_p}\;F_{2n}(\widetilde{x},Q^2), \tag{B12}$$

where we have used that $x_d = x/2$, $\widetilde{x} = x/(2-\alpha_p)$, and $F_{2n}(\widetilde{x},Q^2) = \widetilde{x}F_{Tn}(\widetilde{x},Q^2)$.

Appendix C: Elastic scattering amplitude

In this appendix we give an empirical parametrization of the nucleon–nucleon elastic scattering amplitude at small angles and incident momenta $p \lesssim 1\,\mathrm{GeV}$ (in the rest frame of the target nucleon), for use in our calculation of FSI in tagged DIS on the deuteron.

Measurements of nucleon–nucleon elastic and total cross sections at incident momenta $p \sim 1\,\mathrm{GeV}$ have been performed in several experiments; see Ref. [83] for a review of the data. Neutron–proton scattering measures directly the strong–interaction cross section; in proton–proton scattering one also has to account for electromagnetic interactions (Coulomb scattering) [84, 85]. For both channels (np, pp) the differential strong–interaction cross section for elastic scattering at forward angles can be parametrized as

$$\frac{d\sigma_{\mathrm{el}}}{dt} \;=\; |f(0)|^2\,e^{bt}, \tag{C1}$$

where $f(t)$ is a complex amplitude and b the exponential slope. The amplitude is of the form

$$f(t) \;=\; A(t) \;+\; \text{spin-dependent amplitudes}, \tag{C2}$$

where the central term $A(t)$ is non-zero at $t = 0$ and can be expressed as

$$A(0) \;=\; \mathrm{Im}\,A(0)\,(i+\rho_0), \qquad \rho_0 \;\equiv\; \mathrm{Re}\,A(0)/\mathrm{Im}\,A(0). \tag{C3}$$

The imaginary part at $t = 0$ is related to the nucleon–nucleon total cross section by the optical theorem

$$[\mathrm{Im}\,A(0)]^2 \;=\; \frac{\sigma_{\mathrm{tot}}^2}{16\pi}. \tag{C4}$$

The contribution of spin–dependent amplitudes at $t = 0$ can be described by the parameter

$$\beta_0 \;=\; |\text{spin-dependent amplitudes at } t=0|^2/[\mathrm{Im}\,A(0)]^2. \tag{C5}$$

The differential cross section Eq. (C1) can then be represented as

$$\frac{d\sigma_{\mathrm{el}}}{dt} \;=\; \frac{\sigma_{\mathrm{tot}}^2}{16\pi}\,(1+\rho_0^2+\beta_0)\,e^{bt}. \tag{C6}$$

Experimental values of the parameters $\sigma_{\mathrm{tot}}, \rho_0, \beta_0$, and b at several energies are summarized in Table I.

In terms of the invariant amplitude Eq. (6.14) the differential cross section for nucleon-nucleon elastic scattering is expressed as

$$\frac{d\sigma_{\mathrm{el}}}{dt} \;=\; \frac{|\mathcal{M}(s,t)|^2}{64\pi s\,p_{\mathrm{cm}}^2} \tag{C7}$$

where s is the squared CM energy and $p_{\mathrm{cm}} = \sqrt{s/4 - M_N^2}$ is the CM momentum. Comparing Eq. (C7) with the empirical formula Eq. (C6), we parametrize the invariant amplitude as

$$\left.\begin{aligned} |\mathcal{M}(s,0)|^2 \;&=\; 4sp_{\mathrm{cm}}^2\sigma_{\mathrm{tot}}^2(1+\rho_0^2+\beta_0) \qquad & |\mathcal{M}(s,t)| \;&=\; |\mathcal{M}(s,0)|\,e^{bt/2}, \\ \mathrm{Im}\,\mathcal{M}(s,t) \;&=\; \frac{|\mathcal{M}(s,t)|}{\sqrt{1+\rho_0^2}}, & \mathrm{Re}\,\mathcal{M}(s,t) \;&=\; \frac{\rho_0\,|\mathcal{M}(s,t)|}{\sqrt{1+\rho_0^2}} \end{aligned}\right\}. \tag{C8}$$

	p [GeV]	T [GeV]	$\sigma_{\rm tot}$ [mb]	ρ_0	β_0	b [GeV^{-2}]
np	1.26	0.633	36.1	-0.253	0.181 ± 0.074	5.09 $\pm$0.51
	1.68	0.985	~ 40	-0.414	< 0.01	5.35 $\pm$0.49
pp	1.28	0.648	41.1	0.202	0.096 ± 0.030	3.56 $\pm$1.09
	1.69	0.992	47.5	-0.178	0.025 ± 0.012	6.24 $\pm$0.37

TABLE I. Parameters of the small–angle elastic scattering amplitude measured in np [84] and pp [85] scattering experiments. Here p is the momentum of the incident nucleon in the target rest frame (lab momentum), and $T = \sqrt{p^2 + M_N^2} - M_N$ is the incident kinetic energy (lab energy).

These formulas apply at fixed s, and the parameters $(\sigma_{\rm tot}, \rho_0, \beta_0, b)$ generally depend on s. Equation (C8) can be adapted to the cases of np and pp scattering by choosing appropriate parameters (cf. Table I) and provide a sufficient description of the nucleon–nucleon elastic amplitude for our purposes. For a simple parametrization of the average np and pp amplitude we take the average of the parameter values at the lower energy of Table I ,

$$\sigma_{\rm tot} \;=\; 39\,{\rm mb}, \qquad \rho_0 \;=\; -0.03, \qquad \beta_0 \;=\; 0.14, \qquad b \;=\; 4.3\,{\rm GeV}^{-2}, \tag{C9}$$

For a more realistic parametrization one may use the energy–dependent parameters quoted in Ref. [83]. We note that the Re/Im ratio of the amplitude, ρ_0, is poorly constrained by experimental data and relies on theoretical calculations.

Appendix D: Rescattering integral

In this appendix we evaluate the rescattering integral determining the FSI correction to the current matrix element, Eq. (6.23). It is usesful to consider a phase space integral for hadron–proton scattering of the general form

$$I(p_h, p_p, \ldots) \;\equiv\; \int [dp_{p1}]\, \frac{2\pi}{p^+_{h1}}\, \delta(p^-_{h1} + p^-_{p1} - p^-_h - p^-_p)\, F(p_{p1}, p_h, p_p, ...), \tag{D1}$$

$$p^+_{h1} \;=\; p^+_h + p^+_p - p^+_{p1}, \tag{D2}$$

$$\boldsymbol{p}_{h1T} \;=\; \boldsymbol{p}_{hT} + \boldsymbol{p}_{pT} - \boldsymbol{p}_{p1T}, \tag{D3}$$

$$p^-_{h1} \;=\; (|\boldsymbol{p}_{h1T}|^2 + M_h^2)/p^+_{h1}. \tag{D4}$$

Here p_{h1} and p_{p1} are the hadron and proton 4–momenta in the initial state, and p_h and p_p are the 4–momenta in the final state, with $p^2_{h1} = p^2_h = M^2_h$, $p^2_{p1} = p^2_p = M^2_N$. LF plus and transverse momenta are conserved in the scattering process, cf. Eqs. (D2) and (D3), and the integration is over the initial–state phase space defined by the LF minus momentum– (or energy–) conserving delta function. The integral is regarded as a function of the final–state momenta. The integrand depends on the initial and final hadron and proton 4–momenta, as well as on other 4–momenta, e.g. the momenta associated with the current matrix element of the high–energy scattering process.

The integral Eq. (D1) can be converted to a manifestly relativistically invariant form. Using the conditions of momentum conservation, Eqs. (D2) and (D3), one easily shows

$$\frac{1}{p^+_{h1}}\, \delta(p^-_{h1} + p^-_{p1} - p^-_h - p^-_p) \;=\; \delta[p^+_{h1}(p^-_{h1} + p^-_{p1} - p^-_h - p^-_p)] \;=\; \delta[(p_h + p_p - p_{p1})^2 - M_h^2], \tag{D5}$$

so that

$$I(p_h, p_p, \ldots) = \int [dp_{p1}]\; 2\pi\, \delta[(p_h + p_p - p_{p1})^2 - M_h^2]\; F(p_{p1}, p_h, p_p, ...) \tag{D6}$$

$$= \int \frac{d^4 p_{p1}}{(2\pi)^4}\; 2\pi\, \delta(p^2_{p1} - M^2_N)\; 2\pi\, \delta[(p_h + p_p - p_{p1})^2 - M_h^2]\; F(p_{p1}, p_h, p_p, ...). \tag{D7}$$

The last integral has the form of a cut Feynman integral, where the hadron and proton propagators are replaced by mass–shell delta functions, as appears in the invariant formulation of nuclear rescattering processes (virtual nucleon formulation).

It is convenient to evaluate the rescattering integral in the invariant form Eq. (D6). We choose a collinear frame (cf. Sec. II C) and describe the 4–momenta by their LF components, with the plus components given as multiple of

$p_d^+/2$,

$$\left.\begin{aligned} p_h^+ &= \frac{\alpha_h p_d^+}{2}, \qquad \boldsymbol{p}_{hT}, \qquad p_h^- = \frac{2(|\boldsymbol{p}_{hT}|^2 + M_h^2)}{\alpha_h p_d^+}, \\ p_p^+ &= \frac{\alpha_p p_d^+}{2}, \qquad \boldsymbol{p}_{pT}, \qquad p_p^- = \frac{2(|\boldsymbol{p}_{pT}|^2 + M_N^2)}{\alpha_p p_d^+}, \\ p_{p1}^+ &= \frac{\alpha_{p1} p_d^+}{2}, \qquad \boldsymbol{p}_{p1T}, \qquad p_{p1}^- = \frac{2(|\boldsymbol{p}_{p1T}|^2 + M_N^2)}{\alpha_{p1} p_d^+} \end{aligned}\right\}. \tag{D8}$$

We introduce the total plus momentum fraction and transverse momentum of the hadron–proton system,

$$\alpha \equiv \alpha_h + \alpha_p, \qquad \boldsymbol{P}_T \equiv \boldsymbol{p}_{hT} + \boldsymbol{p}_{pT}, \tag{D9}$$

and the invariant mass of the hadron–proton system,

$$s \equiv s_{hp} \equiv (p_h + p_p)^2 = \alpha \left(\frac{|\boldsymbol{p}_{hT}|^2 + M_h^2}{\alpha_h} + \frac{|\boldsymbol{p}_{pT}|^2 + M_N^2}{\alpha_p} \right) - \boldsymbol{P}_T^2, \tag{D10}$$

such that

$$\frac{p_d^+ (p_h^- + p_p^-)}{2} = \frac{|\boldsymbol{p}_{hT}|^2 + M_h^2}{\alpha_h} + \frac{|\boldsymbol{p}_{pT}|^2 + M_N^2}{\alpha_p} = \frac{\boldsymbol{P}_T^2 + s}{\alpha}. \tag{D11}$$

The argument of the delta function in Eq. (D6) can now be expressed as

$$(p_h + p_p - p_{p1})^2 - M_h^2 = \frac{\alpha}{\alpha_{p1}} \left[R^2 - \left(\boldsymbol{p}_{p1T} - \frac{\alpha_{p1}}{\alpha} \boldsymbol{P}_T \right)^2 \right], \tag{D12}$$

where

$$R^2 \equiv -\frac{\alpha_{p1}^2}{\alpha^2} s + \frac{\alpha_{p1}}{\alpha} (s + M_N^2 - M_h^2) - M_N^2. \tag{D13}$$

From Eq. (D12) it follows that the argument can reach zero only if $R^2 > 0$. According to Eq. (D13) this is the case if

$$x_{\min} < \frac{\alpha_{p1}}{\alpha} < x_{\max}, \tag{D14}$$

where

$$x_{\min,\,\max} \equiv \frac{s + M_N^2 - M_h^2 \mp \sqrt{(s + M_N^2 - M_h^2)^2 - 4 s M_N^2}}{2s} = \frac{\sqrt{p_{\rm cm}^2 + M_N^2} \mp p_{\rm cm}}{\sqrt{s}}. \tag{D15}$$

In the last step we have introduced the center–of–mass momentum of the hadron–nucleon system, $p_{\rm cm}$,

$$(s + M_N^2 - M_h^2)^2 - 4 s M_N^2 = 4 s p_{\rm cm}^2. \tag{D16}$$

The ratio α_{p1}/α in Eq. (D14) represents the fraction of the LF plus momentum of the hadron–nucleon system carried by the initial nucleon. The condition Eq. (D15) has a simple physical meaning. In the CM frame the LF plus momentum fraction is given by the ratio of the nucleon plus momentum, $\sqrt{p_{\rm cm}^2 + M_N^2} + p_{\rm cm}^z$, to the mass of the system, $\sqrt{s}$, and the minimum and maximum values correspond to the situation that the nucleon momentum is opposite to, or along, the z–axis, $p_{\rm cm}^z = \mp p_{\rm cm}$. The bounds satisfy $0 < x_{\min,\,\max} < 1$, and the limiting values for small and large energies are

$$\left.\begin{aligned} x_{\min,\,\max} &\to 1/2, \qquad s \to (M_h + M_N)^2, \qquad \text{or} \qquad p_{\rm cm} \to 0, \\ x_{\min,\,\max} &\to 0, 1, \qquad s \to \infty, \qquad\qquad\ \ \text{or} \qquad p_{\rm cm} \to \infty \end{aligned}\right\}. \tag{D17}$$

In sum, the phase space for the initial nucleon momentum p_{p1} in the rescattering integral Eq. (D6) is defined by the conditions that the LF fraction lie in the interval Eq. (D14), and that the transverse momentum lie on the (shifted) circle corresponding to zero value of Eq. (D12),

$$\left| \boldsymbol{p}_{p1T} - \frac{\alpha_{p1}}{\alpha} \boldsymbol{P}_T \right| = R. \tag{D18}$$

It remains to express the phase space element in the LF momentum variables and account for the Jacobian factors. Using Eqs. (3.4) and Eq. (D12) we obtain

$$I \;=\; \int [d^4p_{p1}]\; 2\pi\,\delta[(p_h + p_p - p_{p1})^2 - M_h^2]... \tag{D19}$$

$$\;=\; \frac{1}{8\pi^2\alpha}\int_{\alpha x_{\min}}^{\alpha x_{\max}} d\alpha_{p1}\int d^2p_{p1T}\;\delta\left[\left(\boldsymbol{p}_{p1T} - \frac{\alpha_{p1}}{\alpha}\boldsymbol{P}_T\right)^2 \;-\; R^2\right]... \tag{D20}$$

Finally, introducing the shifted transverse momentum as integration variable,

$$\boldsymbol{p}_{p1T} \;=\; \frac{\alpha_{p1}}{\alpha}\boldsymbol{P}_T \;+\; \boldsymbol{l}_T, \tag{D21}$$

and using that

$$\delta(|\boldsymbol{l}|^2 - R^2) \;=\; \frac{\delta(|\boldsymbol{l}| - R)}{2R}, \tag{D22}$$

we obtain

$$I \;=\; \frac{1}{16\pi^2\alpha}\int_{\alpha x_{\min}}^{\alpha x_{\max}} d\alpha_{p1}\int_0^{2\pi} d\phi_l\; F[|\boldsymbol{l}_T| = R]. \tag{D23}$$

Equation (D23) represents a practical formula for the evaluation of the phase space integral. As a test we compute the phase volume, i.e., the integral of unity, $F = 1$, and obtain

$$\frac{1}{16\pi^2\alpha}\int_{\alpha x_{\min}}^{\alpha x_{\max}} d\alpha_{p1}\int_0^{2\pi} d\phi_l \;=\; \frac{x_{\max} - x_{\min}}{8\pi} \;=\; \frac{p_{\rm cm}}{4\pi\sqrt{s}}, \tag{D24}$$

which agrees with the standard phase volume obtained by evaluating the invariant integral Eq. (D7) in the CM frame.

ACKNOWLEDGMENTS

This work was motivated by Jefferson Lab's Laboratory-Directed R&D project LD1403/LD1506 "Physics potential of polarized light ions with EIC@JLab" (see Ref. [78]). We are indebted to W. Cosyn, V. Guzey, D. Higinbotham, Ch. Hyde, K. Park, P. Nadel-Turonski, and M. Sargsian, for numerous discussions of theoretical and experimental aspects of nuclear DIS with spectator tagging. We thank R. Schiavilla for helpful communications regarding scattering theory and FSI in deuteron breakup.

This material is based upon work supported by the U.S. Department of Energy, Office of Science, Office of Nuclear Physics, under contract DE-AC05-06OR23177. The research of M.S. was supported by the U.S. Department of Energy, Office of Science, Office of Nuclear Physics, under Award No. DE-FG02-93ER40771.

[1] L. L. Frankfurt and M. I. Strikman, Phys. Rept. **160**, 235 (1988). doi:10.1016/0370-1573(88)90179-2
[2] M. Arneodo, Phys. Rept. **240**, 301 (1994).
[3] L. Frankfurt, V. Guzey and M. Strikman, Phys. Rept. **512**, 255 (2012) [arXiv:1106.2091 [hep-ph]].
[4] S. Malace, D. Gaskell, D. W. Higinbotham and I. Cloet, Int. J. Mod. Phys. E **23**, 1430013 (2014) [arXiv:1405.1270 [nucl-ex]].
[5] D. Boer *et al.*, arXiv:1108.1713 [nucl-th].
[6] A. Accardi *et al.*, arXiv:1212.1701 [nucl-ex].
[7] U.S. Department of Energy Office of Science Nuclear Science Advisory Committee (NSAC) 2015 Long Range Plan for Nuclear Science, `http://science.energy.gov/np/nsac`
[8] A. Accardi, V. Guzey, A. Prokudin and C. Weiss, Eur. Phys. J. A **48**, 92 (2012) [arXiv:1110.1031 [hep-ph]].
[9] S. Abeyratne *et al.*, arXiv:1209.0757 [physics.acc-ph].
[10] A. J. Baltz *et al.*, Phys. Rept. **458**, 1 (2008) doi:10.1016/j.physrep.2007.12.001 [arXiv:0706.3356 [nucl-ex]].
[11] L. L. Frankfurt and M. I. Strikman, Phys. Rept. **76**, 215 (1981).
[12] L. Frankfurt, V. Guzey and M. Strikman, Phys. Lett. B **381**, 379 (1996); doi:10.1016/0370-2693(96)00625-9
[13] F. Bissey, V. Guzey, M. Strikman and A. Thomas, Phys. Rev. C **65**, 064317 (2002); doi:10.1103/PhysRevC.65.064317
[14] C. Boros, V. Guzey, M. Strikman and A. Thomas, Phys. Rev. D **64**, 014025 (2001). doi:10.1103/PhysRevD.64.014025

[15] M. Sargsian and M. Strikman, Phys. Lett. B **639**, 223 (2006) [hep-ph/0511054].
[16] S. Tkachenko *et al.* [CLAS Collaboration], Phys. Rev. C **89**, 045206 (2014).
[17] K. A. Griffioen *et al.*, Phys. Rev. C **92**, no. 1, 015211 (2015) doi:10.1103/PhysRevC.92.015211 [arXiv:1506.00871 [hep-ph]].
[18] S. Bueltmann et al., *"The Structure of the Free Neutron at Large x-Bjorken,"* Jefferson Lab 12 GeV Experiment E12-06-113, `https://www.jlab.org/exp_prog/proposals/06/PR12-06-113.pdf`
[19] E. C. Aschenauer *et al.*, arXiv:1409.1633 [physics.acc-ph].
[20] For current information on the EIC machine designs, see: `https://eic.jlab.org/wiki/` (JLab), `https://wiki.bnl.gov/eic/` (BNL).
[21] V. Guzey, M. Strikman, C. Weiss, in preparation.
[22] A. Arvidson *et al.* [European Muon Collaboration], Nucl. Phys. B **246**, 381 (1984). doi:10.1016/0550-3213(84)90045-2
[23] J. Ashman *et al.* [European Muon Collaboration], Z. Phys. C **52**, 1 (1991). doi:10.1007/BF01412322
[24] M. R. Adams *et al.* [E665 Collaboration], Z. Phys. C **61**, 179 (1994). doi:10.1007/BF01413096
[25] M. R. Adams *et al.* [E665 Collaboration], Phys. Rev. Lett. **74**, 5198 (1995) Erratum: [Phys. Rev. Lett. **80**, 2020 (1998)]. doi:10.1103/PhysRevLett.74.5198
[26] A. Airapetian *et al.* [HERMES Collaboration], Eur. Phys. J. C **20**, 479 (2001) doi:10.1007/s100520100697 [hep-ex/0012049].
[27] A. Airapetian *et al.* [HERMES Collaboration], Nucl. Phys. B **780**, 1 (2007) doi:10.1016/j.nuclphysb.2007.06.004 [arXiv:0704.3270 [hep-ex]].
[28] M. Strikman, M. G. Tverskoii and M. B. Zhalov, Phys. Lett. B **459**, 37 (1999) doi:10.1016/S0370-2693(99)00627-9 [nucl-th/9806099].
[29] L. Trentadue and G. Veneziano, Phys. Lett. B **323**, 201 (1994); doi:10.1016/0370-2693(94)90292-5
[30] J. C. Collins, Phys. Rev. D **57**, 3051 (1998) [Erratum-ibid. D **61**, 019902 (2000)].
[31] P. A. M. Dirac, Rev. Mod. Phys. **21**, 392 (1949).
[32] H. Leutwyler and J. Stern, Annals Phys. **112**, 94 (1978).
[33] F. Coester, Prog. Part. Nucl. Phys. **29**, 1 (1992). doi:10.1016/0146-6410(92)90002-J
[34] S. J. Brodsky, H. -C. Pauli and S. S. Pinsky, Phys. Rept. **301**, 299 (1998) [hep-ph/9705477].
[35] T. Heinzl, hep-th/9812190.
[36] W. Cosyn and M. Sargsian, Phys. Rev. C **84**, 014601 (2011) doi:10.1103/PhysRevC.84.014601 [arXiv:1012.0293 [nucl-th]].
[37] W. Cosyn, W. Melnitchouk and M. Sargsian, Phys. Rev. C **89**, no. 1, 014612 (2014) doi:10.1103/PhysRevC.89.014612 [arXiv:1311.3550 [nucl-th]].
[38] W. Cosyn and M. Sargsian, arXiv:1704.06117 [nucl-th].
[39] W. Cosyn, M. Sargsian, C. Weiss, in preparation.
[40] L. L. Frankfurt and M. I. Strikman, Nucl. Phys. A **405**, 557 (1983). doi:10.1016/0375-9474(83)90518-3
[41] C. Ciofi degli Atti and B. Z. Kopeliovich, Eur. Phys. J. A **17**, 133 (2003) doi:10.1140/epja/i2002-10140-7 [nucl-th/0207001].
[42] C. Ciofi degli Atti, L. P. Kaptari and B. Z. Kopeliovich, Eur. Phys. J. A **19**, 145 (2004) doi:10.1140/epja/i2003-10117-0 [nucl-th/0307052].
[43] V. Palli, C. Ciofi degli Atti, L. P. Kaptari, C. B. Mezzetti and M. Alvioli, Phys. Rev. C **80**, 054610 (2009) doi:10.1103/PhysRevC.80.054610 [arXiv:0911.1377 [nucl-th]].
[44] C. Ciofi degli Atti and L. P. Kaptari, Phys. Rev. C **83**, 044602 (2011) doi:10.1103/PhysRevC.83.044602 [arXiv:1011.5960 [nucl-th]].
[45] L. L. Frankfurt, W. R. Greenberg, G. A. Miller, M. M. Sargsian and M. I. Strikman, Z. Phys. A **352**, 97 (1995) doi:10.1007/BF01292764 [nucl-th/9501009].
[46] W. Boeglin and M. Sargsian, Int. J. Mod. Phys. E **24**, no. 03, 1530003 (2015) doi:10.1142/S0218301315300039 [arXiv:1501.05377 [nucl-ex]].
[47] V. B. Berestetskii, E. M. Lifshitz and L. P. Pitayevskii, in: Course of Theoretical Physics, Vol. IV: Relativistic Quantum Theory, Pergamon Press, Oxford, 1973.
[48] R. K. Ellis, W. Furmanski and R. Petronzio, Nucl. Phys. B **212**, 29 (1983).
[49] S. Weinberg, Phys. Rev. **150**, 1313 (1966). doi:10.1103/PhysRev.150.1313
[50] J. R. Cooke and G. A. Miller, Phys. Rev. C **66**, 034002 (2002) doi:10.1103/PhysRevC.66.034002 [nucl-th/0112037].
[51] J. R. Cooke, Ph.D. thesis, University of Washington, 2001, nucl-th/0112029.
[52] G. A. Miller and R. Machleidt, Phys. Rev. C **60**, 035202 (1999) doi:10.1103/PhysRevC.60.035202 [nucl-th/9903080].
[53] G. A. Miller, Prog. Part. Nucl. Phys. **45**, 83 (2000) doi:10.1016/S0146-6410(00)00103-4 [nucl-th/0002059].
[54] M.V. Terentev, Yad. Fiz. 24 (1976) 207.
[55] R. B. Wiringa, V. G. J. Stoks and R. Schiavilla, Phys. Rev. C **51**, 38 (1995) [nucl-th/9408016].
[56] J. B. Kogut and D. E. Soper, Phys. Rev. D **1**, 2901 (1970). doi:10.1103/PhysRevD.1.2901
[57] J. M. Cornwall and R. Jackiw, Phys. Rev. D **4**, 367 (1971). doi:10.1103/PhysRevD.4.367
[58] O. Benhar, N. Farina, H. Nakamura, M. Sakuda and R. Seki, Phys. Rev. D **72**, 053005 (2005) [hep-ph/0506116].
[59] C. Ciofi degli Atti, L. L. Frankfurt, L. P. Kaptari and M. I. Strikman, Phys. Rev. C **76**, 055206 (2007) doi:10.1103/PhysRevC.76.055206 [arXiv:0706.2937 [nucl-th]].
[60] K. M. Hanson, *Inclusive and Exclusive Virtual Photoproduction Results from Cornell,* Report CLNS-317
[61] M. Arneodo *et al.* [European Muon Collaboration], Phys. Lett. B **149**, 415 (1984). doi:10.1016/0370-2693(84)90436-2
[62] M. Arneodo *et al.* [European Muon Collaboration], Phys. Lett. B **150**, 458 (1985). doi:10.1016/0370-2693(85)90466-6
[63] M. Arneodo *et al.* [European Muon Collaboration], Z. Phys. C **31**, 1 (1986). doi:10.1007/BF01559586
[64] C. Alexa *et al.* [H1 Collaboration], Eur. Phys. J. C **73**, no. 4, 2406 (2013) [arXiv:1302.1321 [hep-ex]].
[65] V. Andreev *et al.* [H1 Collaboration], Eur. Phys. J. C **74**, no. 6, 2915 (2014) [arXiv:1404.0201 [hep-ex]].

[66] F. D. Aaron *et al.* [H1 Collaboration], Eur. Phys. J. C **68**, 381 (2010) [arXiv:1001.0532 [hep-ex]].
[67] S. Chekanov *et al.* [ZEUS Collaboration], JHEP **0906**, 074 (2009) [arXiv:0812.2416 [hep-ex]
[68] M. Derrick *et al.*, Phys. Rev. D **17**, 1 (1978). doi:10.1103/PhysRevD.17.1
[69] P. Allen *et al.* [Aachen-Bonn-CERN-Munich-Oxford Collaboration], Nucl. Phys. B **188**, 1 (1981). doi:10.1016/0550-3213(81)90101-2
[70] P. Allen *et al.* [Aachen-Bonn-CERN-Munich-Oxford Collaboration], Nucl. Phys. B **214**, 369 (1983). doi:10.1016/0550-3213(83)90239-0
[71] A. Arriaga and R. Schiavilla, Phys. Rev. C **76**, 014007 (2007) [arXiv:0704.2514 [nucl-th]].
[72] C. Granados and C. Weiss, JHEP **1507** (2015) 170 doi:10.1007/JHEP07(2015)170 [arXiv:1503.04839 [hep-ph]].
[73] G. Schierholz, Nucl. Phys. B **7**, 432 (1968). doi:10.1016/0550-3213(68)90094-1
[74] F. Coester, Helv. Phys. Acta **38**, 7 (1965).
[75] J. M. Namyslowski, Phys. Rev. D **18**, 3676 (1978). doi:10.1103/PhysRevD.18.3676
[76] W. Cosyn *et al.*, J. Phys. Conf. Ser. **543**, 012007 (2014) doi:10.1088/1742-6596/543/1/012007 [arXiv:1409.5768 [hep-ph]].
[77] V. Guzey, D. Higinbotham, C. Hyde, P. Nadel-Turonski, K. Park, M. Sargsian, M. Strikman and C. Weiss, PoS DIS **2014**, 234 (2014) [arXiv:1407.3236 [hep-ph]].
[78] C. Weiss *et al.*, *"Physics potential of polarized light ions with EIC@JLab,"* Jefferson Lab 2014/15 Laboratory–directed R&D Project, `https://www.jlab.org/theory/tag/`
[79] W. Melnitchouk, M. Sargsian and M. I. Strikman, Z. Phys. A **359**, 99 (1997) doi:10.1007/s002180050372 [nucl-th/9609048].
[80] O. Hen, L. B. Weinstein, S. Gilad and S. A. Wood, *"In Medium Nucleon Structure Functions, SRC, and the EMC effect,"* Jefferson Lab 12 GeV Experimental Proposal PR12-11-107, arXiv:1409.1717 [nucl-ex].
[81] G. Wolf, Rept. Prog. Phys. **73**, 116202 (2010) doi:10.1088/0034-4885/73/11/116202 [arXiv:0907.1217 [hep-ex]].
[82] B. C. Tiburzi and G. A. Miller, Phys. Rev. C **63**, 044014 (2001) [nucl-th/0011074].
[83] C. Lechanoine-LeLuc and F. Lehar, Rev. Mod. Phys. **65**, 47 (1993).
[84] B. H. Silverman *et al.*, Nucl. Phys. A **499**, 763 (1989).
[85] A. V. Dobrovolsky *et al.*, Nucl. Phys. B **214**, 1 (1983).